7-5-2012

Dual neutral particle induced transmutation

William Martin

William Joseph Martin

Candidate

Nuclear Engineering

Department

This dissertation is approved, and it is acceptable in quality and form for publication:

Approved by the Dissertation Committee:

Cassiano de Oliveira , Chairperson

Anil Prinja

Evangelos Coutsias

Edward Arthur

Adam Hecht

Dual Neutral Particle Induced Transmutation

by

William Joseph Martin

B.S., Nuclear Engineering, University of New Mexico, 2008
M.S., Nuclear Engineering, University of New Mexico, 2010

DISSERTATION

Submitted in Partial Fulfillment of the
Requirements for the Degree of

Doctor of Philosophy
Engineering

The University of New Mexico

Albuquerque, New Mexico

May, 2012

Dedication

I dedicate this dissertation to both of my grandfathers. Kamel Bowlus, you first got me interested in science and that passion has never left. Bill Martin, I never really got to know you but I always try to make you proud. Both of you will be eternally missed but will never be forgotten.

Acknowledgments

I'd like to first and foremost thank my wife, Stephanie, for everything. You've kept me sane through everything and I only hope to be there for you like you've been there for me.

Next I'd like to thank my advisor, Dr. Cassiano de Oliveira, for all his help over the last few years. Also, a deep gratitude to Dr. Shannon Holloway for setting up the groundwork for this research.

Finally, a big thanks to Rodney Keith for always being around to bounce ideas back and forth and to my family for all of their support and encouragement.

Dual Neutral Particle Induced Transmutation

by

William Joseph Martin

B.S., Nuclear Engineering, University of New Mexico, 2008
M.S., Nuclear Engineering, University of New Mexico, 2010

Ph.D., Engineering, University of New Mexico, 2012

Abstract

Although nuclear transmutation methods have been around for decades, they all focus solely on neutron induced reactions. Recent novel concepts have sought to use neutrons as well as photons for active interrogation of cargo to detect the smuggling of highly enriched uranium – a concept that would require modeling of the transmutation caused by both neutrons and photons. As photonuclear transmutation has yet to be modeled, new methods need to be developed.

The CINDER2008 nuclear transmutation code from Los Alamos National Laboratory is extended from neutron only applications to dual particle applications specifically for this modeling. To couple these calculations to a dual particle transport for the determination of reaction rates, both deterministic and Monte Carlo methods are used. By doing this through a single code, TINDER (Transport-coupled CINDER), transport and transmutation calculations can be completed with no human interaction after the start of the calculation, cutting down on the uncertainties and errors that come with human manipulation of data.

A necessary verification and validation of these methods has taken place, especially in terms of the photonuclear data, which is sparse or non-existent in some cases. This has proven any data translations and uses are appropriate and correct and the code has been modified correctly. A final demonstration has been performed based on the intended use of this code, active interrogation of nuclear cargo. These results match to within a few percent of experimental data and the extension to dual particles can bolster the output signal by over 15%. As transport methods come at a cost, a sensitivity analysis has been performed to see the effect of variations in the flux on the final output. These results show that although the output beta-delayed photon spectrum is sensitive to the input flux, the results are still on the correct order for practical purposes.

Contents

List of Figures

List of Tables

List of Tables

Chapter 1

Introduction

Activation and depletion analysis methods have recently grown in popularity, especially with computational speeds growing to the point where these calculations can be done efficiently and directly in line with transport calculations. There are numerous codes that do these calculations, from the standard stand-alone activation and depletion methods (e.g. CINDER, ORIGEN) to newer integrally coupled depletion methods (e.g. CASMO, SERPENT). However, a commonality between all of these codes is their restriction to only neutron induced reactions. Generally speaking, for reactor depletion calculations this practice is well accepted since the environment is dominated by neutrons. In other situations, such as dual particle active interrogation[6], photon induced reactions become just as important, thus creating a need for what is not presently available.

Additionally, these activation and depletion analysis tools generally need to be coupled to a particle transport code for that portion of the physics. While Monte Carlo methods have been the popular choice for transport, as well as depletion and activation, they are not without limitations. Not only can Monte Carlo methods be computationally expensive, they also can introduce error into the depletion modeling if sufficient convergence is not met[7, 8]. In order to guarantee sufficient convergence,

even more computational time must be spent on the calculation. To alleviate this burden, deterministic methods can be used to perform the transport as well as the activation/depletion calculations.

Although a popular choice of deterministic transport is the discrete ordinates (S_N) method, the even-parity method is becoming more attractive with the advances in computational power. The even-parity transport method, especially when using spherical harmonics and finite elements, is extremely powerful for computationally efficient modeling of particle transport in arbitrary geometries. These methods will be described further in Section 1.1.

With these thoughts in mind, a great opportunity arises not only to just create a one-of-a-kind dual particle activation/depletion code but to join it with neutral particle transport to create a coupled modeling capability that has not been seen before. This is the goal of the research conducted herein.

First, an review of the background on each method will be discussed in detail. Following that, the methodology behind the dual particle transmutation code will be given. The methodology for the transport coupling method and its capability will is then discussed. Next, results containing the verification and validation of the additions to the transmutation code will be laid out, followed by a sensitivity analysis of the transmutation code and a code demonstration. Finally, a summary, conclusions, and any further work are presented.

1.1 Background

Although there has not been a large motivation in the past for dual particle activation and depletion analysis (or in today's vernacular transmutation or burn-up analysis), new novel concepts have now led to the need for such models. Because of the previous lack of motivation for the work, little to no progress has been made in terms of the modeling and simulation of such physics.

Photofission and photonuclear reactions are by no means new phenomena. In 1939, shortly after the discovery of fission, Bohr and Wheeler [9] predicted that the interaction of high energy quanta with thorium and uranium could also result in fission, or what is now referred to as photofission. To test this theory, only a few years later in 1941 Haxby et.al. [10] conducted experiments with 6.3 MeV monoenergetic gamma rays and measured the cross section for fission of thorium and uranium. To corroborate and extend these results, Arakatu et. al. [11] conducted similar experiments with both 6.3 MeV and 17 MeV photons on thorium and uranium. Since those first tests, countless other experiments have taken place to measure pertinent information about photofission and other reactions. Duffield, Schmitt, and Sharp [12] nearly two decades later summarized a good portion of this information for general consumption.

Measurements of not only cross-section data (summarized succinctly in a single report by Berman [13]) but also the fission yield data [14, 15, 12, 16, 3, 1, 17, 5, 18, 19, 20, 21, 22, 23, 24, 25, 4, 26, 27, 28, 29, 30, 31, 32] are extremely important information for any modeling that is desired. Unfortunately, there is very little that has actually been recorded in the first place. This is extremely true with the photofission yield data as there are usually only one or two experiments for each target isotope, at perhaps five different energies. The current state of recorded data can be observed in Table 1.1. These energies are fairly well spaced in the spectrum of plausible photon energies; however they do not nearly cover all the ground. Additionally, a single

Table 1.1: List of isotopes where photofission yields have been experimentally measured with applicable notes.

Isotope	Notes
^{232}Th	Many experiments and multitude of energies[23, 24, 25, 30]
^{234}U	Single experiment at multiple energies, provisional results given graphically[28]
^{235}U	Many experiments and multitude of energies, well defined[14, 15, 1, 18, 27, 20, 26]
^{236}U	Single experiment at single energy[33]
^{238}U	Many experiments and multitude of energies, well defined[14, 15, 3, 34, 18, 29, 26]
U-natural	Single experiment at several energies, limited tabular results[5]
^{239}Pu	Few experiments at several energies[4, 20]
^{240}Pu	Single experiment at multiple energies, provisional results given graphically[31]
^{242}Pu	Single experiment at multiple energies, provisional results given graphically[32]
^{244}Pu	Single experiment at multiple energies, provisional results given graphically[19]

experiment is not always sufficient to truly capture all of the physics, due to experimental biases, imperfections, human error, etc. In particular, with the plutonium isotopes other than ^{239}Pu, a provisional set of data is only given graphically and does not always follow expected trends, as mentioned in the reports. Tabular results for these experiments were never published.

Photon cross section data has been slightly better in its abundance than the yield data, but it is still not as well known as the neutron cross sections. Whereas there are 393 of isotopes with evaluated neutron cross sections, there are only 163 isotopes with evaluated photonuclear cross sections [35]. Some examples will be presented in Section 2.1.

This lack of data places a limitation from the start on the modeling capabilities for photonuclear reactions, including photofission. Thankfully, due to the fact that there are physical similarities between neutron fission and photofission, the product yield

data can be translated from one to the other. This allows for the greater knowledge base of product yields from neutron induced fission to be used as a supplement. This is possible because current theory on fission points to the fact that there does not appear to be much of any difference in the scission process of compound nuclei excited to the same state by photoabsorption compared to de-excitation of similar compound nuclei produced by other means [36, 37, 38, 39]. Therefore, the resulting processes from fission post-excitation of the nucleus can be treated essentially the same no matter how the excitation occurred. Details of how this process is done will be discussed later in Section 2.1. Additionally, others have used this concept to model the fission yields for many incident particles like alpha particles and protons with success. [40, 41].

Recently there has been an interest in using photons in unique and new ways. One such example is for active interrogation of shielded nuclear material [42, 6]. This involves shining a beam of photons or neutrons (and in some cases both) onto shielded special nuclear material to see the response – with the intention of using this method to verify that there is/isn't special nuclear material in the media in question. The responses most desired are the delayed gamma signals that come from the decay of the daughter products produced in fission, both photon and neutron induced. Although there are no problems in constructing experiments to conduct this, there are simply no models capable of the simulation for the daughter products and released gammas from photonuclear interactions.

Because of these and other interests, a consortium began with the intent to gather all of the photonuclear cross section data and put it for the first time in the ENDF-B libraries [43]. Since this work, photonuclear cross sections have their own subsection in the ENDF-B libraries, from version VI onward [35]. These additions only cover photonuclear cross sections.

To attempt to address the second data need for delayed photon simulations, Verbeke, Hagmann, and Wright [44] gathered data on the neutron and gamma number and

energy distributions resulting from photofission. The intent of this work was to be used in transport codes, namely MCNPX and GEANT4, in conjunction with the photonuclear cross section data now in ENDF-B/VI (and all later versions) to produce the output gamma and neutron signal from photofission. This data covers the needs of new ideas in terms of the ultimate output signal. However, it does gloss over the underlying physics that produce that data. The physics that have been removed from the process include the splitting of the excited atom into fission products, which then decay to produce delayed neutrons and delayed gammas. There is also a lack of the ability to track the build-up of those fission products from the reactions and decays. By omitting the build-up, the method lacks a possible feedback mechanism to the transport calculation, as would happen in the real world. Although this type of integral data can serve a specific purpose, it is not highly generalizable.

To take full advantage of all of the data that is available, a more fundamental and rigorous method for this type of analysis would be a full transmutation analysis tool for photonuclear interactions. Similar types of codes have been around for decades but are limited neutron induced reactions [45, 46, 47, 48, 49]. Due to a lack of need and data, these codes all have not included the ability to process photonuclear reactions and the transmutation caused by them. An effort had taken place several years ago to attempt to put the photonuclear capability in the CINDER'90 activation/depletion code [50, 51, 52, 53, 54]. Unfortunately, the effort did not produce a final releasable product and to date there is still no product that has this capability. Not only could these models and data be useful in the aforementioned proposed active interrogation but also it can help refine the calculations made on reactor or pulsed systems or even simply photon-driven systems. Modeling of photonuclear transmutation for such systems as accelerators would help bring a better understanding of the contribution to background radiation by material activation and depletion in the system. These could lead to lower uncertainties in, for example, photonuclear cross section measurements, which would be beneficial to entire industry. At the same

time, in terms of reactors, the inclusion of both neutrons and photons could possibly bring closer to experimental data the modeling of reactor lifetime and spent fuel isotope inventories. In systems with a high gamma flux, this would be very useful. Because of these drivers, a dual neutral particle (neutrons and photons) transmutation analysis code would be extremely beneficial and is one goal of the research at hand.

While the transmutation calculation is extremely beneficial for many purposes, not just those listed above, it is only one piece of the modeling puzzle. In order for these codes to work, they need to be supplied an average particle flux. This flux is generally calculated through a particle transport code that models the entire medium at hand and averages the particle flux for the volume that is to have the transmutation analysis performed.

In general, there are two types of methods used for the transport calculation. The first, Monte Carlo method [55], is a stochastic method that uses probabilities and individual particle tracking to determine how the particles distribute themselves in the medium. Tallies are then performed to determine the flux in the region of interest. Although extremely popular for their ability to easily model arbitrary geometries with making few assumptions to reduce the phase space, Monte Carlo methods have a big drawback – they are extremely expensive to run and can take days and even months for a single result in a complicated model. Additionally, as mentioned in the Introduction, if sufficient convergence has not been met in terms of the flux for the problem, large error can propagate throughout the transmutation analysis, resulting in off-the-mark calculations [7, 8]. That being said, Monte Carlo codes are still the most widely used for this purpose [56, 57, 58].

The second class of methods used for transport calculations are deterministic. Deterministic methods are based on the direct solution of the Boltzmann transport equation [59, 60]. Due to the fact that the transport equation is integro-differential, it is not possible to be solved as is using current numerical techniques. Therefore,

approximations must be made in order to reduce the equation to simply a differential equation or an integral equation.

Perhaps the most common of these reduction techniques is the discrete ordinates, or S_N, method [61]. This method removes the integral portion of the equation by reducing the phase space through an assumption in angle–reducing the problem to solution only along discrete directions, or ordinates. By reducing the equation in such a way, simple "marching" schemes can be used to solve the problem, sweeping through the discretized space. This simplified solution scheme is popular as there is no need for large amounts of memory when solving on a computer. However, because of how this method reduces the phase space, non-physical ray effects can appear in the results. In terms of the front-end transport calculation for a transmutation analysis, S_N is the primary deterministic method that has been used in the past [56].

Another method that is similar to the S_N method is the so-called P_N method. Instead of reducing the angular variable of the transport equation into discrete directions, it uses Legendre polynomials to eliminate the integral portion of the equation [59, 60]. Unlike the discrete ordinates method, the solution to this reduced form of this equation is not as straight forward. A large system of equations is created through this reduction, and when solved as a matrix problem, the matrix structure and size cause the solution to be prohibitively expensive computationally. Historically, the P_N method has not been as popular as S_N.

A third method to reduce the integro-differential equation into a form that's more amenable to numerical solution is the integral method [59]. This method does the opposite of the previous two, as it removes the differential portion of the transport equation, leaving only integrals. Although straightforward to solve, the integral method only solves for the scalar flux, not the angular flux which can be desirable for other parameters that can be calculated from it. As with the P_N method, the integral method has not been as popular historically as the S_N method.

Yet a fourth method for the reduction of the transport equation is the even parity

or second order method [60]. This method splits the angular flux variable space into two parts, the even- and odd-parity fluxes. By using algebraic reductions and differentiating the entire equation, a second order differential equation is created on half the angular space. By then using a P_N-type approximation (using Legendre polynomials or spherical harmonics in three dimensions) on the angular dependence, the integral portion of the equation is removed. This reduction can be solved similar to P_N equation, using a system of equations. However, with the reductions done to arrive at the second order equation, the matrix created by this system is extremely well suited for off-the-shelf numerical solvers as it is symmetric positive definite. Because of the ability to use common numerical methods on the nicely structured system of equations, the even-parity method has the potential to beat the S_N method for computational speed.

Due to its potentially large impact on transport calculations, the even-parity method is being considered for use in coupled calculations. As these types of calculations could need numerous transport calculations for a single model, the numerical advantages of deterministic methods with the flexibility and capabilities of even parity transport can have a large impact. Additionally, the capability for the extremely popular Monte Carlo method to be coupled to the transmutation method is necessary. This will allow an apples to apples comparison of the transmutation method versus existing computational methods. This code coupling development and methodology are the focus of the second half of the research in this report.

1.2 Problem Statement

Bearing in mind all of the past work that has and hasn't been done in terms of photonuclear transmutation and the coupling to transport calculations, there is an apparent hole in current modeling capabilities. As mentioned, current novel applications of photonuclear interactions, especially photofission, have brought this missing capability to light. Methods are therefore sought to fill this void, which is the thrust of this research.

There are several steps that need to be taken in order to fill the gap. First on the transmutation side of the process, an activation/depletion code is needed, either existing or created for this purpose. Being as it would be most useful if the program was capable of processing both neutron and photon interactions simultaneously and being as there is no need in this case to reinvent the wheel, an existing transmutation code will need to be modified to accept both particles.

The code that has been chosen for this purpose is the CINDER2008 (beta) code from Los Alamos National Laboratory [48]. A large advantage of this code over others is its ability to have a user-created data library with a user-defined energy group structure. Therefore, unlike the previous version of CINDER (CINDER'90) [62] and the ORIGEN code [45, 47], the energy bin structure of the input flux can be defined and modified by the user. This allows for better modeling of a wide range of problems, other than those similar to light water reactor (LWR) and accelerator systems–as the libraries for these codes were previously designed for those applications. Additionally, CINDER2008 is a modern implementation of a deterministic transmutation code in Fortran 95 with double and quad precision options.

For the purpose of this research, CINDER2008 source code will be modified to allow for photonuclear interactions and data. This includes the creation of a library with the ENDF-B/VII [35] photonuclear cross-sections and fission product yield data. The code modifications will include the ability to not only read this file, but also

read the input data (especially photon flux) for each problem. The goal of the code modifications is to ensure backward compatibility, as is best practice. These modifications will then enable CINDER2008 to process both a neutron and photon flux simultaneously (with the ability to also turn one or both off), create and destroy material through transmutation and fission, and decay the products of all processes. In order for these modifications to work, the library must be populated with photofission product yield data. As mentioned in the Background Section, no evaluations of this data exist, and experimental data is sparse. Therefore, a physics translation of the neutron induced fission product yield data will be performed using similarities in the processes. This will enable the library to be populated with physically similar data that can be validated with the sparse experimental results. The addition of the photonuclear cross section data will be much easier as evaluations and codes to process this data exist.

As the research is not solely focused on the dual-particle transmutation code, a second track of work will take place on connecting the transport calculation that feeds into CINDER2008. To show the use and power of the two types of transport methods when coupled to transmutation, both deterministic and Monte Carlo codes will be used.

Again, to avoid duplication of past work, especially with the feature-rich programs that have been in development for decades, an existing three-dimensional even parity transport code will be used as the transport code that will be coupled to the transmutation. Not many codes using the even parity method exist, but a great choice is the EVENT code by de Oliveira [63]. EVENT is a multigroup three-dimensional even parity transport code using finite elements and spherical harmonics with anisotropic scattering. It sets itself apart from other transport codes because not only does the finite element derivation allow for easy modeling of most any complicated geometry that can be meshed but also it allows for anisotropic scattering.

Similar to the transmutation code, a library will be needed for EVENT with coupled

neutron and photon cross sections. Since during the activation and depletion routine new nuclides will be created, the transport library will need to either be recreated at each step using the current inventory of nuclides or one large library will need to be created beforehand. As the first method will be prohibitively expensive computationally, the second method will be used. Therefore, a large library with as many nuclides as possible will be created as part of this research.

Additionally, the MCNPX Monte Carlo transport code [64, 65] will be used for the most popular transport method. This will allow for high energy physics and photofission to be modeled in the transport method, providing a full coverage of the physics of the problem. It will also bring in a widely used computer code into the mix of transport methods that will be coupled with the transmutation code. Version 2.7.E additionally brings many improvements for photonuclear transport, including better models for photofission neutron multiplication.

The final step of the project will be focused on bringing the two codes together into one coherent system. This will allow for EVENT/MCNPX to model how the particles arrange themselves in the media, CINDER2008 to take that resulting flux to produce the transmutation that has occurred, then that information to be fed back into EVENT/MCNPX to model the new arrangement of particles due to the creation and destruction of material. This cycle can continue for each time step. The coupling code is a driver program that calls both CINDER2008 and a wrapper for EVENT/MCNPX and handles the communication and bookkeeping between the two externally. This option, although not necessarily elegant, allows for driver to be written for virtually any transport method. The user could invoke nearly any transport method or code and couple it to the dual particle transmutation inside CINDER2008.

Additional to each step will be a verification and validation of the code additions and modifications, including the libraries. This is a key part of the research to be sure what has been done is preforming as expected and is modeling reality. A demon-

stration of the code system will also be performed to prove its effectiveness on real world problems.

Although there are many portions to this research, the final product will be a truly unique software that fills a rising need. A dual neutral particle transmutation code with coupled dual particle three-dimensional finite element even parity transport or widely used Monte Carlo transport is an engineering tool that has yet to be seen in the nuclear industry.

Chapter 2

Methodology

Given the current drive for the a dual neutral particle activation/depletion code with coupled three-dimensional transport, it is necessary to describe the method behind each component. Since these are novel interpretations and extensions of existing methods, brief discussions will be given on the current state of the art with respect to both transmutation and coupled transmutation/transport calculations.

Section 2.1 will discuss transmutation calculations through the scope of the CINDER2008 code. Discussions will then move to how these methods can be extended to model both neutrons and photons simultaneously. Finally, the implementation of these extensions will be introduced.

Finally, Section 2.2 will discuss the methodology and implementation of the combined calculations for transmutation and transport with dual particles. This will be performed using the TINDER code developed for this purpose, which has been extended to perform transport calculations with EVENT, the 3-D even-parity deterministic transport code, and MCNPX, the high energy Monte Carlo transport code.

2.1 Transmutation

2.1.1 Single Particle Transmutation

As outlined in the Introduction, one of the first steps in the research at hand is the creation of a dual neutral particle activation and depletion code. Historically, this type of analysis has gone by many names, based mainly on the application. For accelerator and shielding analysis, the term activation and/or depletion analysis has been commonly used. This is due to the fact that the accelerator is activating the material causing subsequent depletion or that the shielding is being activated by some incident radiation, again leading to a depletion of the material. In terms of reactor analysis, this has most commonly been referred to as burn-up analysis, as the calculations are tracking the usage, or burning, of the material in the reactor. Due in part to the concept of converting some of the long-lived isotopes created in reactors into isotopes that have much shorter half-lives, this type of computation has been termed transmutation analysis as well. The models are used to track the transmuting of long-lived isotopes to other, hopefully more manageable materials. Throughout the paper the different terms will be used interchangeably to reflect the different research areas this method can be used.

In order to make a dual particle activation and depletion code, it is best to take stock of current off-the-shelf products that are available. Because these methods have been used for decades [46, 49], there is no reason to attempt to reinvent the wheel, especially when there are new implementations of these programs [48].

Unfortunately, although there have been long standing deterministic transmutation codes, none of them are able to handle both neutrons and gammas. Allowances had been made in the past for the inclusion of photons [49], but those plans were never completed and the feature remains inactive. That has led to the project at hand. It is still wise to use the existing updated framework upon which the dual particle

portion can be built. Due to its flexibility and recent update, the CINDER2008 code has been chosen as the base code.

Even though the method being used is well established, it is useful to review the method before modifying it for the dual particle capability. This is especially true as there are several methods of solution for transmutation, and CINDER2008 takes a quite different approach than other popular codes.

Transmutation analysis is essentially a tracking of the rate of change of the number, or atom, density of materials. To describe this process, a simple differential equation is used to relate the gains and losses to the rate of change of a nuclide m. The losses are due to transmutation, both the radioactive decay of nuclide m producing daughter nuclides and the particle absorption reactions of nuclide m producing residual nuclides different from m. The gains are due to the transmutation of other nuclides in the system, where the residual or daughter is nuclide m. The relationship describing this differential equation for nuclide m can be written as

$$\frac{d\mathcal{N}_m}{dt} = -\mathcal{N}_m(t)\beta_m + \sum_{k \neq m} \mathcal{N}_k(t)\gamma_{k \to m} \ , \tag{2.1}$$

where $\gamma_{k \to m}$ is the probability of nuclide k transmuting to m and β_m is the total transmutation probability for nuclide m. Equation 2.1 is known as the Bateman equation [66]. This transmutation probability for m can be broken into its components as

$$\beta_m = \lambda^m + \boldsymbol{\varphi}^n \boldsymbol{\Sigma}_a^m \ . \tag{2.2}$$

In this relationship, $\boldsymbol{\varphi}^n$ is the neutron flux vector (in energy) and $\boldsymbol{\Sigma}_a^m$ is the vector (in energy) of cross sections for neutron absorption by nuclide m, and λ^m is the decay constant for nuclide m. Absorption reactions, denoted in Equation 2.2 by $\boldsymbol{\Sigma}_a^m$, are all reactions on nuclide m with residual nuclides other than m. For the purposes of the code, that includes everything other than scattering that results in the same nuclide.

Since CINDER uses the multigroup approximation to reduce the energy variable, the energy regime must be finite, generally reaching only around 20 MeV. Because in many cases meaningful physics will happen above this energy, a constant is added into the governing equations to account for this possible addition/subtraction. By introducing the constant $\overline{Y_m}$, Equation 2.1 transforms into

$$\frac{d\mathcal{N}_m}{dt} = -\mathcal{N}_m(t)\beta_m + \overline{Y_m} + \sum_{k \neq m} \mathcal{N}_k(t)\gamma_{k \to m} \; . \tag{2.3}$$

Once compiled for the entire inventory of possible chains, a large coupled set of differential equations is reached since each equation depends on the information from another about atom density for each nuclide. However, this set of equations can be easily reduced to a set of independent, linear differential equations through the Markov method. Solutions are then obtained for all contributions $N(t)$ to $\mathcal{N}_m(t)$. Additionally, each contribution $N_i(t)$ occurs as the i^{th} element in a linear chain. The rate of change of the i^{th} element, $N_i(t)$, is only coupled to the preceding element in the sequence for which all parameters are known and solutions have been obtained in turn. This is described by the differential equation

$$\frac{dN_i}{dt} = \overline{Y_m} + N_{i-1}(t)\gamma_{i-1} - N_i(t)\beta_i \; . \tag{2.4}$$

At this point, densities are now indexed by their relative order in the sequence and γ_i is the transmutation probability for forming the i^{th} nuclide from the $i-1$ nuclide. The solution to these linear differential equations, as shown by England [67], is:

$$N_n(t) = \sum_{m=1}^{n} \left\{ \prod_{k=m}^{n-1} \gamma_k \right\} \left(\overline{Y_m} \left[\frac{1}{\prod_{l=m}^{n} \beta_l} - \sum_{j=m}^{n} \frac{e^{-\beta_j t}}{\beta_j \prod_{i=m, \neq j}^{n} (\beta_i - \beta_j)} \right] + N_m^0 \sum_{j=m}^{n} \frac{e^{-\beta_j t}}{\prod_{i=m, \neq j}^{n} (\beta_i - \beta_j)} \right) \; . \tag{2.5}$$

This equation propagates N_m^0, or the initial number densities, of all nuclides $m = 1$ to n to the current n^{th} nuclide density, N_n, while also allowing for a constant production term from all nuclides, $\overline{Y_m}$. While this was the standard method for all pre-CINDER'90 versions, the modern implementation makes a simplification to limit the length of chains followed. Mainly the purpose of this is to allow on-the-fly chain following instead of only propagating along predetermined chains. Each chain is followed until its significance is below a tolerance. Additionally, the algorithm only propagates the initial density and constant production rate of the first nuclide in the chain to effectively define the total inventory of all nuclides in the system of chains beginning with that first nuclide.

By applying the identity

$$\frac{1}{\prod_{l=m}^{n} \beta_l} \equiv \sum_{j=m}^{n} \left\{ \frac{1}{\beta_j \prod_{i=m,\neq j}^{n} (\beta_i - \beta_j)} \right\}, \tag{2.6}$$

to Equation 2.5, the general solution can be rewritten as

$$N_n(t) = \sum_{m=1}^{n} \left\{ \prod_{k=m}^{n-1} \gamma_k \right\} \left(\overline{Y_m} \sum_{j=m}^{n} \frac{1-e^{-\beta_j t}}{\beta_j \prod_{i=m,\neq j}^{n} (\beta_i - \beta_j)} + N_m^0 \sum_{j=m}^{n} \frac{e^{-\beta_j t}}{\prod_{i=m,\neq j}^{n} (\beta_i - \beta_j)} \right) . \tag{2.7}$$

For the modern versions of CINDER, including CINDER2008, the final algorithm is reached by imposing the conditions

$$N_m^0 = 0, \quad m \neq 1 , \tag{2.8}$$

and

$$\overline{Y_m} = 0, \quad m \neq 1 , \tag{2.9}$$

on Equation 2.7, resulting in

$$N_n(t) = \sum_{m=1}^{n} \left\{ \prod_{k=m}^{n-1} \gamma_k \right\} \left(\overline{Y_1} \sum_{j=m}^{n} \frac{1-e^{-\beta_j t}}{\beta_j \prod_{i=m,\neq j}^{n} (\beta_i - \beta_j)} + N_1^0 \sum_{j=m}^{n} \frac{e^{-\beta_j t}}{\prod_{i=m,\neq j}^{n} (\beta_i - \beta_j)} \right) . \tag{2.10}$$

To reduce the equation to a more manageable form, the definitions

$$Y_n(t) = \sum_{j=1}^{n} \frac{1 - e^{-\beta_j t}}{\beta_j \prod_{i=1,\neq j}^{n} (\beta_i - \beta_j)} = \sum_{j=1}^{n} Y_n^j(t) \tag{2.11}$$

and

$$X_n(t) = \sum_{j=1}^{n} \frac{e^{-\beta_j t}}{\prod_{i=1,\neq j}^{n} (\beta_i - \beta_j)} = \sum_{j=1}^{n} X_n^j(t) \tag{2.12}$$

can be inserted into Equation 2.10 to reach the simple form

$$N_n(t) = \sum_{m=1}^{n} \left\{ \prod_{k=m}^{n-1} \gamma_k \right\} \left(\overline{Y_1} Y_n(t) + N_1^0 X_n(t) \right) \ . \tag{2.13}$$

The algorithm continues through this equation on all possible linear chains for the system until the path is found to be insignificant or insufficiently accurate. The significance is determined by a value called the "pass-by," which is the time-step integrated transmutation of the nuclide. This can also be thought of as the number of atoms of nuclide n that are transmuted during that time step. This value is close to the number of atoms residing in all unexamined paths that come from nuclide n. The equality of the two is separated by the transmutations that yield more than one nuclide, e.g. an (n, α) reaction where both ^{4}He and a residual nuclide are created. The pass-by as defined is

$$P_n(t) = \beta_n \int_0^t N_n(t')dt' \ . \tag{2.14}$$

In order to handle cases that will cause numerical problems with Equation 2.13, several limiting cases have been derived to attempt to alleviate the problem. These numerical problems are caused because of the solution of the Markov equations where quantities of potentially differing signs and magnitudes are summed. Because of this possible problem, the number of significant figures in each number density calculation in CINDER2008 is calculated. Each pass-by having less than two significant

figures is set to zero. Additionally, an atom density contribution with fewer than two significant digits is also set to zero and the chain is ended. A running tally of the pass-bys that are not followed due to this lack of significant digits is made and then output as "Losses" in the CINDER2008 output.

Several special conditions within Equation 2.13 can cause issues to arise. The main three are: small transmutation probabilities, $\beta \to 0$; similar transmutation probabilities, $\beta_i - \beta_j \to 0$; and small time steps. Limit solutions are are used in CINDER when the first two cases are reached, and a Taylor series expansion is used for the final case.

When nuclides have a $\beta < 10^{-10}\mathrm{s}^{-1}$, the first limiting case is reached and the following equations replace the calculations for $X_n(t)$ and $Y_n(t)$.

$$X_n(t) = \frac{1}{\prod_{i=1}^{n} \beta_i} \sum_{m=0}^{s-1} \left\{ \sum_{|\alpha|=s-1-m} \left(\left[\prod_{i}^{n} (\beta_i)^{\alpha_i} \right]^{-1} \right) \frac{t^m}{m!} (-1)^{s-1-m} \right\} \tag{2.15}$$

$$Y_n(t) = \frac{1}{\prod_{i=1}^{n} \beta_i} \sum_{m=0}^{s-1} \left\{ \sum_{|\alpha|=s-1-m} \left(\left[\prod_{i}^{n} (\beta_i)^{\alpha_i} \right]^{-1} \right) \frac{t^{m+1}}{(m+1)!} (-1)^{s-1-m} \right\} \tag{2.16}$$

In these equations, only chain elements with large β values contribute and small values are omitted. The variable $\alpha = (\alpha_1, \ldots, \alpha_n)$ is an n-tuple of non-negative indices that satisfy $\sum_i \alpha_i = |\alpha| = s - 1 - m$.

If the second case is reached, when $\beta_i - \beta_j < 10^{-14} s^{-1}$, the second set of limit equations is used to calculate $X_n(t)$ and $Y_n(t)$.

$$X_n^l(t) = \frac{e^{-\beta_l t}}{\prod_{i=1}^{n} (\beta_i - \beta_j)} \sum_{m=0}^{l-1} \left\{ \sum_{|\alpha|=l-1-m} \left(\left[\prod_{i}^{n} (\beta_i - \beta_l)^{\alpha_i} \right]^{-1} \right) \frac{t^m}{m!} (-1)^{l-1-m} \right\} \tag{2.17}$$

$$Y_n^l(t) = \frac{1}{\prod_{i=1}^{n}(\beta_i - \beta_j)} \sum_{m=0}^{l-1} \left\{ \sum_{|\alpha|=l-1-m} \left(\left[\prod_i^n (\beta_i - \beta_l)^{\alpha_i} \right]^{-1} \right) \times \left[\frac{1}{\beta_l^{m+1}} - \frac{e^{-\beta_l t}}{\beta_l} \sum_{k=0}^{m} \frac{t^k}{k! \beta_l^{m-k}} (-1)^{l-1-m} \right] \right\} \tag{2.18}$$

In these equations, all $\beta_i \approx \beta_j$ are omitted.

When contributing terms to the summations in Equations 2.11 and 2.12 have large unique transmutation probabilities, they are calculated without approximation by Equations 2.15- 2.18.

Finally, when the time step is small, Taylor series approximations can be used to obtain the solutions to Equations 2.11 and 2.12.

$$X_n(t) = \sum_{m=0}^{\infty} \frac{X_n^m(0)}{m!} t^m \tag{2.19}$$

$$Y_n(t) = \sum_{m=0}^{\infty} \frac{Y_n^m(0)}{m!} t^m \tag{2.20}$$

$$X_n^m(0) = \begin{cases} 0 & m < n-1 \\ 1 & m = n-1 \\ (-1)^{m-n+1} \sum_{|\alpha|=m-n+1} \prod_i^n (\beta_i)^{\alpha_i} & m \geq n-1 \end{cases} \tag{2.21}$$

$$Y_n^m(0) = \begin{cases} 0 & m < n \\ 1 & m = n \\ (-1)^{m-n} \sum_{|\alpha|=m-n} \prod_i^n (\beta_i)^{\alpha_i} & m \geq n \end{cases} \tag{2.22}$$

The Taylor series solution has a limited convergence for large values of β and is therefore only implemented when accurate solutions cannot be obtained using the full or limit solutions.

2.1.2 Dual Particle Transmutation

Now that the methodology behind the burn-up calculations in CINDER2008 has been explained, the modifications for photons can be introduced. Although not trivial, these modifications to the full algorithm are minimal due to the way transmutation reactions are included.

In Equation 2.2, the transmutation reactions are all based on neutrons, which are given by the vector product term, $\boldsymbol{\varphi}^n \boldsymbol{\Sigma}_a^m$. This is the only spot where the flux and cross sections for neutrons are required as the reaction rate and knowledge of the products from that reaction are sufficient to describe the problem after that point. Therefore, in order to add photons, the flux and cross sections are required in the same way, so long as the products are duly described in the library for use later in the calculation. Equation 2.2, with the addition of a photon flux vector, $\boldsymbol{\varphi}^\gamma$, and a photonuclear absorption cross section vector, $\boldsymbol{\Sigma}_{a,\gamma}^m$, becomes

$$\beta_m = \lambda^m + \boldsymbol{\varphi}^n \boldsymbol{\Sigma}_a^m + \boldsymbol{\varphi}^\gamma \boldsymbol{\Sigma}_{a,\gamma}^m \; . \tag{2.23}$$

Through this addition and the subsequent information about the nuclides produced from these reactions, CINDER has the capability to handle both neutron and photon induced reactions. Being as the decay of daughter nuclides is the same no matter how they are produced, the main portion of the transmutation code does not need modification. In essence, including photonuclear reactions is like including other types of neutron induced reactions but the rate is calculated using a different flux.

One great property of Equation 2.23 is the fact that as the neutron and photon reaction portions are independent, they can be vectors of differing length. In real terms, this means that the number of energy bins (vector length) for the neutron energy spectrum can be different than those of the photon energy spectrum.

The energy bin structure is predefined in the library that is used by CINDER2008. When the user inputs the flux spectrum for that particle, they obviously need to use an identical structure. This ensures that the vector product is being computed

on the same length vectors, both the cross section vectors from the library and the input flux profile. In the newest CINDER release, the user is given a tool to create libraries with their own data (from ENDF-B/6 style files, e.g. ENDF-B/VII, JEFF-3.1.1, JENDL-4.0, etc. evaluated data files) using their own energy bin structure.
The energy bin structure is needed to reduce the continuous energy variable into something amenable to numerical solution. The multigroup method uses a weighting function – the flux – to collapse this continuous variable into a histogram, or a piecewise constant. The choice of the weighting function is based on prior knowledge of the system at hand as this method is only exact if the weighting function matches the resulting flux. Therefore, a flux weighting function should be carefully chosen when using the multigroup method as the usefulness of the reduced data goes down as the actual flux diverges from the weighting function.
CINDER2008 comes prepared with four neutron induced reaction libraries, all based on different needs and using different weighting functions. They are: CINDER'90 63-group library weighted with the Maxwellian, 1/E, Watt fission spectrum, and fast fission spectrum distributions at thermal, low, intermediate, and high energies, respectively; CINDER2008 66-group fission library weighted with the Maxwellian, 1/E, and Watt fission spectrum for thermal, low, and intermediate to high energies, respectively; CINDER2008 175-group fusion library weighted the same way as the CINDER'90 library; and CINDER2008 321-group constant library using a constant weighting function. These libraries not only contain the information about cross sections, but also the decay data for each nuclide in the library as well as the fission product yield data for those nuclides that have available data. The data source is generally ENDF-B/V (for CINDER'90) and ENDF-B/VII (for CINDER2008) but other sources, such as JEFF and JENDL, are used to fill in gaps in the data.
To extend the capability of CINDER2008 into the coupled incident particle regime, the cross sections for photonuclear interactions are needed. A second library is therefore a necessary addition. However, it does not need to have the same extent of

information as the neutron library, as the decay data is independent of the reaction data. A library is then needed to have only the interaction and photofission product yield data.

The first component is fairly straightforward thanks to previous work [50, 51, 52, 53, 54] in pursuit of the same research. This can easily be put into multigroup format using the NJOY99 nuclear data processing code [68] and any of the recently created ENDF-B/6 style photonuclear data files.

It is important now to note some features of photonuclear cross sections. First, photonuclear cross sections are generally much much less than neutron cross sections. This can range from a factor of two lower to several orders of magnitude. Therefore, a much higher flux is required to bolster the photonuclear reaction rate to that of neutrons in a similar problem. For the purposes of this research, the photofission cross section is important. These cross sections generally reach the measurable range around 5 MeV, giving a perceived threshold. In fact, physically, there is no threshold for photofission and measurements have been made much lower [33, 69, 34]. The cross sections become effectively zero, however, in these very low ranges.

In addition to the effective threshold, a giant dipole resonance appears in the photo absorption cross sections, with a peak around 14 MeV. The cross section jumps an order of magnitude in this region, as can be seen in Figures 2.1, 2.2 and 2.3[35]. Additionally, in these figures the relative cross sections for the different photonuclear absorption cross sections

Other photonuclear cross sections have a similar shape to that listed in Figures2.1-2.3, both the single and double humped resonance. All of these cross sections, as listed in the ENDF files, can then be reduced using the multigroup approximation for use in CINDER.

The main problem that is encountered is in attempting to populate the photofission yield data section. As this section is extremely important since it describes the probability distribution of nuclides after a photofission event, it is extremely important

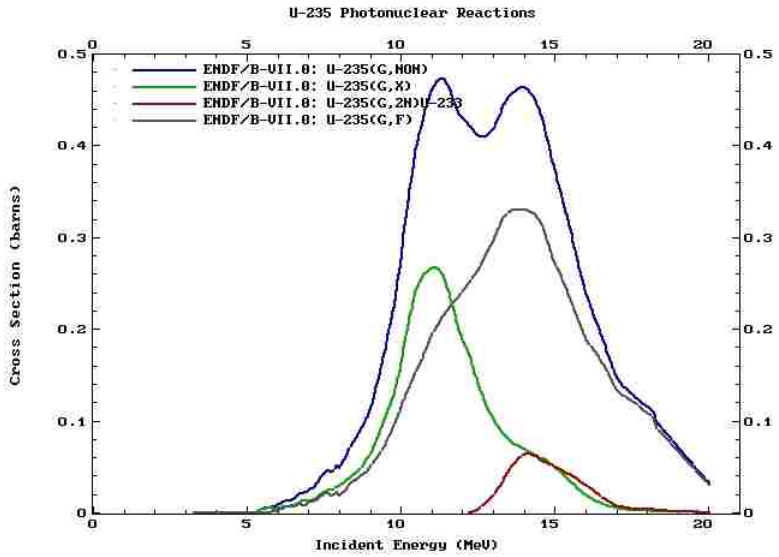

Figure 2.1: U-235 Photonuclear cross sections

to have as much reputable data populated as possible. Unfortunately, due to a lack of need and generally a lack of experimental data, there are no concise, evaluated data files for photofission product yields. There are only a limited number of experiments [33, 14, 15, 12, 3, 1, 17, 34, 5, 18, 19, 20, 21] with this data and no evaluated data file includes an evaluation for these yields.

To fill this need, the physics of fission induced by a photon is investigated to see if it can be tied in some way to fission induced by a neutron, since evaluations and much more data exist for those reactions. In order to do this, the physics of the fission reaction should be investigated and compared depending on the incident particle.

Particle induced fission occurs when an incident particle, traveling with a certain energy, mass, spin and parity, collides with the nucleus of an atom. With some probability (the cross section), the particle is essentially absorbed into the nucleus. This creates a compound nucleus, in a quasi-equilibrium state, with the extra mass from the particle, the extra energy (minus any energy required to bind it to the nucleus), and with its spin and parity modified. From this excited and unstable compound

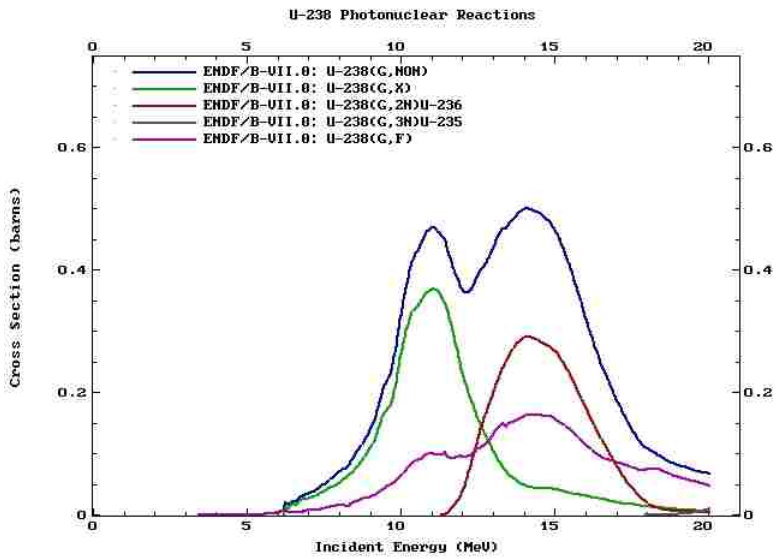

Figure 2.2: U-238 Photonuclear cross sections

state, the nucleus splits into generally two main parts, with extra neutrons and gammas being emitted to account for excess mass and energy. This splitting is not fully understood, but in some theories can be compared to a water droplet splitting after being deformed by the impact of another drop.

These fission events are described by not only the target nucleus and incident particle (with the properties listed above), they are also defined by the distribution of the fragments that come from the splitting nucleus. In terms of the research at hand, this distribution is described by the mass of the two fragments coming from fission. Except in high energy collisions, this distribution is a double humped curve with one peak below and one above the half mass of the fissioning nucleus, connected by a low probability region of two similarly sized products.

As this is the distribution that will be used in the research at hand, it is best to investigate what input properties help define its ultimate shape. One obvious property is the mass of the excited nucleus that will undergo scission. This will help to define where the peaks are located in terms of the two daughter nuclei. Another

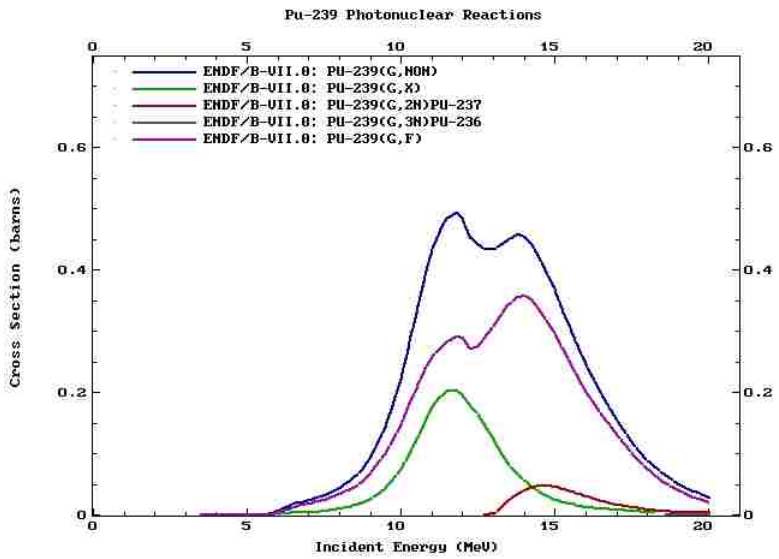

Figure 2.3: Pu-239 Photonuclear cross sections

property that is very important is the excitation energy of the excited nucleus. When the excitation energy is low (as with spontaneous fission when it is essentially zero), the peaks are extreme, with very little chance of producing similarly sized products. However, when the excess energy is high, the nucleus has a better chance of splitting into something other than the typical light/heavy combination, causing the peaks of the curve to drop and the valley between to rise up. These two properties are the major defining variables in the mass distribution.

Although they do not play as big a role, it is believed that spin and parity of the incoming particle can cause the mass distribution to be slightly modified[37], compared the results of similar fissioning systems, one with an incident neutron and the other with an incident alpha particle. They observed at maximum a 17% difference in the distribution between the two, assuming the mass and energy contributions are the same. However, they attributed these difference not necessarily on the spin and parity of the particles, but second chance reactions that can happen at energies over 25 MeV. So long as the distribution is compared below this energy, we will treat it

as being independent of the incident particle and its spin and parity. In the end, the authors still recommend that fission product yield data can essentially be used for different incident particles, assuming the possible differences are noted. This is the conclusion of others as well [70, 71, 38, 39].

In addition to these results and comments by previous authors, a program called UKFY [40, 41] from the United Kingdom (part of the JEFF project) operates on this basis. It takes prototypical results and trends to create fission product yield data for incident neutrons, protons, deuterons, alpha particles and photons, as well as for spontaneous fission. It operates under the assumption that spin and parity offer such a little effect on the final outcome, that the main parameters that need be tracked are the masses and energies of the incident particle and target.

Since there are several examples on this physics translation of measured data, providing a backbone to the assumption that the neutron data can be used as a surrogate, it is used in place of the sparse and unevaluated experimental data that is available in the open literature. Additionally, the physics of the reactions, as far as they are known currently, point to an independence of the incident particle and product yield distribution. The sparse measured data, though, will serve as a perfect vehicle to perform validation calculations for the current assumption. This process of translating the data can now be addressed.

When fission occurs by a photon, the target nucleus absorbs the photon and its kinetic energy, exciting it above the ground energy state. With some probability, scission will occur at that excited state, splitting the nucleus into two daughter nuclei, some number, ν, of neutrons, energy in the form of prompt photons and other byproducts. Put simply, this reaction can be represented as

$$ {}^{A}_{Z}W + \gamma + \mathrm{KE}_{\gamma} \rightarrow {}^{A}_{Z}W^{*} \rightarrow {}^{A_1}_{Z_1}X + {}^{A_2}_{Z_2}Y + \nu \mathrm{n}^{1}_{0} + \mathrm{E} \tag{2.24} $$

where the mass numbers balance as

$$ A = A_1 + A_2 + \nu \tag{2.25} $$

and the number of protons balance as

$$Z = Z_1 + Z_2 \ . \tag{2.26}$$

On the other hand, neutron induced fission varies slightly on how it arrives at the excited state. Fusing a neutron to the nucleus will add energy to the system. Therefore, not only does the reaction include the addition of a neutron to the compound nucleus causing an increase in the mass number, A, by one, but the compound nucleus is produced in an excited state. Most of the neutron kinetic energy goes into exciting the compound nucleus, since the compound nucleus recoil is minimal. Additional excitation energy comes from the increase in total binding energy of the nucleus with the additional neutron, which is equal to the single neutron separation energy (Sn, on the order of 5 MeV) of the compound nucleus. Again written as an equation, neutron fission can be represented as

$$^{A-1}_{Z}V + \mathrm{n}^1_0 + (\mathrm{KE_n} + \mathrm{S_n}) \rightarrow {}^{A}_{Z}W^* \rightarrow {}^{A_1}_{Z_1}X + {}^{A_2}_{Z_2}Y + \nu\mathrm{n}^1_0 + \mathrm{E} \tag{2.27}$$

where the mass numbers and proton numbers balance as described in Equations 2.25 and 2.26.

The excited compound nucleus has no memory of how it arrived at that state, so the the reaction during the transition from exited state to fission products (the second transition) is identical no matter how the excited compound state was produced. As mentioned, according to current theory and experiment this is essentially the case as the fission process is Markovian, or has no prior knowledge of the reactions that led up to it [36]. No matter how the excited nucleus, ${}^{A}_{Z}W^*$, got to that state, it will have the same probabilities of producing products on some distribution (with a possibly slight variation due to spin and parity of the incident particle).

A translation can then be used to relate the production of a given excited nucleus by an incident photon or neutron. Since the energy of the exited state is extremely important to the outgoing products, a translation in energy must also be made.

The first relationship that must be described to translate from neutron fission to

photofission is the mass number. Since photofission lacks the inbound neutron in the initial reaction, there will be one fewer neutron in the excited nucleus if the target is the same. By the way Equations 2.24 and 2.27 are written, they end up at the same excited nucleus. Therefore, their left sides must be similar and the photofission on a nuclide is equivalent to neutron fission on a nuclide with one less mass number, as shown in Equation 2.28.

$$ {}^{A}_{Z}W + \gamma \rightarrow {}^{A}_{Z}W^{*} \sim {}^{A-1}_{Z}V + \mathrm{n}^{1}_{0} \rightarrow {}^{A}_{Z}W^{*} \tag{2.28} $$

As mentioned, the mass balance is not the only hurdle to jump for the translation to hold. The excitation energy of the fissioning nucleus must also be the same. Again relating Equations 2.24 and 2.27, this time in terms of energy leading to the excited nucleus yields

$$ \mathrm{KE}_{\gamma} \rightarrow \mathrm{E}\left({}^{A}_{Z}W^{*}\right) \sim \mathrm{KE}_{\mathrm{n}} + \mathrm{S}_{\mathrm{n}} \rightarrow \mathrm{E}\left({}^{A}_{Z}W^{*}\right) \ . \tag{2.29} $$

Therefore, the excitation energy of a fissioning compound nucleus is equal for the photon or neutron induced case when the kinetic energy of the photon causing fission is equal to the kinetic energy of the neutron causing fission plus the single neutron separation energy for the compound nucleus (taking also into account the loss of energy due to the recoil of the nucleus). Note that the neutron's energy must be calculated in the center of mass frame. Since nearly all energy is transferred from the photon for the mass ranges that have been translated in this exercise, its total kinetic energy is used and no conversions are necessary. This can easily be proven for the lightest mass and highest energy photon that will be encountered in the later validation and demonstration of this code, ^{235}U and 70 MeV photons. Because of conservation of momentum, the energy lost in the recoil of the nucleus after this collision is given by

$$ \mathrm{KE}_{\mathrm{nucleus}} = \frac{p_{\gamma}^{2}}{2m_{\mathrm{nucleus}}} = \frac{490\frac{\mathrm{MeV}^{2}}{c^{2}}}{470,000\frac{\mathrm{MeV}}{c^{2}}} \simeq 0.001\mathrm{MeV} \ , \tag{2.30} $$

where p is the momentum of the photon, m_{nucleus} is the mass of the compound nucleus, and $\text{KE}_{\text{nucleus}}$ is the kinetic energy of the recoil nucleus.

Therefore, for an incident photon, the excitation would be its incident energy minus a maximum of this kinetic energy. Since this is much lower than the incident energy (70 MeV in this case), it is assumed to be insignificant. The total incident energy is assumed to go entirely into exciting the nucleus.

For neutrons, as the kinetic energy that is reported in evaluations and experiments is generally in the lab frame of reference, it must first be converted before relating the two sets of energies. To convert the kinetic energy from the lab to center of mass frames, the following equation is given [72], where the superscript ^{C} denotes center of mass frame, ^{L} denotes the lab frame, the target nuclide mass is M_A, and the projectile mass is m.

$$\text{KE}^{C} = \frac{M_A}{m_{\text{n}} + M_A}\text{KE}^{L} \tag{2.31}$$

Using Equation 2.31 on the neutron and photon induced system, the excitation energy of the nucleus after absorbing the incident particle is given as

$$\text{E}\left({}^{A}_{Z}W^{*}\right) = \left[\frac{M_A}{m_{\text{n}} + M_A}\text{KE}^{L}_{\text{n}} + \text{S}_{\text{n}}\right] \leftrightarrow \left[\text{KE}_{\gamma}\right] \ , \tag{2.32}$$

where m_{n} is the neutron mass.

Similar to the situation for photons, the recoil energy is negligible. This can be shown by again assuming the lightest mass considered in this library, ^{234}U and the fastest neutron, 14 MeV. By a similar equation to Equation 2.30, the neutron reaction recoil energy is determined to be

$$\text{KE}_{\text{nucleus}} = \frac{p_n^2}{2m_{\text{nucleus}}} = \frac{\sqrt{\left(2 \times \text{KE}_n \times m_n\right)}^2_n}{2m_{\text{nucleus}}} \simeq \frac{225\frac{\text{MeV}^2}{c^2}}{470,000\frac{\text{MeV}}{c^2}} \simeq 0.0005\text{MeV} \ , \tag{2.33}$$

where again the kinetic energy of the recoil nucleus is given by $\text{KE}_{\text{nucleus}}$, the incident neutron's mass, momentum and kinetic energy are given by m_n, p_n and KE_n,

respectively, and the mass of the compound nucleus is given by m_{nucleus}.

As with the photon case, the energy lost to the recoil of the nucleus is below the precision of the single neutron separation energy and excitation energies for each fission product yield distribution. Therefore, this value is negligible and not carried through the calculations. This assumption is valid for the range of energies and target masses considered in this research. Equations 2.30 and 2.33 should be readdressed if the library is expanded to lighter nuclei or higher energy neutrons.

Using the concept in Equation 2.28 and the math in Equation 2.32, neutron fission product yield data can be translated for use on photofission reactions. As a matter of practicality, neutron induced fission product yields are given at three discrete incident energies: thermal (0.025 eV), fast (500 keV), and high energy (14 MeV). Therefore, translations of only these fission product yield data must be made. As an example, the equivalent excitation energy for a fast energy neutron on ^{234}U is given by (creating the compound nucleus ^{235}U)

$$\mathrm{E}\left({}^{235}_{92}\mathrm{U}^{*}\right) = \left[\frac{234.0409}{1.0087 + 234.0409} 0.5\mathrm{MeV} + 5.2975\mathrm{MeV}\right] = 5.7954\mathrm{MeV}\ . \quad (2.34)$$

In terms of energy, Table 2.1 gives the translation energies for several of the common nuclides. Also listed are the ground state single neutron separation energies for the compound nuclei [73].

It is apparent from this table that the values for equivalent excitation energies, and therefore incident photon kinetic energies, are somewhat loosely correlated between nuclides. For practical applications, at the lower bound of the photofission cross section and below, approximately the photofission barrier energy to 6 MeV, the thermal fission product yield should be most appropriate. In the intermediate range from approximately 6-14 MeV, the fast fission product yield data should be most appropriate. Finally, in the high energy range, anything above 14 MeV, the high energy fission product yield data should be most appropriate. As CINDER2008 does not interpolate between these discrete energy yields, it is on the user to choose the most appropriate data for the physics at hand. This restriction was carried through

Table 2.1: Equivalent incident photon energies for translating neutron fission product yields of select nuclides at the discrete neutron energy groups. Thermal equivalent excitation and the single neutron separation energy are separated by 0.025 eV, repeated for clarity. Single neutron separation energy (S_n)is given for the compound nucleus for that reaction.

γ-Fission Reaction	Surrogate Reaction (n-fission)	S_n (MeV)	Equiv. Thermal Neutron Excitation (MeV)	Equiv. Fast Neutron Excitation (MeV)	Equiv. High Energy Neutron Excitation (MeV)
γ+^{235}U	n+^{234}U	5.2975	5.2975	5.7954	19.2374
γ+^{236}U	n+^{235}U	6.5455	6.5455	7.0434	20.4857
γ+^{237}U	n+^{236}U	5.1258	5.1258	5.6237	19.0662
γ+^{238}U	n+^{237}U	6.1542	6.1542	6.6521	20.0949
γ+^{239}U	n+^{238}U	4.8064	4.8064	5.3043	18.7473
γ+^{238}Np	n+^{237}Np	5.4883	5.4883	5.9862	19.4289
γ+^{239}Pu	n+^{238}Pu	5.6462	5.6462	6.1441	19.5871
γ+^{240}Pu	n+^{239}Pu	6.5342	6.5342	7.0321	20.4754
γ+^{241}Pu	n+^{240}Pu	5.2415	5.2415	5.7394	19.1829

from neutron reactions because of the uncertainty that could overtake the problem when interpolation is used between these sparse points.

These energy region boundaries are applicable to the current suite of isotopes in the initial library. If the photofission data was expanded to much lower or higher mass numbers, these regions may not be applicable. Therefore, a table such as Table 2.1 should always be used with the isotopes currently in play and a best approximation of the energy region should be made.

Now that the translation between neutron fission product yield data and photofission product yield data has been illuminated (validations will follow in Section 3.1), the photon reaction library has been fully introduced and can be compiled. To do the compilation, a tool has been created for this research, a modification of the distributed neutron library creator. This tool, *make_libg*, takes NJOY99 processed ENDF-B/6 style photonuclear cross section data along with existing CINDER library neutron fission product yield data to create a library that is of the same form

as the neutron library. *make_libg* determines the energy group structure as created in NJOY99 as well as does the translation of the neutron fission product yield data into photofission product yield data.

After creation of the library of photonuclear data and the algorithm modification to handle the transmutation by photon interactions, the task remains to modify the source code of CINDER2008. Being as it is not necessary to describe the process of coding, suffice it to say that CINDER2008 has been modified to now processes dual neutral particle transmutation. The code modifications were made to be backward compatible with CINDER'90 and CINDER2008 input files as to reduce problems when running existing neutron models. The input changes include the choice of the photofission product yield set, photon flux in the appropriate group structure, and flux multipliers to modulate the photon flux over all time steps and/or individual steps.

A validation and verification of the modified CINDER2008 is given in Section 3.1. This is a required step as to ensure not only that the code is performing as intended (coded correctly) but also to validate it against experiment to compare the models to reality.

2.2 Coupled Transport/Transmutation

In order to make use of the dual particle transmutation code, it is necessary to know the average flux in the material that is to be transmuted. Therefore, a transport code must be plugged onto the front end of the calculation to first see how the neutrons and photons distribute in the medium.

As mentioned, there are many ways to do this transport calculation. For this research, the two codes chosen are EVENT and MCNPX. By giving these two codes as options, the user can choose either the computationally cheap but less rigorous deterministic method or the computationally expensive but highly detailed Monte Carlo method. Both codes are capable of calculating the average flux in a specific region but have somewhat different scopes and purposes. The even parity deterministic method is a great choice for a scoping exercise when many calls to the program will be made, as in a parametric study. Monte Carlo on the other hand is useful for the big end of research calculation when a single number is desired, but with great detail.

Additional to the front end transport calculation for the flux, a back end calculation for retransporting the beta-delayed photons[1] is a must. Both of these codes are capable of taking a new source in the transmuted region and transporting those photons through the system, perhaps to detectors. This is useful in not only the active interrogation systems as described in Chapter 1, but also in lifetime calculations for reactor systems or spent fuel.

In addition to this retransporting of delayed photons, some calculations will have the goal of tracking the effect of the changing nuclide densities on the system. This is the main idea behind reactor burn-up calculations. To do this, a transport calculation is done, followed by a transmutation calculation. From this transmutation

[1]The photons created from the natural decay of fission/absorption reaction daughter products.

calculation, the new material densities are sent back to the transport code to see the new equilibrium state of the particles. This process then marches in time to see the system evolve.

To capture the needs of all of the different potential models, a generalized code has been developed. It not only allows for the feedback from one code to the other in terms of fluxes and new sources, but also in terms of material number density changes. As this code is coupling a transport code and CINDER2008, it has been named TINDER (Transported (C)INDER).

Before delving into the details of TINDER, an overview of how the calculations are performed is necessary. The first items that are needed are the input files. For the code, there are actually two input files that are needed: the TINDER input file and a transport template input file. The TINDER input file gives the general information that is need by CINDER2008 to perform the calculation, including temporal information, material data, flags for which fission product yield sets to use, etc. This information is all that TINDER needs to perform its portion of the calculation, as well as populating the CINDER2008 input files. The transport template input file, on the other hand, is a template for the input file that the transport code will use, with special flags to denote where the material information and source information will go. These flags will enable a wrapper code to take the new material data at each step, as well as the photon source from the decay (if applicable), and input it into the transport code.

TINDER has been designed on the concept of flexibility. Therefore, it only calls CINDER2008 and handles material inventories and photon source information. It does not physically call the transport code. Instead, the user supplies the name of a specially created wrapper that will take the results from CINDER (nuclides and photon source), modify the transport template input file, call the transport code, and prepare the output (the neutron and/or gamma flux) for use by TINDER. This concept allows for the user to plug the code into virtually any transport solver by

simply writing a simple wrapper script. Additionally, it enables the user to change the transport code that will be used in the calculation without needing to create a new TINDER input file.

Although flexibility has been built into the code, it was still built for a main purpose. That purpose is active interrogation systems, which have special modeling requirements. These requirements are much different than, say, burn-up calculations. Active interrogation modeling requires only two transport calculations with a single transmutation calculation in between. This allows for the system flux to be calculated, the beta-delayed photon source to be found, then for the retransport of those photons to the detectors to be modeled.

On the other hand, burn-up calculation require a large number of iterations back and forth the transport and transmutation codes. This is done at a minimum of 18 months of reactor operation to properly characterize the system, with perhaps 10 iterations in the first year to capture the initial transients. This method also relies more heavily on the created nuclides to be properly accounted for and passed between codes and does not depend as much on the delayed photons. Additionally, it has been shown that during each time step that is performed in the transmutation code, a corrector transport step improves the accuracy of the model without having to perform a full step. This step essentially uses a better approximation for each timestep and "corrects" the initial estimates.

Because active interrogation has been the driver for this research, the features for a reactor burn-up code are not as detailed. This is mainly due to the fact that there is no predictor-corrector performed during the time step. To better model these types of systems, shorter time steps are recommended. Additionally, the material inventory passing has a feature that allows the user to set a low limit on the number density that will be transferred to the transport code. This speeds up the calculation by eliminating extremely rare nuclides in that system. In terms of reactor systems, though, certain nuclides can appreciably modify the system even at low levels. Care

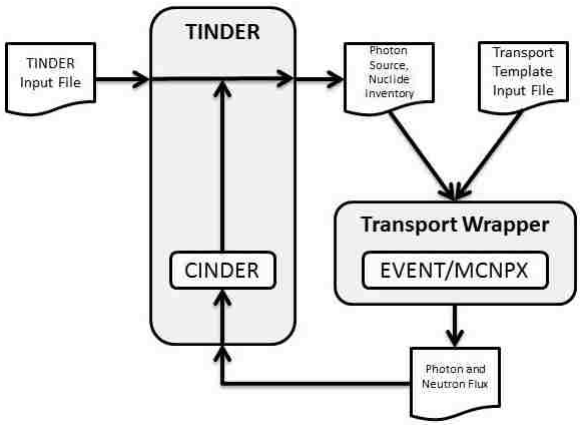

Figure 2.4: TINDER program flow

must be taken with this parameter.

With those limitations being noted, TINDER is capable of modeling active interrogation systems, accelerators, reactors, and spent fuel assemblies, to name a few. Figure 2.4 shows the flow of the program. This program flow iterates at each new timestep given in the transmutation code. The initial pass through, the nuclide inventory and the photon source are unperturbed and zero, respectively, for the first transport calculation.

Looking into each step in this process a little deeper yields the meat of the TINDER code. When the input file is read, the time steps for the transmutation calculation are brought in. These time steps will determine the number of times the transport code will be called. In all cases, there will be a transport calculation called first and last – therefore the most simple calculation is a single transmutation step with an initial and final transport calculation. It is important to note that each transmutation step can in fact have many substeps, producing a better characterization within the step. However, for the transfer of photon source and nuclide inventory information, only the final substep's information will be used.

The first transport step is taken with a clean nuclide inventory (no transmutation of

the given materials) and with a zero photon source. Within the transport wrappers, allocations can and have been made for an initial source to be used in the transport calculation. For example, in the active interrogation problem, there would be an initial photon and neutron source irradiating the material. This would then create the flux that would be fed to CINDER. Additionally, this can be turned off for subsequent steps where only the retransported source is necessary. The transport wrapper prepares the current transport input file, runs the transport code, then parses the output file for the flux information that is passed back. This information is placed in a file and the wrapper is finished for that step.

Next, TINDER kicks back on and reads the information created by the transport code and prepared by the wrapper. This flux information is used along with material and other settings (specified in the TINDER input file) to create the input files for CINDER2008. The time information supplied to CINDER is strictly for the current time step. The transmuted nuclide inventory and beta delayed photon source are then created. This information is transferred to holding files for the transport wrapper to access.

The transport wrapper is then called again, which reads in the information from the CINDER calculation and proceeds the same way as the first time (with flags for sources turned on/off). If this was the final time step in the series, the calculation is concluded when the transport code finishes. Otherwise, the process is repeated until that final time is reached. The final nuclide population, transport flux, etc. are all output for the user. Additionally, each step's information and results are saved so that a clear picture can be build for that model from the start to end times.

As mentioned, the code has been written to allow for nearly any transport code to be plugged into the system. In order for this to happen, a simple wrapper must be written that reads the nuclide and photon source information saved by TINDER, creates/modifies the transport input file, calls the transport code, and outputs the calculated fluxes to a single file. This type of plug and play code makes allowances

for changes in transport input/output files without the need for a full overhaul of the driver code. A simple wrapper modification is all that's necessary.

Chapter 3

Results

In order to test the capability of the newly created code systems, several example cases have been run. Two types of results are presented in this chapter. The first set of examples, presented in the following Section, 3.1, are validation and verification cases. Hand calculations and experimental results are introduced to ensure the dual particle additions described in Section 2.1 are physically correct and implemented properly. The second set of results, given in Section 3.2, are demonstration problems for the TINDER code system. An active interrogation problem is introduced to demonstrate the effect of a dual particle transmutation modeling on this type of system. In addition to showing the results from this method and contrasting the two transport methods, a sensitivity analysis is given.

For the validation cases, Table 3.1 gives a quick note about each of the isotopes identified in Table 1.1. This identifies each case that will be run in the photofission validation section, or gives a note as to why that isotope was not included in the validation suite. Additionally, for the validation and verification of the CINDER code additions, the cross sections are taken as is since the evaluations for inclusion in the ENDF-B library has already performed necessary validation. The surrogate reactions are therefore focused solely on the fission product yield data.

Table 3.1: Notes on each isotope with experimentally measured photofission product yield data for their use in this validation.

Isotope	Notes
^{232}Th	No surrogate reaction (^{231}Th(n,f)) data exists. Experimental data not used.
^{234}U	Graphical results are provisional and publishing authors noted limitations and inconsistencies with the data.
^{235}U	Experimental results used for validation.
^{236}U	Mass distribution not given in publication.
^{238}U	Experimental results used for validation.
U-natural	Experimental results used for validation.
^{239}Pu	Experimental results used for validation.
^{240}Pu	Graphical results are provisional and publishing authors noted limitations and inconsistencies with the data.
^{242}Pu	Graphical results are provisional and publishing authors noted limitations and inconsistencies with the data.
^{244}Pu	Graphical results are provisional and publishing authors noted limitations and inconsistencies with the data.

3.1 Validation and Verification of CINDER2008

In order to properly test the dual neutral particle extension of the CINDER2008 code, a series of verification and validation models should be run. These not only ensure that the code behaves as expected but also determines how well it can model real world problems. Seven separate examples are given below. The first is a verification problem to ensure the user inputs and photonuclear data are being read in correctly, and the processing within CINDER in terms of a simple non-fission photon transmutation problem is being done correctly. The second verification problem extends the first to include a flux of neutrons to exercise the dual particle capabilities. Next, a validation case is run using a photofission transmutation case to ensure the fission product distributions that have been translated from neutron induced fission mimic one of the few photofission experimental results available. The second validation case again allows all types of transmutation to occur, ensuring the proper fission product distribution is being used. The fission product distribution is additionally verified against the similar neutron induced fission case (from where the distribution was translated as described in Section 2.1). Two additional photofission validation cases are given to further show the validity of the yield translation from incident neutrons to photons. These cover not only a different proton number than the first two validation cases, but also a multiple isotope material case. Finally, a photofission validation case is given to show the differences in the yields for isotopes with the same mass number, but different proton numbers. This final case will help illuminate subtle differences in the yields for this situation and will further validate the translated yield sets.

For all validation and verification problems, a photonuclear library is required. One such library was created using the *make_libg* tool. For the group structure, the CINDER standard gamma energy bin structure (as used for the photon spectra output) as outlined in Table 3.2. The cross section data was taken from the ENDF-B/VII

photonuclear evaluated sublibrary and collapsing was done with a flat weighting function.

To ensure the photon library's compatibility with the neutron based counterpart

Table 3.2: Energy boundaries for the 25-group photonuclear cross section library

Grp #	E_{min} (MeV)	Grp #	E_{min} (MeV)	Grp #	E_{min} (MeV)
1	0.00E+00	10	7.50E-01	19	6.00E+00
2	1.00E-02	11	1.00E+00	20	7.00E+00
3	3.00E-02	12	1.33E+00	21	8.00E+00
4	6.00E-02	13	1.66E+00	22	9.00E+00
5	1.00E-01	14	2.00E+00	23	1.00E+01
6	2.00E-01	15	2.50E+00	24	1.20E+01
7	3.00E-01	16	3.00E+00	25	1.70E+07
8	5.00E-01	17	4.00E+00	cut	3.00E+07
9	5.25E-01	18	5.00E+00		

that will be called simultaneously, the isotope numbering must be consistent (to ensure isotope number X refers to some isotope ${}^{Z}_{A}W$ in both libraries). This is due to the fact that CINDER2008 refers to isotopes by sequential numbering by increasing mass. If one library has isotopes the other does not, zero data entries must be inserted into the library to ensure consistent numbering. As CINDER'90 and CINDER2008 libraries contain different amounts of data because of their differing sources, the number of isotopes represented in each is different. Therefore the photonuclear CINDER library *C08lib_gamma_v1.3* has been created using the isotope numbering of the more established CINDER'90 library. Similar libraries can be created for use with CINDER2008 neutron library by simply using the created tool.

3.1.1 Photonuclear Absorption Verification Case

The first step in any code verification and validation is to ensure that it is performing as expected, processing information correctly, and is giving proper results. This is

best done on a simple case that can be also calculated through a second method that is known to be correct. For the case of the verification of CINDER2008's new photon-induced reaction capability, this is most simply done on a non-fissioning nuclide with a simple cross section and a constant flux. Although this problem may not have any physical bearing, it is a simple method to ensure the data flow in the code is happening properly. This ensures the proper products and paths in the data are being followed.

Consider the simple case of an volume averaged photon flux vector of $\boldsymbol{\varphi}^{\gamma} = \{0.01\,{}^{\gamma}/_{cm^2\,sec\,bin}\}$ in a 1 cm^3 sample of pure ^{14}N that has a number density of $0.01\,{}^{\#}/_{b\,cm}$. Assume that the flux multiplier applied to the problem is set to 10^{10} as well. This case is handy as ^{14}N has only one absorption reaction with photons[1], the (γ, p) reaction, which happens at a single discrete resonance when E_{γ} is 9.17225 MeV. This cross section is given in Figure 3.1.

This case is also useful as it creates two discrete nuclides in a single reaction, both ^{13}C and ^{1}H (essentially a single proton). Through this case, not only can the reaction rates be checked but also the identical creation of two separate daughter products.

Given the input parameters above, the only missing information in order to process this by hand is the microscopic cross section. Since the cross section is a single resonance at 9.17225 MeV, which falls into energy bin 22 as shown in Table 3.2, there is only a single group with a non-zero cross section. As processed by NJOY99, the value in this group for the absorption is $\Sigma_{a,\gamma} = 3.6970 \times 10^{-4} b$. Since the reaction rate for group g is defined by

$$\left(\text{Reaction Rate}\right)_g = R_g = \varphi_g^{\gamma} \times \text{mult}_{\varphi^{\gamma}} \times N \times \Sigma_{a,\gamma}^{g} \tag{3.1}$$

[1] ^{14}N also has a photon radiative capture reaction where a photon is also emitted; however, as the same nuclide is created, it is not considered a transmutation absorption reaction.

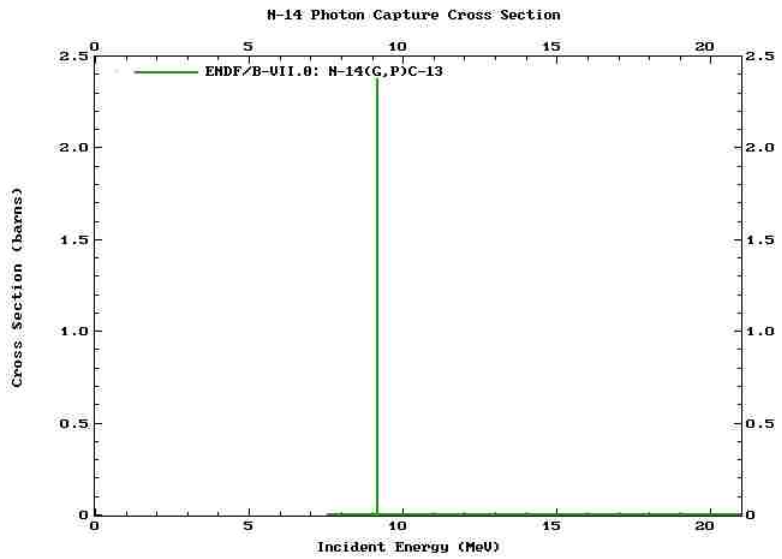

Figure 3.1: N-14 Photonuclear cross sections

where N is the number density of the material and $\text{mult}_{\varphi^\gamma}$ is the flux multiplier, the reaction rate for group 22 is

$$\begin{aligned} R_g &= 0.01\,{}^{\gamma}/_{cm^2\,sec\,bin} \times 10^{10} \times 0.01\,{}^{\#}/_{b\,cm} \times 3.6970 \times 10^{-4}\,b \\ &= 3.6970 \times 10^{2}\,{}^{\#}/_{cm^3\,sec} \\ &= 3.6970 \times 10^{-22}\,{}^{\#}/_{b\,cm\,sec}\ . \end{aligned} \tag{3.2}$$

Since there is one single reaction to consider, each event results in a set of ^{1}H and ^{13}C nuclides. Therefore, the production at the end of the time step is

$$\text{Production of } {}^{1}\text{H and } {}^{13}\text{C} = 3.6970 \times 10^{-22}\,{}^{\#}/_{b\,cm}\ . \tag{3.3}$$

When run through CINDER2008 given the same inputs, the results are identical, producing $3.6970 \times 10^{-22}\,{}^{1\text{H}}/_{b\,cm}$ and $3.6970 \times 10^{-22}\,{}^{13\text{C}}/_{b\,cm}$. Since the results match exactly to the hand calculation done in Equation 3.3, this verification problem has shown that for a simple absorption transmutation reaction, the additions to CINDER2008 properly handle and process the data.

The photoabsorption portion of the code is therefore verified for simple, photon only models.

3.1.2 Photonuclear and Neutron Absorption Verification Case

The second verification test is an extension of the first case given in Subsection 3.1.1. This tests the code's ability to handle both neutrons and photons incident simultaneously, causing multiple reactions on the same material through different sources. Before this can be done, in addition to the baseline case of photons only, a baseline case of neutrons only must first be run.

Keeping the material information constant from the previous case and setting the neutron flux to a constant $\boldsymbol{\varphi}^{\mathrm{n}} = \{0.01\ {}^{\mathrm{n}}/_{cm^2\ sec\, bin}\}$ with a multiplier of 10^7, the problem is rerun with a 0 photon flux. This can be run on the neutron only CINDER2008 code which has been validated for that capability, and comparisons have confirmed the same results between codes. As such, there is no need to attempt to do this problem by hand. The resulting nuclide composition for the neutron only case is given in Table 3.3. As there are many more neutron induced reactions in ^{14}N, this product list is much more extensive. Additionally, unlike the photonuclear case, the products of these reactions do interact with the incident particle, causing even further transmutation. It should be noted that the number of significant digits reported is due to the limitation of CINDER2008 output. This number of significant digits is enough to verify the current code additions.

Now that the baselines for both sets of product distributions after a 1 second irradiation have been made, the combined case can be run. As the two beams are independent, this case should produce a distribution of nuclides post-irradiation that is equal to the sum of the independent cases, plus some additional transmutation caused by the interplay of the two incident particles. The interplay of the two particles comes from the interaction of one particle with the daughter product of an

Table 3.3: Atom density of all nuclides in sample after irradiation of ^{14}N with a constant flux of neutrons.

Nuclide	Atom Density ($\#/_{b\,cm}$)	Nuclide	Atom Density ($\#/_{b\,cm}$)
^{1}H	1.827×10^{-21}	^{10}Be	4.379×10^{-24}
^{2}H	3.926×10^{-22}	^{11}Be	1.076×10^{-40}
^{3}H	1.051×10^{-22}	^{9}B	6.273×10^{-48}
^{4}H	1.848×10^{-53}	^{10}B	1.056×10^{-23}
^{3}He	3.345×10^{-23}	^{11}B	1.405×10^{-21}
^{4}He	1.157×10^{-21}	^{12}B	8.559×10^{-30}
^{5}He	1.189×10^{-63}	^{13}B	1.545×10^{-28}
^{6}He	1.084×10^{-43}	^{14}B	2.203×10^{-42}
^{7}He	5.026×10^{-65}	^{12}C	1.051×10^{-22}
^{5}Li	2.081×10^{-68}	^{13}C	4.592×10^{-22}
^{7}Li	2.066×10^{-22}	^{14}C	5.990×10^{-20}
^{8}Li	4.993×10^{-42}	^{15}C	8.085×10^{-42}
^{9}Li	4.111×10^{-45}	^{13}N	3.595×10^{-23}
^{10}Li	4.066×10^{-53}	^{14}N	1.000×10^{-02}
^{8}Be	2.602×10^{-40}	^{15}N	1.241×10^{-21}
^{9}Be	3.153×10^{-24}	^{16}N	4.507×10^{-44}

interaction from the other particle. Keeping all inputs the same but enabling both particles, the distribution of nuclides in Table 3.4 was produced.

By summing the results from Subsection 3.1.1 and Table 3.3, it can be seen that the two combine to create the distribution in Table 3.4, with some slight but expected differences. The differences, other than those in ^{1}H and ^{13}C, are due to the interplay of the two particles on the nuclides that are created from the interactions of the other. For example, the creation of extra ^{5}He and ^{6}He are due to neutron induced reactions on the ^{13}C created by the initial ^{14}N(γ,p) reaction. Additionally, isotope ^{11}C comes from the (γ,n) reaction on ^{12}C which is created by neutron induced reactions on ^{14}N. Verification of each of these discrepancies through the requested chain print-out was performed, proving to be products of similar interplay. Since the performance of the code on dual particle absorption transmutation reactions has thus been performed, that portion of the code has been deemed verified as well.

Table 3.4: Atom density of all nuclides in sample after irradiation of ^{14}N with a constant flux of neutrons and photons. Similar to Table 3.3.

Nuclide	Atom Density ($\#/_{b\,cm}$)	Nuclide	Atom Density ($\#/_{b\,cm}$)
^{1}H	2.196×10^{-21}	^{11}Be	1.076×10^{-40}
^{2}H	3.926×10^{-22}	^{9}B	6.273×10^{-48}
^{3}H	1.051×10^{-22}	^{10}B	1.056×10^{-23}
^{4}H	1.848×10^{-53}	^{11}B	1.405×10^{-21}
^{3}He	3.345×10^{-23}	^{12}B	8.559×10^{-30}
^{4}He	1.157×10^{-21}	^{13}B	1.545×10^{-28}
^{5}He	1.192×10^{-63}	^{14}B	2.203×10^{-42}
^{6}He	1.373×10^{-43}	^{11}C	1.421×10^{-41}
^{7}He	5.026×10^{-65}	^{12}C	1.051×10^{-22}
^{5}Li	2.081×10^{-68}	^{13}C	8.289×10^{-22}
^{7}Li	2.066×10^{-22}	^{14}C	5.990×10^{-20}
^{8}Li	5.052×10^{-42}	^{15}C	8.085×10^{-42}
^{9}Li	4.111×10^{-45}	^{13}N	3.595×10^{-23}
^{10}Li	4.066×10^{-53}	^{14}N	1.000×10^{-02}
^{8}Be	2.602×10^{-40}	^{15}N	1.241×10^{-21}
^{9}Be	3.153×10^{-24}	^{16}N	4.507×10^{-44}
^{10}Be	4.379×10^{-24}		

As the decay portion of the code is untouched, it as well is verified through the comparison of the CINDER2008 results for the simple neutron only source case and the CINDER2008 results from the same case. Using the same decay data, they arrive at the same distribution. Therefore, all neutron, photon, and neutron/photon absorption and decay cases have been verified against either hand calculations or the previously validated and verified code.

3.1.3 Photofission Validation Case 1

The next portion of the code that needs verification and validation is the photofission section. This addition is not much different than the portion listed above except for the fact that instead of a few products from the reaction, there are over a thousand

daughters produced in fractional quantities. The physics of the decay and transmutation after the initial reaction are the same. Therefore, a validation needs to be made that a proper fission product distribution is being created and these results should be validated against experiment. This is especially important as the neutron fission product yield data has been translated for photofission yields.

The first photofission problem to be used is ^{238}U(γ,f). It is worth noting that, as mentioned in the Methodology section, the photofission yield data comes from the equivalent neutron fission system. For this case, that equivalent system is the yield of ^{237}U(n,f). Unfortunately, there is very little data for this fissioning system as it is not as commonly encountered as other isotopes and does not have extensive measured data. Nonetheless, it is a good example of the use of the data because it is simple.

Due to this limited amount of data for neutron induced fission on ^{237}U, the distribution is only given at a single incident neutron energy in the ENDF-B/VII library, 500 keV. As shown in Table 2.1, the incident gamma energy range that this data should be most applicable is 6-14 MeV. Luckily, experiments by Jacobs et. al. [3] have covered some of this range. Photofission yields at four different nominal incident photon energies are given in the paper: 9.7, 11.6, 13.4, and 14.7 MeV. It should be expected that since 500 keV nominal incident neutron energy corresponds to approximately 6.6521 MeV incident gamma energy; the further away from that value, the less representative the data for the yield will be. This prediction shows to be true by visual inspection of Figures 3.2 through 3.5.

For the modeling of this system, the photon flux was set to an even energy distribution from 5 MeV and up at a total strength of 1×10^{10} $^{n}/_{cm^2\ sec}$. This ultimately does not have bearing on the yield distribution in the program (because the discrete energy range for the product distribution must be chosen prior to running), only the magnitude. Since the yield comparisons being made are normalized to 200%, this input is not of concern. The time exposure was set to 15 minutes in a single time step as to allow ample time for the system to equilibrate and irradiate, as with the

experiment. The time of exposure was not given in the experimental report, therefore this was chosen as most representative.

By visual inspection, experimental results match up well to the data that has gone

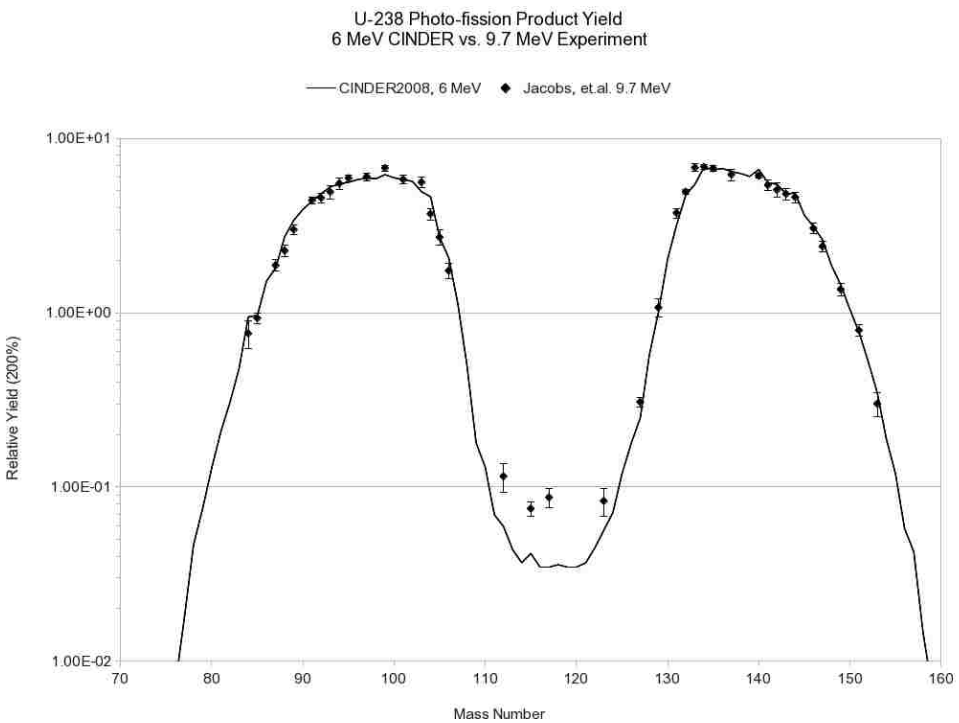

Figure 3.2: ^{238}U (γ,f) product yield at 9.7 MeV (experimental) versus CINDER at 6.6521 MeV

into the photon reaction library for CINDER2008. The diverging trend at higher energy was to be expected and the shapes are aligned throughout.

A more rigorous comparison of the data that is common among fission product yields is a comparison of the peak mass numbers and the peak to valley (the section between the two peaks) ratio. This ratio is essentially the average of the peak values divided by the valley value, measuring how far it is from a symmetric, single peaked distribution. As there are daughters with two distinct masses produced in fission, depending on the mass of the fissioning nuclide, these peaks will shift around. In

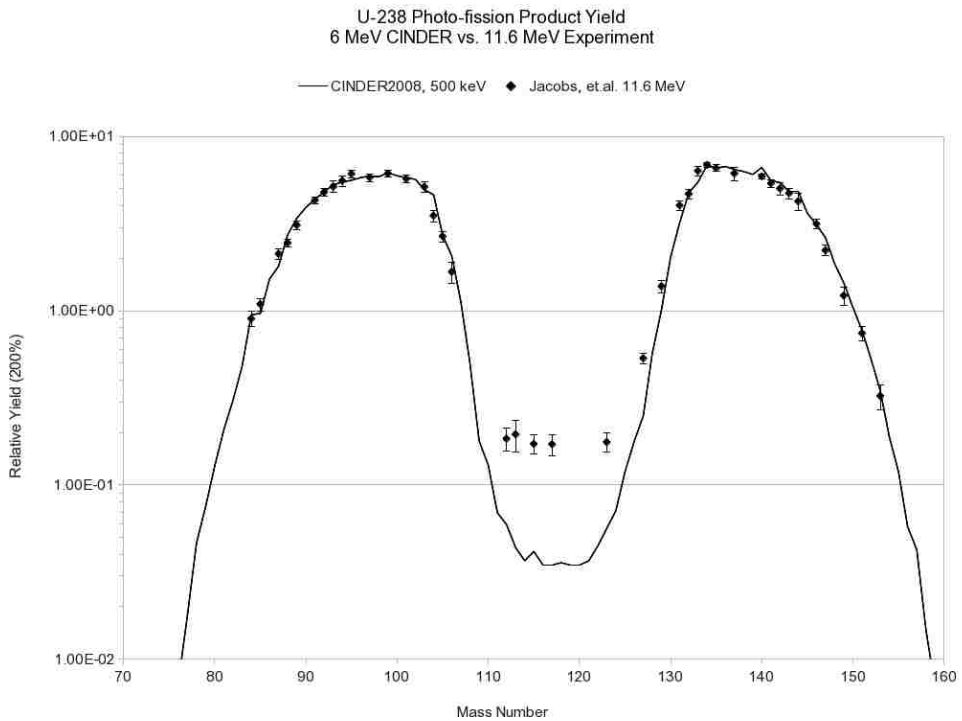

Figure 3.3: ^{238}U (γ,f) product yield at 11.6 MeV (experimental) versus CINDER at 6.6521 MeV

the case of photofission on ^{238}U, the experimental peaks happen at masses 99 and 134 and the valley happens at mass 115 for the 9.7 MeV case and mass 117 for the others. CINDER has determined these peaks to be at masses 99 and 134, and the valley to occur at mass 117. By these matching up, as well as they do, it is apparent that they come from systems of the same original mass number prior to fission. The discrepancy in the 9.7 MeV case for the valley can be noted by visual inspection of the data. Due to the sparsity of data in the valley region and the low readings, there is some variability in the results. A curve-fit of the data near the valley would likely result in a closer result, but as this is a comparison to measured data, no predictions are made and thus the data is taken at face value.

The second parameter, the average peak to valley yield ratio can be just as easily

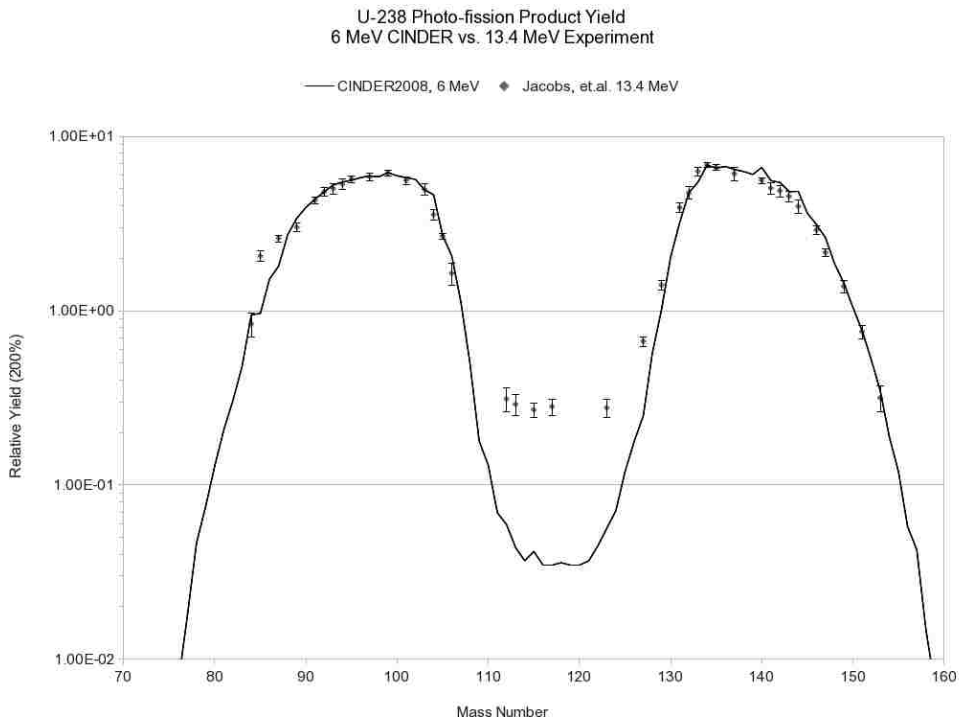

Figure 3.4: ^{238}U (γ,f) product yield at 13.4 MeV (experimental) versus CINDER at 6.6521 MeV

compared. Due to the physics of the reaction, as the excitation energy increases, the valley value is raised and the peaks are slightly lowered, giving a slightly more even probability distribution. Since the energies in this comparison stretch the range of applicability of the data, and even exceed it, these results aren't expected to match up well. Other than more experiments and evaluations, there is little that can be done to remedy these discrepancies. The CINDER2008 results yield a ratio of 188.7, typical of the lower incident energy distribution. The four experimental cases yield ratios of 90.9, 38.0, 23.1, and 14.1 for the 9.7, 11.6, 13.4, and 14.7 MeV incident energies, respectively. These results are summarized in Table 3.5. Although these results are not close, they are indicative of the expected trend by incident energies and keep with results presented elsewhere [41].

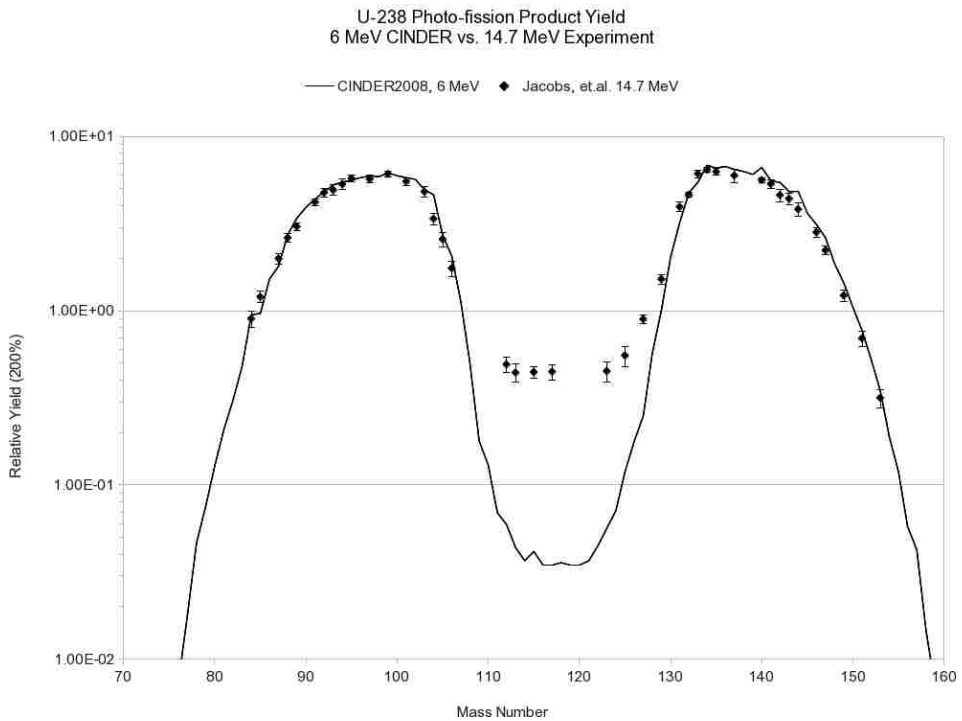

Figure 3.5: ^{238}U (γ,f) product yield at 14.7 MeV (experimental) versus CINDER at 6.6521 MeV

There is one last extremely useful parameter that enables a quantitative analysis of

Table 3.5: Photofission yield results for ^{238}U(γ,f), experimental and CINDER library

Incident Photon Energy (MeV)	9.7 (Exp)	11.6 (Exp)	13.4 (Exp)	14.7 (Exp)	6.6521 (C08)
Ratio of Peak to Valley	90.9	38.0	23.1	14.1	188.7
Peak Mass Numbers (Low/High)	99/134	99/134	99/134	99/134	99/134
Valley Mass Number	115	117	117	117	117
Error: Experiment vs CINDER library	0.37	0.36	0.46	0.46	-

how close the results are to each other. A error measure can be found by taking the L-2 vector norm of the difference between the measured (^{238}U(γ,f) translated) and

library (^{237}U(n,f)) data. Equation 3.4 gives how this vector is calculated, where N is the total number of product yield values.

$$\text{Error} = \sqrt{\frac{\sum_1^N \left(\text{Measured}_i - \text{Library}_i\right)^2}{N^2}} \tag{3.4}$$

These values, as seen in Table 3.5, are very small. They are also consistent. If these values were large (> 1 as will be shown in the next section), it is indicative of more than just the noise in the results. That type of result would indicate that the fission product yields are misaligned, causing large differences in the individual points. Misalignment happens when the excited nucleus that undergoes scission is not the same in terms of mass. When the error values are small, as with this case, an assumption can be made that the curves are representing the same mass system. Overall, the photofission product yield of ^{238}U was shown to match up very well to experimental data. The shape and peak/valley locations were all aligned, indicating that the dataset in the library matches with the physical problem in terms of the fissioning mass. However, the lack of evaluated data was apparent as the single energy that the library can be built on was not able to closely model a wide range of incident photon energies. This was to be expected and is simply a known limitation of the library. The correct compilation and processing of the data has verified the photofission capability in CINDER2008 and the fission product yields in this example are therefore considered valid as compared to experiment.

3.1.4 Photofission Validation Case 2

Although the comparison on a single simple photofission case is useful, it does not cover enough ground for a full validation and verification of the method. Therefore, a second, albeit similar, photofission validation case is needed.

In order to properly validate the code and data library, comparison with experimental results is perhaps the best way to go. Jacobs et. al. [1], one year later from

the experiments used in Subsection 3.1.4, performed a similar experiment on ^{235}U. In this experiment, results for the photofission yields were once again measured and reported for as tallies for each mass number.

To reproduce this, another case was run in CINDER2008. The same input parameters were used as with the ^{238}U case above, both in flux and time of exposure. This time, however, there are two energy choices for the fission product yield in the library since U^{234} is more well known in terms of fission product yields than U^{237}. The choices are between the fast energy range (6-14 MeV) and the high energy range (>14 MeV), which cover the experimental levels. Therefore, what should be expected, especially in light of the results from Subsection 3.1.4, is that the experimental yield distributions should progressively move from the fast to the high range results from CINDER. The nominal incident photon energies from the experiment are 9.7, 11.6, 14.1, and 70 MeV. For CINDER2008, as there are two choices for the fission energy, fast and high, both are given on the plot to show their applicability. The fission product yield results are given in Figures 3.6 through 3.9.

As with the previous validation case, the photofission yields match up quite well overall. The shapes are consistent between experimental results and the model, with the peaks again aligning nicely, albeit not as exact as in the case of ^{238}U. This can be, in part, attributed to the sparsity of the experimental results. There is no data recorded where the model's peaks lie, but trends in the experiment suggest that they would be aligned if data was present. The peak to valley ratios are where the main discrepancies are, which was to be expected. This is due to the models being for a single incident particle energy, which does not match exactly the experimental incident energies. The overall behavior of the distributions trending from the fast to high energy spectra from the models was anticipated, but the 70 MeV experimental result should have been predicted to have a lower peak to valley ratio than the fast energy CINDER model. In fact, in comparison to results given in [39], this 70 MeV result seems to not quite capture the expected shape. The valley should be raised

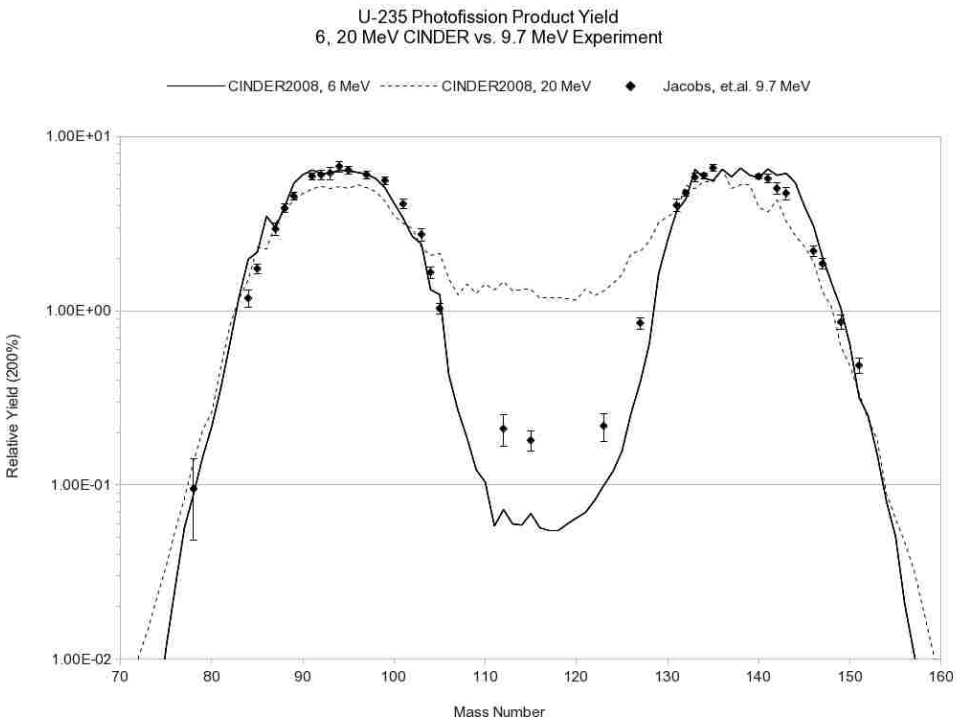

Figure 3.6: ^{235}U (γ,f) product yield at 9.7 MeV (experimental) versus CINDER at 5.7954 and 19.2374 MeV

to nearly the level of the peaks at that excitation level. This discrepancy could be partially, if not fully, attributed to the fact that photon source is a Bremsstrahlung source, not monoenergetic. Therefore, the energy of the source photons are actually a continuum up to a maximum, with the most probable at approximately 30 MeV. With these types of distributions, there are still plenty of photons below that level, which could skew the results. [1]

These peak to valley ratio results and peak/valley mass numbers can be seen in Table 3.6.

As with the first photofission validation problem, the relative error was found for each distribution. Since this case had two library distributions, the energy range that each experiment fell into was used decide which library set to use. The 9.7 and

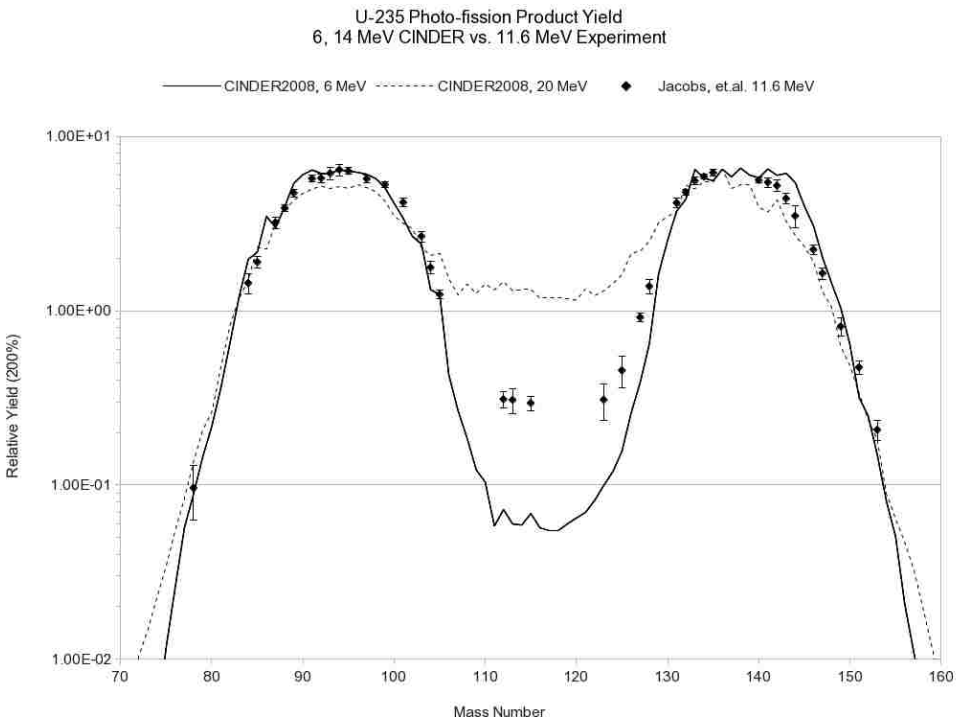

Figure 3.7: ^{235}U (γ,f) product yield at 11.6 MeV (experimental) versus CINDER at 5.7954 and 19.2374 MeV

Table 3.6: Photofission yield results for ^{235}U(γ,f), experimental and CINDER library

Incident Photon Energy (MeV)	9.7 (Exp)	11.6 (Exp)	14.1 (Exp)	70 (Exp)	9.7 (^{238}U) (Exp)	5.7954 (C08)	19.2374 (C08)
Ratio of Peak to Valley	37.0	21.4	12.1	8.6	90.9	118.7	3.8
Peak Mass Numbers (Low/High)	94/135	94/135	95/137	95/137	99/134	94/141	96/136
Valley Mass Number	115	115	113	115	117	117	116
Error: Experiment vs CINDER library	0.52	0.85	0.76	0.65	1.25	-	-

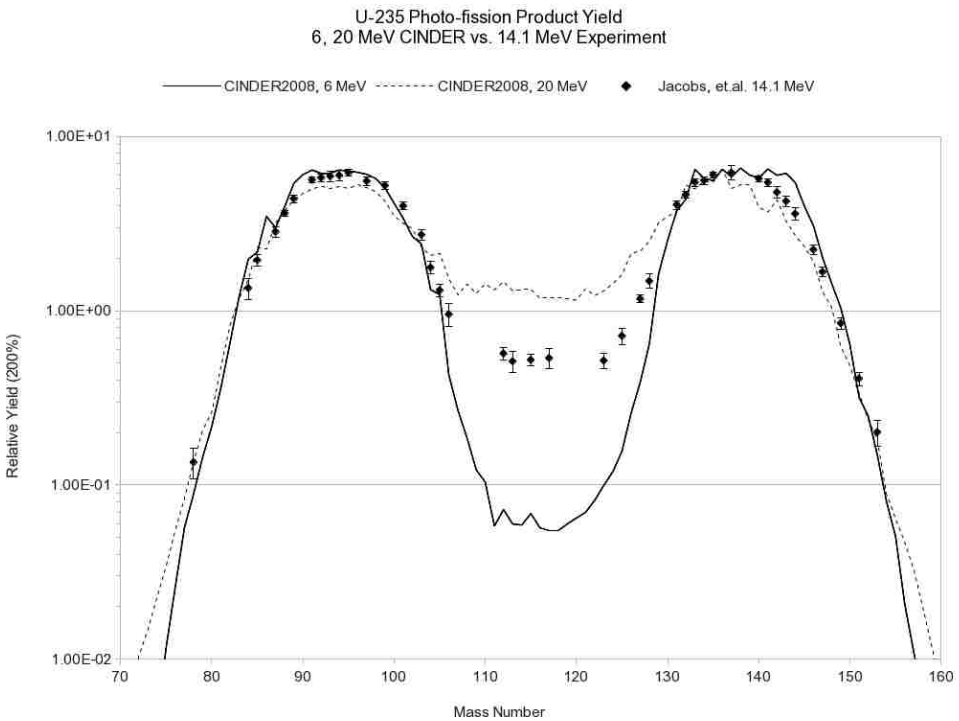

Figure 3.8: ^{235}U (γ,f) product yield at 14.1 MeV (experimental) versus CINDER at 5.7954 and 19.2374 MeV

11.6 MeV cases were taken against the fast energy library (6-14 MeV), while the 14.1 and 70 MeV results were compared against the high energy library (¿14 MeV). It should be noted that these libraries are most applicable for this case at 5.7954 MeV and 19.2374 MeV. Since none of these cases are those energies, they are not expected to align perfectly. However, as with the first validation case, when the relative error is less than one, the correct fissioning system is assumed and the results should be applicable. As can be seen, when closer to the experimental result energy, the library matches quite well (near 0.5 error). Additionally, when in the middle of the two libraries, the results reach 0.85, showing that the results are a bit of a stretch to match reality. As these results still match well, they are assumed again to be from the correct fissioning system, validating the library translation.

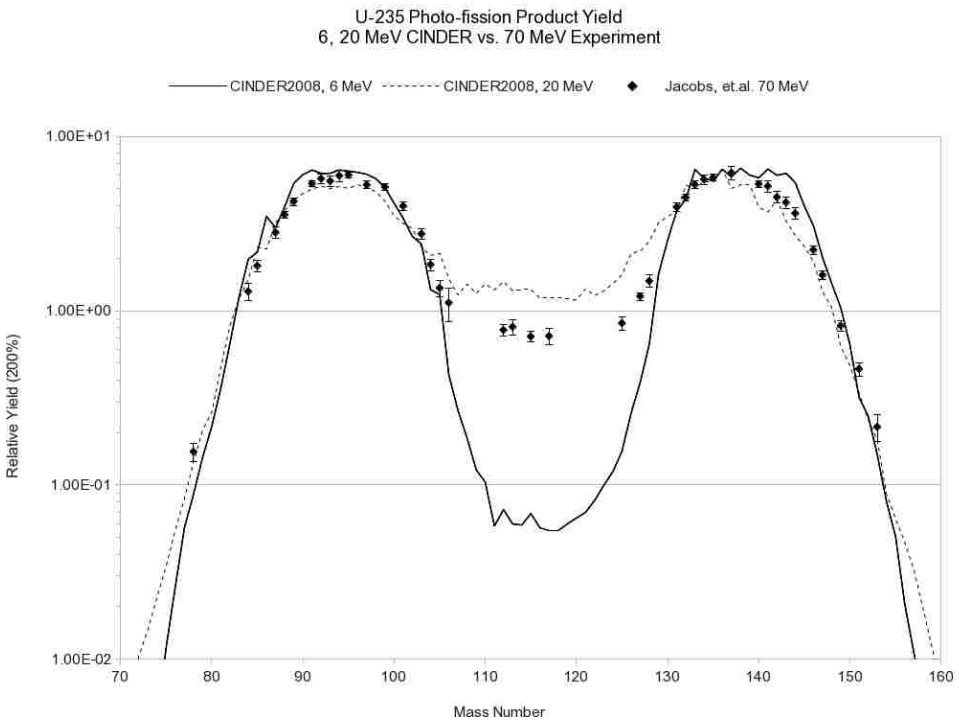

Figure 3.9: ^{235}U (γ,f) product yield at 70.0 MeV endpoint energy (experimental) versus CINDER at 5.7954 and 19.2374 MeV excitation

Although it is good to say that the values match up well, nothing has been presented showing the effect of using the incorrect fissioning system. Figure 3.10 shows a comparison of a ^{238}U(γ,f) set of experimental data versus the library for data for ^{235}U(γ,f). An obvious misalignment is observed immediately, especially in the lower peak. This difference is shown using the parameters of the yield comparison in Table 3.6. Not only do the peaks not align, but the error measure blows up to 1.25. This immediately flags the fact that the peaks are not aligned, causing large errors to be calculated between corresponding mass points. The alignment of the high peak is expected [39].

In addition to the check of the fissioning system in terms of photofission, it is useful to also check that the library matches, when compared to the equivalent neutron

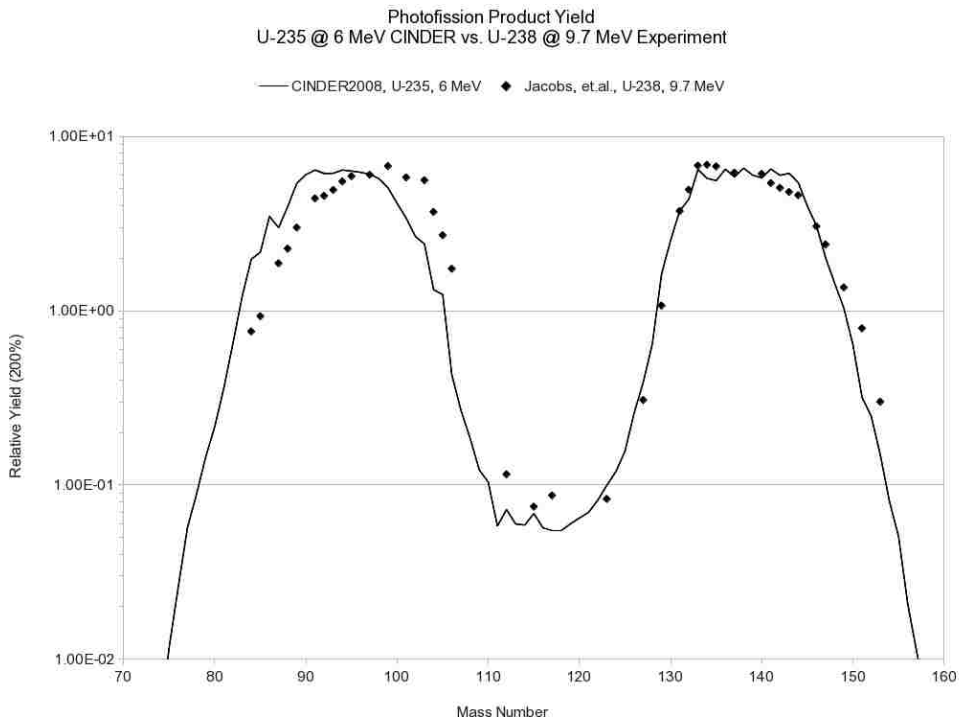

Figure 3.10: ^{235}U(γ,f) CINDER fission product yield results versus ^{238}U(γ,f) experimental results at 5.7954 MeV and 9.7 MeV, respectively

induced fission system. This can simply be done by taking the fissioning system from which the library was translated and compare it against an experiment of that neutron system.

An example of this is an experiment done on ^{234}U with 14 MeV neutrons [2]. This should almost exactly match the high energy library that is given for this system in the new code (equivalent to the 19.2375 MeV ^{235}U(γ,f) system). Figure 3.11 gives the graphical results of this exercise. As can be seen, these results match nearly exact as they represent information that went into the original dataset.

This simple comparison shows that the translation of the data has kept the integrity of the original data as it can still be used in another translation back to neutron induced fission.

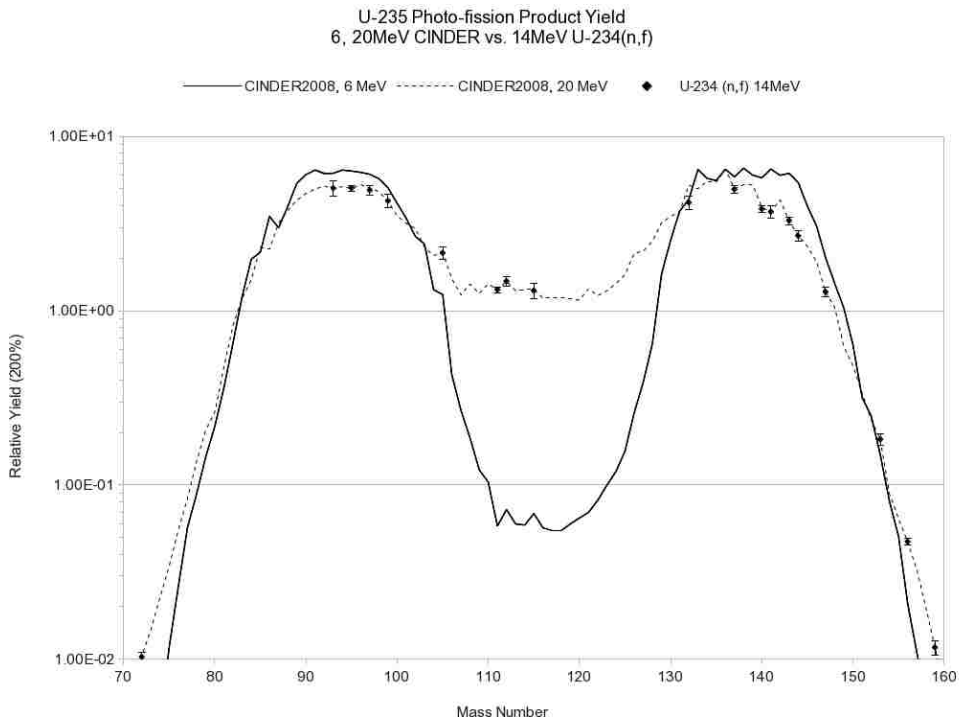

Figure 3.11: Comparison of fission product yields for ^{235}U(γ,f) at 5.7954 and 19.2374 MeV versus ^{234}U(n,f) at 14 MeV

Overall, the photofission product yield of ^{235}U was shown to match up well to experimental data, with noted and explained discrepancies. Again the shape and peak/valley locations were all aligned, indicating that the dataset in the library matches with the physical problem in terms of the fissioning mass. As with the previous validation, this example showed that the lack of experimental data is the main issue to fully validating the model – there are simply gaps in the data that don't allow for true peak and valley locations to be obtained. These validation cases do, however, show the correct compilation and processing of the data for the photofission capability in CINDER2008. They also show that the data has been translated correctly from the neutron induced systems. Slight differences in the library and experiment are observed, but are not due to a different fissioning system, as shown.

3.1.5 Photofission Validation Case 3

The third photofission example involves the photofission of ^{239}Pu. The first two validation examples were focused on uranium cases, where essentially all of the experimental data lies. However, the photofission yield data does not only include the uranium isotopes. For CINDER2008 to be able to model photofission, the cross section and product yield data must both be present. Of the materials that have experimental results for photofission, plutonium is the only other element that fits the criteria. In addition, the one isotope of plutonium that has experimental tabulated fission product yield data for comparison is ^{239}Pu. This validation therefore is a useful comparison of a different proton number isotope.

Kondrat'ko et. al. performed an experiment in 1981 to measure this photofission yield [4]. Unlike the two uranium cases given previously, this work was done by a Russian group, which expands the code to being validated by work by multiple sources. The experimental setup included a 28 MeV endpoint energy Bremsstrahlung source – equating to approximately to a most probably energy of 13 MeV. The irradiation saturated the material, as with the other cases, so an identical setup was used as in the first two photofission cases.

The CINDER2008 input again requires the choice of a fission product yield set. As the translation of yield products has come from the neutron induced data for ^{238}Pu and ^{238}Pu only has data for the high energy range, the choice for this model is simple. For the translation, this set would be most appropriate at an energy of 6.1441 MeV, with a suggested upper limit of applicability of approximately 13 MeV. This experiment is on the upper limit of the range for this fission yield set, but is the best data that is available.

The setup of the model for CINDER2008 followed the details of the previous two

examples in terms of the amount of material, irradiation time, and input tolerances. This model uses a flux that has been placed fully into the bin containing 13 MeV since this is essentially a multiplier for the fission product yield. The same comparisons are therefore able to be used for this set as with previous validations.
Figure 3.12 gives the graphical results of this comparison. The solid line is the data results from CINDER (using the translated neutron data) and the dots with error bars give the experimental results.

As can be observed from Figure 3.12, the results of the simulation match well to

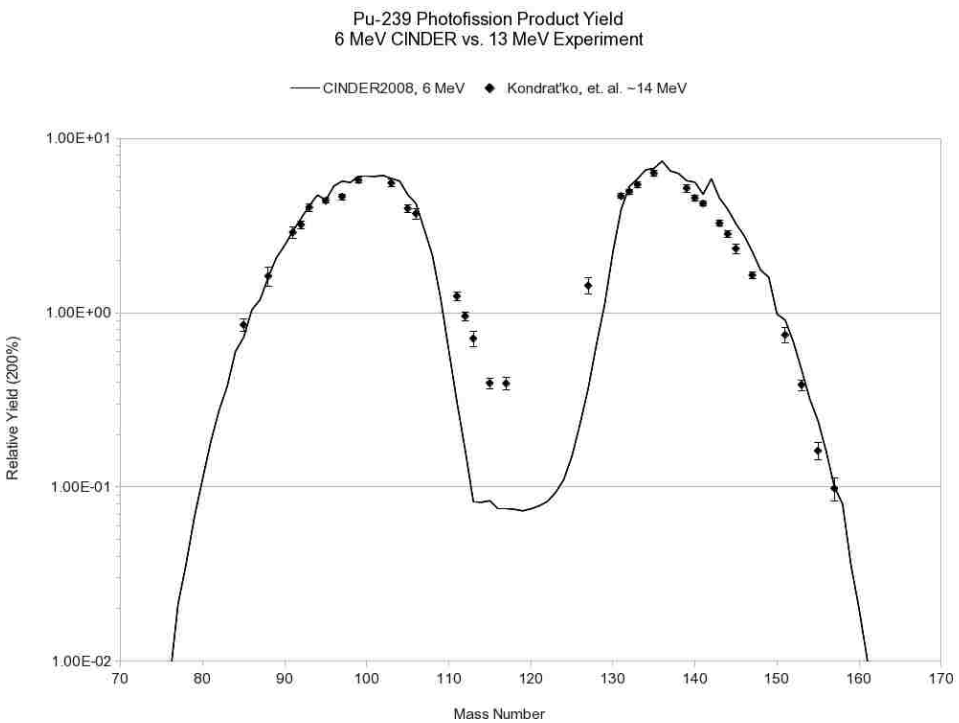

Figure 3.12: ^{239}Pu (γ,f) product yield at 28 MeV endpoint energy (approximately 13 MeV most probable energy) (experimental) versus CINDER at 6.1441 MeV excitation

the experimental results, but perhaps not as well as previous validations. As was expected again with the mismatch of the energy for the fission product yield data, the

Table 3.7: Photofission yield results for ^{239}Pu(γ,f), experimental and CINDER library

Incident Photon Energy (MeV)	∼13 (Exp)	6.1441 (C08)
Ratio of Peak to Valley	16.1	101.7
Peak Mass Numbers (Low/High)	99/135	99/136
Valley Mass Number	117	119
Error: Experiment vs CINDER library	0.62	-

valley region between the light and heavy mass peaks is higher in the experiment. This is do to the fact that the distribution becomes more symmetric with higher incident energy. Additionally, the peaks are slightly lowered for this same reason. Other than these two main differences, the trends are similar between the model and experimental data. There is a slight offset noted at the high end of the mass curve, where the library data appears to be higher than the experimental results. The library seems to have a strange higher trend in this region, perhaps because this comparison is between an evaluated library that is comprised of several experiments and a single set of experimental data. Although this is not a major difference and the trends are still the same, the discrepancy is noted.

In order to better compare the experiment and model, metrics can be used to quantitatively asses the differences. The mass numbers where the peak and valleys lie can be compared to ensure the same fissioning system is being used. Additionally, the peak to valley yield ratio gives the measure of how asymmetric the distribution is. Finally, the error measure as described in Section 3.1.3 can be used to determine how close the curves are in their trend. These results are all given in Table 3.7.

As with the previous validation cases, the sparsity of the yield distribution for the experimental data has an impact on the peak and valley locations for this data. In terms of the valley low point mass number, the experimental results and library differ by two mass numbers. This can be attributed to the lack of experimental results in

this region, where there are large gaps in the data. The overall trend in this region appears consistent. The light mass peak number matches exactly between the model and the experiment, which is perhaps the most important metric that can be used to ensure the same fissioning system was being used. Since the heavy mass peak stays fairly constant regardless of the fissioning mass due to stable proton and neutron shells, the lower peak being the same shows that the remainder of the mass is being attributed consistently. The heavy mass peak is only off by a single mass number, but again this can be attributed to the lack of experimental data in this region. The trends are similar between the two sets of results. Overall, from the peak and valley alignment, the fissioning system is assumed to be correct.

In addition to checking the fissioning system in terms of mass, the excitation energy should be verified. Since the two model and experiment differ in this sense, the trend is what must be checked. As the CINDER library energy is centered around 6.1441 MeV, a higher excitation energy (as in the experiment) should result in a more symmetric distribution. With the current set of metrics, this is verified using the ratio of the peak to valley fractions. The closer the value is to 1, the closer the distribution is to symmetry. The correct trend is observed with these results since the ratio is 16.1 for the higher excitation energy experiment versus 101.7 for the lower excitation energy model. This trend is verified and therefore not only has the fission system been validated in terms of mass numbers, but also in terms of the trends due to excitation energy.

A final measure of how similar the two distributions are is the error metric that was described above in Section 3.1.3. This gives a single value measurement of how similar or dissimilar the two distributions are. When the value is near or greater than 1, the fissioning systems are not similar. Below that, with a error value of around 0.5, the fissioning systems are very similar, with perhaps minor differences in the magnitudes of the numbers, but the overall trends match. For this experiment and model, the error metric shows a value of 0.62. This confirms the observation that

the trends are similar between the model results and experimental data. This is a low error value when compared to some of the previous validations, but all are still within an acceptable range of less than approximately 0.9.

It should be noted also that this error metric is close despite the fact that the excitation energy for the experiment is on the upper energy bound of the library data applicability range. Therefore, the trends are that much more similar and are able to compensate for the expected and observed mismatch in the peak and valley magnitudes. This again corroborates the results of the other metrics.

For the third validation case, again the library has proven to be correct in its fissioning systems by using the translated neutron induced fission product yield data. This validation used not only a different proton number than the other two validations, but also a set of experimental data from a different research group. This further validates the photofission product yields used in CINDER2008.

3.1.6 Photofission Validation Case 4

The fourth photofission validation case is another extension of the method that is yet untested. This includes a mixed isotope case, where there are three different fission product yields that fold into the final result. As there are limited isotopes for this type of comparison in CINDER2008, especially ones that also have experimental results, natural uranium was chosen. The isotopics of this case include 0.72% ^{235}U and 0.0054% ^{234}U, while the rest is ^{238}U. Modeling of this system will therefore be predominantly influenced by the ^{238}U. It will also be perturbed by the yields of the two lighter uranium isotopes. This case will enable the interplay for mixed isotope modeling to be validated.

An experiment in 1954 by Schmitt and Sugarman at the University of Chicago looked at the photofission yields of natural uranium. They were looking for a systematic approach to the yields at several incident energies, which had yet to be done for

heavy isotopes in photofission. Therefore, they started with a 48 MeV endpoint Bremsstrahlung source as the main comparison and then modified the x-ray energies from 7 MeV to 300 MeV to see any effects. The main energy, 48 MeV (or approximately a most probably energy of 15 MeV), was used to get the full yield for the isotope. The yield results were much more sparse in their results due to simply trying to observe the main changes that the excitation energy would make (around the peaks and valley masses only). Since the full distribution is only given for this main energy, a comparison is in order at that level.

Again, the same inputs are used as all the other validation cases, in terms of tolerances, irradiation time for saturation of the material, and material density. The main difference with this case is that the material is spread in the proportions given previously over three separate isotopes. Therefore, three isotopes are used at the start of the irradiation in CINDER. To determine the fission product yield that will be used, the energy of the experiment was taken into account. A high energy yield was therefore selected since that will best describe the isotopes at hand. The high energy range for all of these isotopes is centered around 19-20 MeV excitation, which is closer than the fast energy range which is around 5.5-7 MeV. However, although this is the selection made, for ^{238}U, there is no high energy distribution in the translated library from the ^{237}U(n,f) yield data. Therefore, for ^{234}U and ^{235}U, the high energy curve will be used, but for ^{238}U, the fast energy curve will be used. This will skew the results as seen in the validation of ^{238}U above in Section 3.1.3 toward higher peak fractions and a lower valley fraction.

The results from this CINDER model and the experiment are given as the lines and dots on Figure 3.13.

As can be observed in Figure 3.13, the overall trend again matches. The peak and valley locations seem to align when interpolating a trend between the sparse experimental data points. This is promising considering that three different distributions make up the majority of this curve. At mass number 103, the experimental results

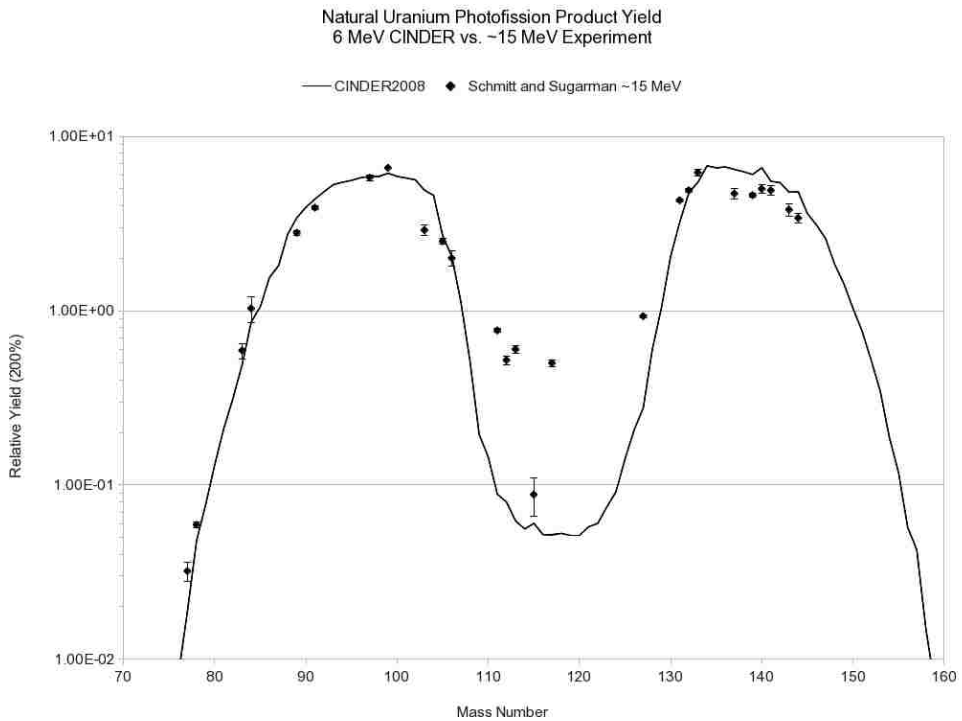

Figure 3.13: U-nat(γ,f) product yield at 48 MeV endpoint energy (approximately 15 MeV most probable energy) versus CINDER at high energy setting.

seem to show a slightly different trend than the library results from CINDER. When observing the whole trend of the data in the down-coming portion of the first peak, though, the trend suggests that this value might be slightly low, but is consistent with a more shallow peak and raised valley. This is therefore attributed to the mismatch in the excitation energy of the library for ^{238}U.

All other slight mismatches in the magnitude also can be attributed to the excitation energy mismatch, as the difference lies mainly in the "flatness" or symmetry of the distribution.

These observations are again not complete without a full investigation into the metrics described previously. The results for these quantitative comparisons are given in Table 3.8.

Table 3.8: Photofission yield results for U-nat(γ,f), experimental and CINDER library

Incident Photon Energy (MeV)	∼15 (Exp)	∼20 (C08)
Ratio of Peak to Valley	75.0	132.9
Peak Mass Numbers (Low/High)	99/133	99/134
Valley Mass Number	117	120
Error: Experiment vs CINDER library	0.87	-

These results are much like the previous three examples in their trends between experiment and model. First, the comparison of the peak and valley mass numbers should be done. It should be noted that for this comparison, the unusually low result at mass number 115 in the valley was discounted as it was well off the trend of the data. However, when looking at the trend of the remainder of the valley, the mass number of 117 is the low point, whereas CINDER predicted a mass of 120. This mismatch yet again can be attributed to the lack of data in the valley region for the experiment. The peak numbers, on the other hand, are in alignment. The low mass peaks are perfectly aligned at mass 99, as was observed in the trend of the data in the figure above. Additionally, the high mass peak was only off by a single mass number. The trends suggest these are aligned and there is no experimental data point at the CINDER predicted heavy peak mass. With these alignments, again the fissioning system (or systems in this case) have been preserved with the translated fission product yield data.

The second metric that is used to do this validation is the peak to valley fraction ratio. This again shows how asymmetric the distribution is, which is based on the excitation energy of the fissioning nuclei. Since the ^{238}U data does not include the most appropriate energy range data, the results from CINDER were expected to be skewed to a more asymmetric result – a higher ratio. This was confirmed in the results, where CINDER predicted a ratio of of 132.9 while the experiment showed a

ratio of 75.0. These results are much closer than previous cases, due in large part to the contribution from the ^{234}U and ^{235}U results that have the high energy product yield data. These yields therefore lifted the CINDER results to match more closely to the experiment. This trend was again expected due to the limitations of the available data.

The final metric for measuring the proximity of the results is the error metric. This tells how well the data matches in terms of the trends. A value of 1 or more generally indicates that the fissioning systems are a mismatch as their product yields are not aligned. For this model, the error metric was at 0.87. This value is higher than some of the previous results, but it was expected. As the fission product yield for ^{238}U did not match the excitation of the experiment, the results from CINDER resulted in a much more asymmetric distribution. As the experimental results are more flat in the low mass range and the peaks are lowered, there is a natural offset in the data. This is the same result that was observed in the case of ^{235}U photofission yields and energy mismatches in Section 3.1.4. As the distributions still have the same general trends – the peaks and valleys line up – the error metric was still below 1.

Although this error metric was not as close as some other cases, due to modeling limitations, it is still well below the cutoff for a mismatched fissioning system.

In all, the metrics for this validation of a three isotope material irradiation and fission product yield comparison show that the fissioning system has been preserved. This of course is with the caveat of the known limitation of the data libraries for CINDER2008 which do not contain a comprehensive set of evaluations at all energies. Through this validation, and the three previous, the fissioning systems have been shown to be preserved, the model results match experiment, and the system is therefore considered valid for use in photofission modeling.

3.1.7 Photofission Validation Case 5

The final photofission validation case is used to show the subtleties that differences in the proton number at the same mass will affect in the final fission product yield distribution. Because the total mass is essentially the same with the same total number of protons and neutrons, the general distribution of photofission products will be the same. However, subtle differences can arise due to the fact that there are different numbers of protons and neutrons in the nucleus.

When the atom scissions, heavy and light mass products are formed. Because of the natural bias to fill neutron and proton shells, the initial number of these particles in the scissioning mass can have an effect on the final distribution of the two products. Therefore, when comparing the distributions from the fissioning mass of nuclides with the same mass but different proton numbers, slight differences are expected.

To do such a comparison, $^{238}_{93}$Np and $^{238}_{92}$U are modeled using CINDER2008 to get their photofission product yields. This can then be compared against the first validation case in Section 3.1.3 to check it against an experimental yield for ^{238}U(γ,f). One issue that arises for this comparison is the lack of evaluated cross section data for ^{238}Np. As this is essentially a multiplier for the fission product yield data and the results are normalized in the end, what is input is inconsequential. A cross section simply must be present for CINDER to process the photofission. All other inputs are kept constant for this comparison from the previous four photofission validation cases.

The experimental data and CINDER2008 results for ^{238}U are exact copies from Section 3.1.3. Full discussion of that validation will not be repeated here.

The photofission product yield distributions are given in Figure 3.14. The experimental results for $^{238}_{92}$U are the black dots, while the $^{238}_{93}$Np and $^{238}_{92}$U CINDER results are given by the solid and dashed lines, respectively.

As can be seen from Figure 3.14, the expected subtle differences were observed.

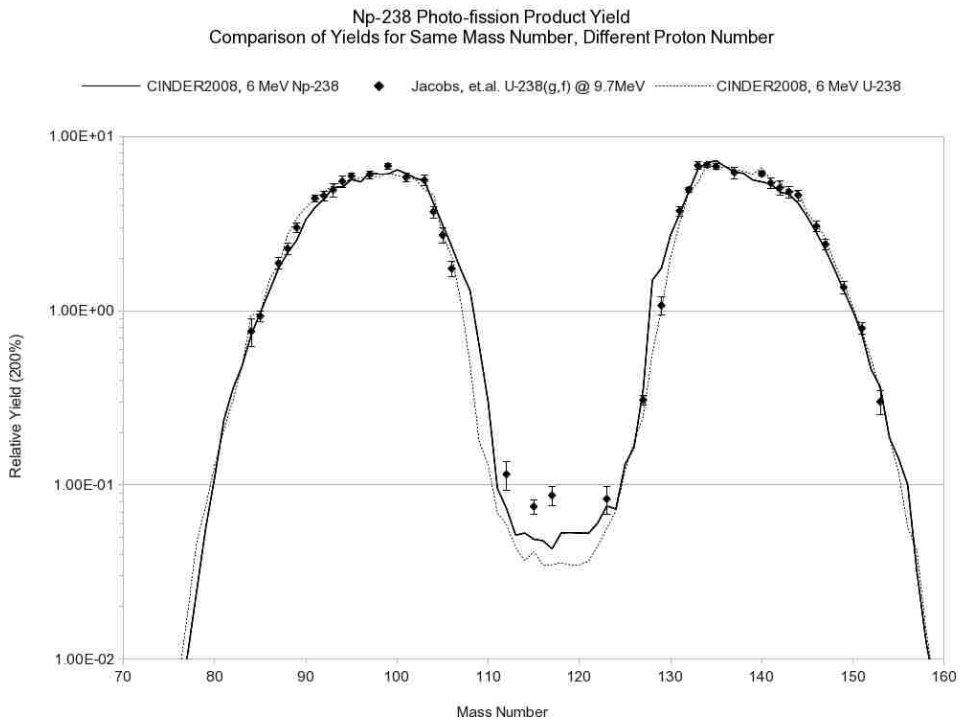

Figure 3.14: $^{238}_{93}$Np(γ,f) product yield at 5.9862 MeV from CINDER2008 versus $^{238}_{92}$U(γ,f) product yield at 6.6521 MeV and 9.7 MeV from CINDER2008 and experiment, respectively.

Overall, the peaks and valleys are aligned due to the masses being the same. However, the transition from the light mass peak to the valley shows a difference between the two isotopes. For ^{238}Np, the shoulder in this region is shifted by a mass number or two. This could be attributed to the difference in neutrons and protons between the two isotopes. Since the heavy mass peak is consistent and well defined for most heavy nuclei, the light mass peak will get the remainder of the neutrons and protons left over from the scission process. As ^{238}Np and ^{238}U will be different in this remainder by a proton and neutron, it is likely that the proton shells will be populated slightly different between the two isotopes. Since neptunium has one more proton than uranium, this is a hypothesis as to why the distribution in the 100-110 mass

Table 3.9: Photofission yield results for the comparison of ^{238}Np and ^{238}U. ^{238}U results are repeated from Table 3.5.

Incident Photon Energy (MeV)	5.9862 (^{238}Np) (C08)	6.6521 (^{238}U) (C08)	9.7 (^{238}U) (Exp)
Ratio of Peak to Valley	159.4	188.7	90.9
Peak Mass Numbers (Low/High)	100/135	99/134	99/134
Valley Mass Number	117	117	115
Error: Experiment vs CINDER library	0.31	0.37	-

number region is skewed high for neptunium. Additional differences could come from the difference in excitation energy, which is approximately 0.666 MeV, but this generally only affects the level of asymmetry in the distribution.

These slight differences do not greatly affect the overall distribution, though. In fact, as can be seen in Table 3.9, the metrics used for checking the overall shapes show that the two distributions are extremely similar though the shoulders are different. Most metrics line up fairly consistent between the sets of data. The trend in the ratio of peak to valley fractions are consistent as in previous sections – higher excitation energy leads to a less asymmetric distribution. Additionally, the valley locations match between the two CINDER results for ^{238}Np and ^{238}U. As well, the similar shapes as noted in the figure can be seen in the error metric, with a consistently low error between the measured values and the two CINDER library models.

These differences and similarities were expected in this validation exercise. Although the mass number of the fissioning nucleus helps to mold the general shape of the fission product distribution, this validation exercise showed the effect of the number of protons and neutrons. Slight nuances are introduced by differences in how the mass is populated by protons and neutrons. Overall, this final validation illuminated these differences and further validated the fission product yields that have been translated from incident neutrons to photons.

3.1.8 Validation and Verification Summary

Through these seven models, the CINDER2008 code for dual processing of neutron and gamma transmutation with natural decay has been verified and validated. It has been tested on all capabilities newly added to the thoroughly validated CINDER2008 code.

First, the data input, output and internal handling was verified through two simple examples. These not only showed that the libraries were being read correctly and that data was being processed consistently, but also that the interplay of the dual particles was being captured. No issues arose in this verification.

Next, the surrogate fission product yield distributions (from A-1(n,f) were validated versus experimental results for photofission. This ensured that the translation in terms of mass and energy was consistent with the actual physics of the reaction. Overall, trends were consistent with the experimental data, even if absolute values were different most likely due to a lack of a full mass curve for experimental data. This closeness was measured by an error metric – a single value denoting how close the library data and experimental results are. These values are summarized in Table 3.10 for all validation cases. The validation of the surrogate reactions proved to be successful as all results were consistent with experiment and as expected.

In addition to ensuring the surrogate reactions were valid, a comparison was made to examine how apparent it would be if an incorrect fissioning system was used. In terms of a different mass altogether, the comparison showed that there are glaring differences in terms of peak and valley locations in addition to simple observation of the distributions. The error metric as well captured this discrepancy. A system that has a slightly different number of protons and neutrons making up the same mass is much more difficult to discern. The distributions were consistent and the error metric proved the shapes are similar. However, slight nuances introduced by how the final products will be created based on the number of protons and neutrons was

Table 3.10: Summary of the error metric denoting the closeness of the CINDER library (surrogate data, using A-1(n,f)) and experimental results for photofission yield distributions (using A(n,f)). Values between 0 and 1 denote a close match (the lower the number, the closer the results), while values above 1 denote a mismatch in the fissioning system. Values are summarized from tables in the previous validation sections. (exp) denotes if experiment other than fissioning system was used for comparison.

Fissioning System	Excitation Energies (CINDER/Experiment) in MeV	Measure of Error	Section
γ+^{235}U	5.7954/9.7	0.52	3.1.4
γ+^{235}U	5.7954/11.6	0.85	3.1.4
γ+^{235}U	19.2374/14.1	0.76	3.1.4
γ+^{235}U	19.2374/70 (endpoint)	0.65	3.1.4
γ+^{238}U	6.6521/9.7	0.37	3.1.3
γ+^{238}U	6.6521/11.6	0.36	3.1.3
γ+^{238}U	6.6521/13.4	0.46	3.1.3
γ+^{238}U	6.6521/14.7	0.46	3.1.3
γ+^{235}U vs. γ+^{238}U(exp)	6.6521/9.7	1.25	3.1.4
γ+^{239}Pu	6.1441/48 (endpoint)	0.62	3.1.5
γ+U-natural	$\sim$20/28 (endpoint)	0.87	3.1.6
γ+^{238}Np vs. γ+^{238}U(exp)	5.9862/9.7	0.31	3.1.7

observed both visually and through the mass peak and valley locations. In all, these special cases do not disprove the surrogate models that were used, further validating the library.

This validation and verification exercise proved successful for library and code modifications introduced into CINDER2008 for the processing of photonuclear transmutation.

3.2 Demonstration of TINDER and CINDER2008

Now that the CINDER2008 code additions for dual particle transmutation have been verified and validated, it is necessary to do a thorough example that tests the new capabilities. Not only should this example test the CINDER additions, but also utilize the driver code, TINDER, to couple these calculations to transport.

As mentioned in Section 2.2, the TINDER code is a driver that connects the transmutation capability of CINDER2008 with different 3D transport solvers. The current solvers that are available are EVENT (even parity, deterministic transport) and MCNPX (Monte Carlo transport with high energy capabilities). These two transport codes cover a wide range of appropriate problems, from the scoping/parametrization cases to complex, all inclusive problems. EVENT is generally better when lower fidelity modeling is appropriate or when computational time is at a premium. Due to the deterministic nature of the code and the simplifications in terms of physics, precision is potentially not as good as Monte Carlo, but the calculation is much faster. MCNPX has the capability to model very fine details in the physics, over wide energy ranges (including very high energy) and intricate geometries. However, MCNPX is limited in that Monte Carlo calculations are extremely time consuming and therefore should be used as a last resort or for a final, intricate design calculation after scoping models have been made with a less expensive tool.

For the demonstration case, both transport codes will be used. This will enable a comparison of the computational time for each method, as well as the differences in the results. It will also allow for a check on each method to ensure the data transfer using the wrappers is performed correctly (as the wrappers for each transport code are different).

The problem that will be addressed and modeled is one that was an experiment performed by Lawrence Livermore National Laboratory for active interrogation. [74, 75, 76, 77, 78, 79, 80, 81, 82, 83, 84] As these systems are the driver of this project,

this type of model is appropriate. The next Section, 3.2.1, will give a description of the problem. This will include not only a description of the experimental setup, but how that system is modeled in the two different transport codes. Additionally, this section will describe the changes that were made from the original experimental setup of solely a neutron source to a dual particle source.
Then, Section 3.2.2 will give the results of this modeling using TINDER. It will compare and contrast the results with the experimental results for a neutron only source, giving indications of the utility of photofission on these types of systems.
After the general results and performance has been outlined, Section 3.2.3 will give the results of a sensitivity analysis performed on the CINDER2008 code. This sensitivity analysis was performed to determine how sensitive the system at hand is to the calculated flux profiles. This will give a measure of how exact the fluxes should be computed in order to properly characterize active interrogation systems.
Finally, the demonstration problem will be summarized in Section 3.2.4. This will give an overview of the performance of the code system as a whole.

3.2.1 Problem Description

In order to move further with the demonstration problem results, a full description of the problem at hand is in order. The model has been slightly adapted from the work by Slaughter et. al. [84] at Lawrence Livermore National Laboratory (LLNL). This work had been done to investigate the viability of active interrogation with neutrons on cargo. It was intended to verify if a delayed photon signal could be seen after fission was induced by a neutron beam.
The general idea is based on irradiating cargo with a high energy beam of particles, which will can then cause fission in enriched uranium, if present. The daughter products of this fission then produce beta delayed photons from their decay, which can be observed for a minute or longer after irradiation. This timing allows for the

standard activation of the host cargo to dissipate enough for the beta delayed signal to be observed. Additionally, these photons that will come from the decay of fission fragments inside an energy range (3-6 MeV) that is uncommon for other types of decay and activation. Therefore, if, after a period of time post-irradiation there is a photon signal in the 3-6 MeV region, there is a high likelihood that fission took place in the cargo. The cargo could then be scrutinized further. This method, although perhaps not a primary screening tool because of the irradiation effects on cargo and the cost, it could easily be used as a secondary tool before actually opening the cargo. The group at LLNL used this concept to see if it was possible to detect a canister of U_3O_8 within a matrix of plywood (among other materials). Their neutron source peaked at 7 MeV, emerging from a source below the cargo. A hole in the floor allowed for an approximate beam spot radius on the cargo of nearly 6.77cm. The source strength through that beam spot is 2×10^8 $^n/_s$.[2] This beam then transports through an essentially homogeneous plywood matrix with a density of approximately 0.55 $^g/_{cc}$, made almost entirely of hydrogen, oxygen, and carbon. The plywood was arranged in a way to mimic the size and shape of cargo that would be scanned and a panel of detectors was erected on one side of the cargo to essentially encompass one of the six sides of the cube. A schematic of the setup is given in Figure 3.15.

In addition to this schematic, Table 3.11 gives the specifics on the model in terms of materials, dimensions, etc.

In this setup, there are several assumptions that have been made in order to model it on a computer. The first assumption has to do with the source. The source is modeled as a 7 MeV monoenergetic neutron beam. In reality, there is a distribution about 7 MeV and there are neutrons that will appear below and above that value. These are assumed to be insignificant since these details will be many (at least 5) orders of magnitude lower than the actual distribution. In addition to the energy of

[2]Calculated based on a source strength of 1×10^{10} $^n/_s$ situated at a distance below the cargo with a 15 degree angular view factor.

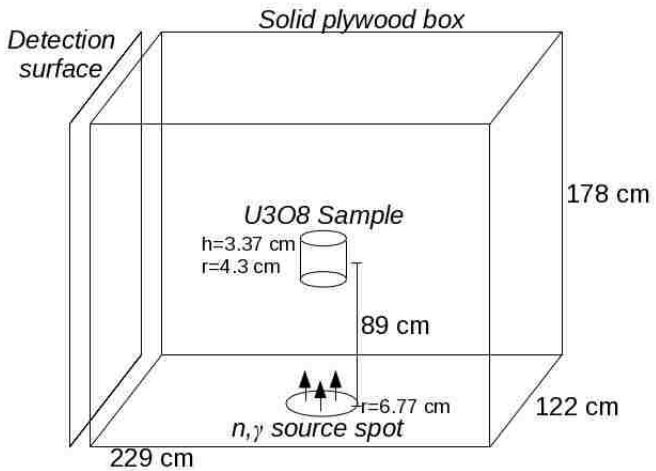

Figure 3.15: Schematic of the experimental setup on which the demonstration is based.

Table 3.11: Detailed parameters for the demonstration model

Plywood box dimension (cm) w×l×h	122×229×178
Plywood composition: Hydrogen Carbon Oxygen	$0.55\ {}^{g}/_{cc}$ 6.45% (weight) 48.55% 45.00%
Target cylinder dimensions (cm) r×h	4.3×3.37
Target composition: Uranium-235 Uranium-238 Oxygen	$2.4\ {}^{g}/_{cc}$ 80.15% (weight) 4.45% 15.4%
Source spot radius (cm)	6.77
Source spot location	Centered on Bottom Face
Source strength ($^{n}/_{s}$ and $^{\gamma}/_{s}$)	2×10^{8}

the source, the strength and direction have been assumed. The strength has been calculated based on flux measurements made in the experiments. An unattenuated flux was given, allowing for a back calculation of the source rate through the beam spot. Also, the neutrons are assumed to be directed inward, normal to the cargo

surface.

The next assumption has to do with the material compositions in the setup. The plywood is assumed to be entirely hydrogen, carbon, and oxygen at a density of $0.55^{g}/_{cc}$. The composition in reality will have traces of other elements, especially in the glue that is used. However, these elements will in general just modify to the scattering and slight absorption of source neutrons. This modification is assumed to be insignificant over the whole cargo. Additionally, the density is assumed to be constant over the whole media. Ignoring heterogeneities in this size of cargo is standard practice but is noted. This assumed content and density of the U_3O_8 target was also done to simplify the model.

The final assumptions are with the detection of the produced photons. The detector is assumed to encompass an entire side of the plywood box. Therefore, every photon that exits the cargo on that surface will pass through (and possibly interact) with the detector. In the models, it is assumed that all photons passing through that surface can be detected, and a detector efficiency can be used at that point (highly dependent on the detector).

With those assumptions in mind, the computer model versions of this experiment can be introduced. As mentioned in the introduction to this section, transport models were built for both EVENT and MCNPX.

The MCNPX model was built directly around the model described previously. As Monte Carlo is able to model minute details in geometry easily, the setup was modeled just as described above. A total of 10 million (50 million for the photon source) source particles were run to properly determine the characterize the flux profiles within the cylindrical target. Unlike the experiment, both neutrons and photons were used as sources for the MCNPX models (run separately). The photon source was kept at the same strength as there are existing sources that are able to reproduce those numbers [85] and was set to be a mono-energetic 12.2 MeV source. This energy is in the heart of the giant dipole resonance region for photofission of ^{235}U, making

it much more effective. Two models were run for MCNPX to model neutrons only, photons only, and a linear addition of the two was used for the dual particle case. All cases were run tracking both neutrons and photons.

For the EVENT model, simplifications were made to show the power of a deterministic transport method. First, the model was reduced to a 2-dimensional cylindrical geometry. This means that the box of plywood was translated into an equivalent volume cylinder. The height was kept constant as the length of travel for the particles to the target is an extremely important parameter. Additionally, the model, due to code constraints, uses an isotropic surface source in the beam spot instead of a monodirectional source. As the neutrons are scattered almost immediately in the plywood, this does not make a large difference, but for photons it does as they stream through the plywood. Therefore, equivalent models have been run in MCNPX to determine the effect of this source change. As the isotropic source with the same strength will cause a lower total flux in the target, a multiplication factor was determined from these models to affect the same total flux from the two sources. This multiplication factor was then applied to the EVENT source. Like the MCNPX models, two cases were run with EVENT: a neutron source problem and a dual particle problem.

Additionally, a multigroup library with 30 neutron groups and 12 photon groups was used. These libraries are from the TRANSX code's [86] MATXS10 library, which is weighted with the following distributions: thermal Maxwellian, 1/E for the resonance region, and Watt fission spectrum for high energies. The use of this validated, off the shelf library not only gives the data library some pedigree but also again exemplifies the low cost of running a deterministic transport method.

These two methods comprise the first transport calculation for the active interrogation problem. Both return the results for the average neutron and photon flux in the target region. In order to get this flux, F4-type tallies were used in MCNPX. This tally uses a track length estimation to determine the flux within a region. EVENT uses the calculated first moment of the angular flux (the scalar flux) in each finite

element of the region to calculate the volume averaged flux.

Once calculated, this flux is input into CINDER, along with the materials and volume for the target, U_3O_8 cylinder. CINDER is then run to determine the transmutation of the materials and the subsequent beta delayed photons released. As is done in the experiment, the beam (the constant flux in the case of CINDER) is turned on for 30 seconds to perform the irradiation and activation. This is done in a single time step. After this is done, the daughter products are left to decay with a zero flux. The delayed gammas in the range of 6 to 7 seconds after the irradiation are used in the re-transport models. This time corresponds to the initial time the detectors were turned on to start detecting radiation in the LLNL experiment.

The delayed spectra that is produced by CINDER not only contains the beta-delayed gammas from fission, but also the photons that are produced from the natural decay of uranium and its daughters. Therefore, it contains the low level background signal that would be observed from the target itself. The next step is to transport these photons to the detector to see how the potential signal that could be seen.

For MCNPX, as it is using a rigorous representation of the experiment, the gammas are emitted as a uniform volume source throughout the target. The rest of the model remains the same as mentioned above. To determine the potential signal, an F1 current tally is taken on the detector faces of the plywood matrix. Since particles are killed in the model when they exit the box, there is no incoming current. The F1 tally will then just show those leaving the box and potentially being detected.

In the EVENT model, another approach is taken. As the model was translated to a 2D cylindrical problem for the first step to save on the computation, a similar approach is used for the second step. It is important for this step for the photons to travel the correct distance to the faces of the box, a 2D x-y geometry has been set up. This means that the inner cylinder and outer box are infinite in the vertical, Z-direction (the beam direction). Additionally, symmetry is used to only model a quarter of this geometry. Figure 3.16 gives the schematic for this 2D problem. The

current through the detector face is then divided by 2 to determine the number of particles that could be detected (as it represents the four quarters through symmetry).

Once the re-transport has been completed, the modeling of the problem is finished.

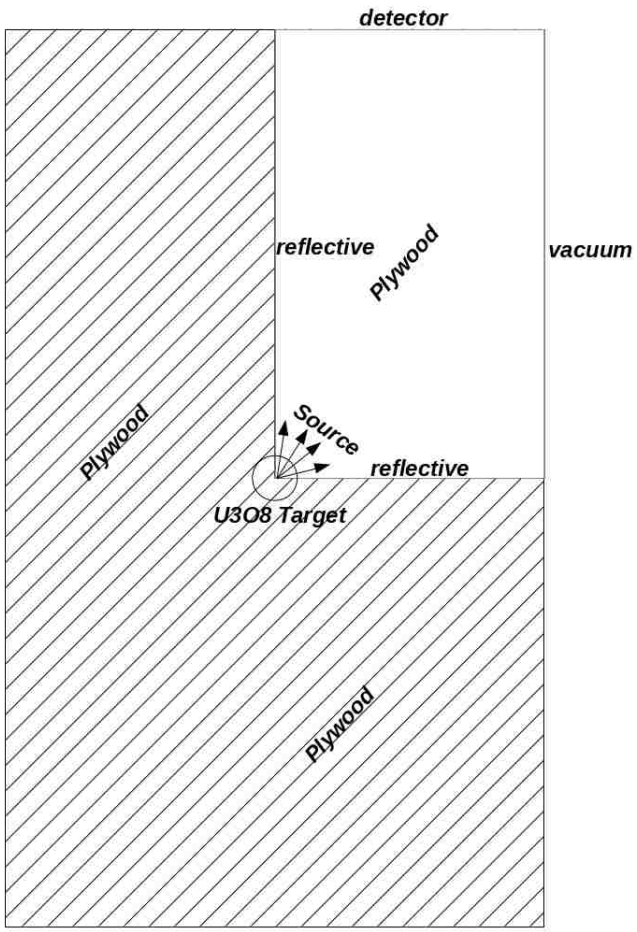

Figure 3.16: 2D X-Y setup of the second EVENT model used for re-transporting the delayed photons. Geometry is infinite into the page and the initial source was directed into the page, also. Hashed portion denotes region ignored due to symmetry. White plywood region is the geometry as modeled, with the U_3O_8 target in the lower left-hand corner.

This "detected" amount of photons can then be combined with a detector efficiency

to determine the actual signal output. In general, detector efficiencies can range anywhere from 10-35%. To compare with the experimental results, an efficiency of 30% is assumed [85], which although on the high side gives a good comparison versus the measurements.

3.2.2 Active Interrogation Results

Now that the problem has been outlined, the results from these models can be introduced. As two codes have been used in the process, both sets of results will be presented, compared, and discussed.

As mentioned in the previous section, the first step in the modeling is the first transport sweep. This models the transport of the neutrons and photons to the target and determines the volume averaged flux for the region. In order to see the effect of the dual particle active interrogation, a neutron source case was run in both transport codes as a baseline. This baseline not only allows for the gains in the dual particle active interrogation to be seen, but also gives set of values to compare to the experimental results for validation.

The MCNPX results were easily found as the model was well defined and could be reproduced in the code directly. However, the EVENT results, as the source is isotropic and not directed, need a multiplication factor to be applied before they can be used. To find this multiplication factor, the standard, directed source case was run in MCNPX, followed by an isotropic source case. This was done both for the neutron and photon source cases. A multiplication factor could then be found from a ratio of the directed source to isotropic source total flux. The following table, 3.12, gives the results of this comparison.

The true impact of this approximation can be seen through the plotting of Monte Carlo particle paths for these calculations. Figures 3.17 through 3.20 give these re-

Table 3.12: Multiplication factor to compensate for EVENT isotropic source

	MCNPX Isotropic	MCNPX Directed	Ratio (compensating factor)
Total neutron flux	2.730×10^{-5}	3.663×10^{-4}	13.417
Total photon flux	8.093×10^{-5}	5.058×10^{-3}	62.498

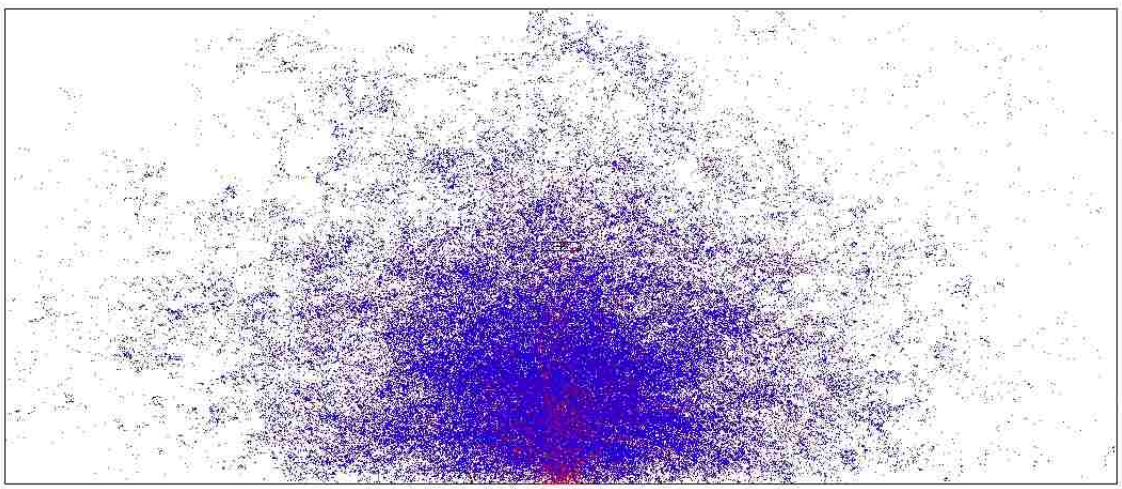

Figure 3.17: Incident neutron tracks for inward normal source in a vertical slice in the centerline of the geometry. Source is located in the bottom center of the figure. U_3O_8 target is located in the center of the box, denoted by a faint black border. Red tracks are those of the initial particle. (1000 source particles graphed)

sults. These figures are a slice through the vertical centerline of the cargo. Therefore, the source is located at the bottom center of the plot (denoted by a red instead of black outline) and the target is located at the center of the cargo box.

Figures 3.17 and 3.19 give the cases where the source is directed inward. This is essentially as was performed in the experiment. It can be easily observed that due to the low-Z and hydrogenous cargo material, even directing the neutrons directly inward does not stop them from being highly scattered by the time they reach the object. On the other hand, the photons have an easier time traversing the cargo as they do not interact as easily with the light materials.

Figures 3.18 and 3.20 show the effect of an isotropic source on the particle tracks.

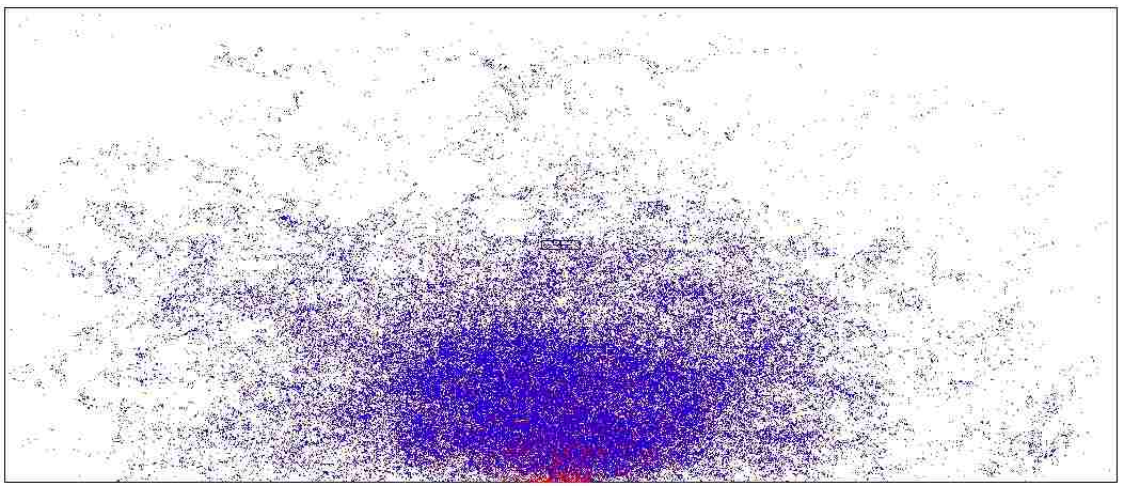

Figure 3.18: Incident neutron tracks for isotropic inward source in a vertical slice in the centerline of the geometry. Source is located in the bottom center of the figure. U_3O_8 target is located in the center of the box, denoted by a faint black border. Red tracks are those of the initial particle. (1000 source particles graphed)

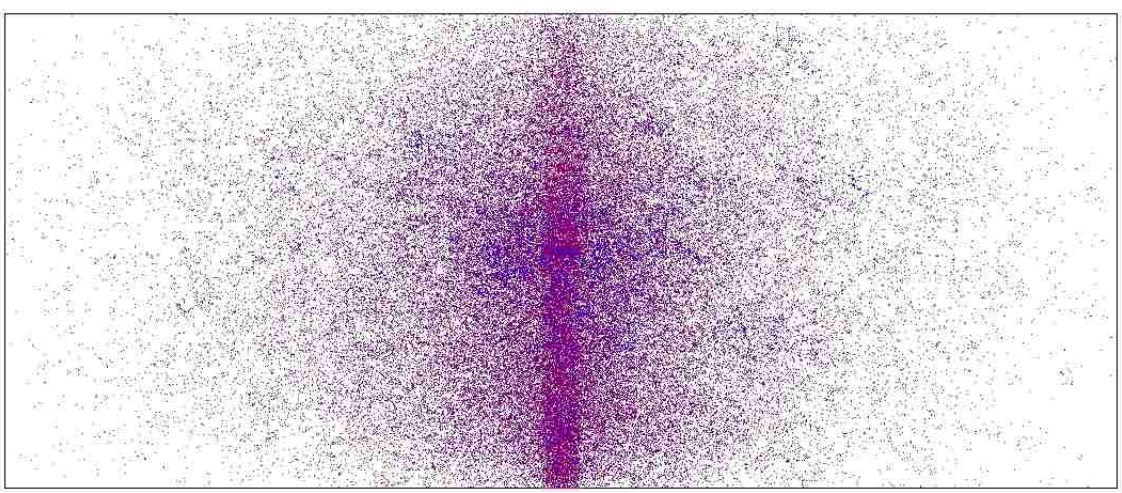

Figure 3.19: Incident photon tracks for inward normal source in a vertical slice in the centerline of the geometry. Source is located in the bottom center of the figure. U_3O_8 target is located in the center of the box, denoted by a faint black border. Red tracks are those of the initial particle. (5000 source particles graphed)

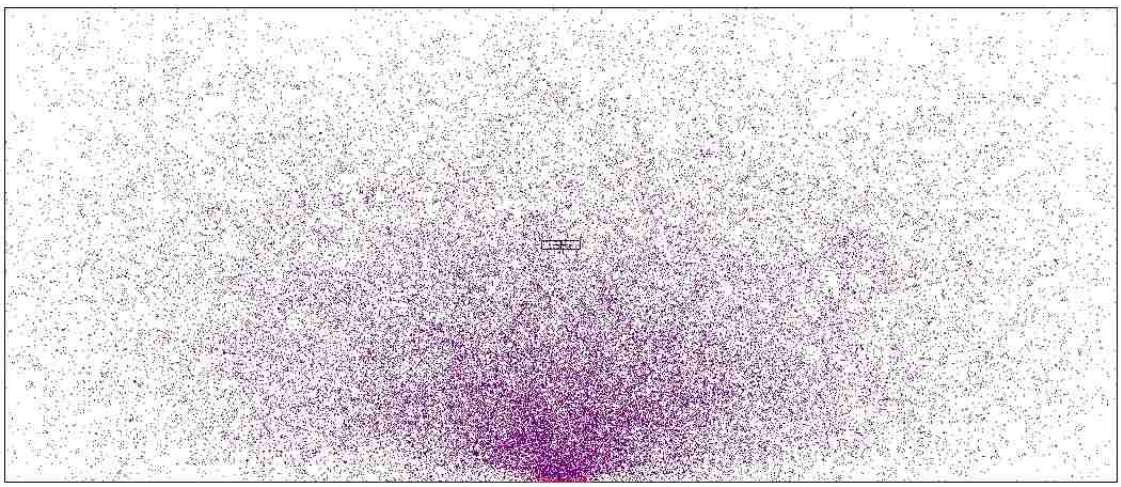

Figure 3.20: Incident photon tracks for isotropic inward source in a vertical slice in the centerline of the geometry. Source is located in the bottom center of the figure. U_3O_8 target is located in the center of the box, denoted by a faint black border. Red tracks are those of the initial particle. (5000 source particles graphed)

Little impact is shown with the neutrons as they were essentially isotropically scattered by the time they reached the target, no matter how they are configured when the enter. However, there is still an impact that can be seen as the epicenter of the tracks is located much closer to the wall of the cargo. The true impact is seen with the photon cases, where the isotropic and inward normal directed cases look very dissimilar. As the photons are the opposite of the neutrons and do not scatter well in this material, the output is much different. The isotropic photon case results in a much lower total flux at the target based on the same number of incident isotropic particles.

Since this is the simplification that must be made with the deterministic code, it is duly noted that there is a significant correction that must be made on the total flux at the target. When accounting for all production through dual particle tracking in these cases, the neutrons and photon fluxes are 7.5% and 1.6% their original values when transferring from directed to isotropic sources, respectively. This factor is therefore added to the results that come from EVENT before they are used

in the transmutation calculation. Subsequent calculations (e.g. the re-transport of photons) do not require such modifications.

By introducing these factors in the source strength of the EVENT models, the volume averaged flux results for the target can be used. Figures 3.21 through 3.24 give a graph of the energy distribution of the flux results from both codes. As the total number of neutrons and photons are lowered through the isotropic approximation, it is necessary to see if there is any impact on the energy distribution of the particles. A visual inspection of these results show a fairly close calculation in both codes.

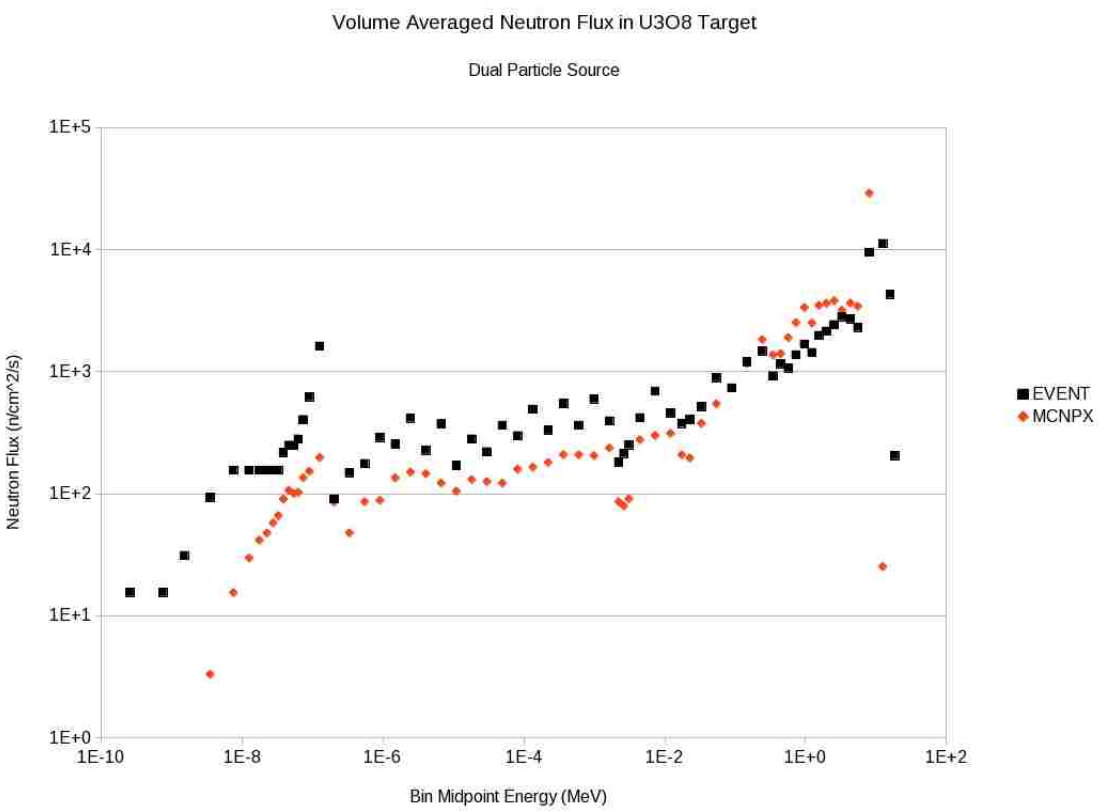

Figure 3.21: Comparison of volume averaged neutron fluxes in the U_3O_8 target due to dual particle source.

For the neutron fluxes, the trends are similar between MCNPX and EVENT, with

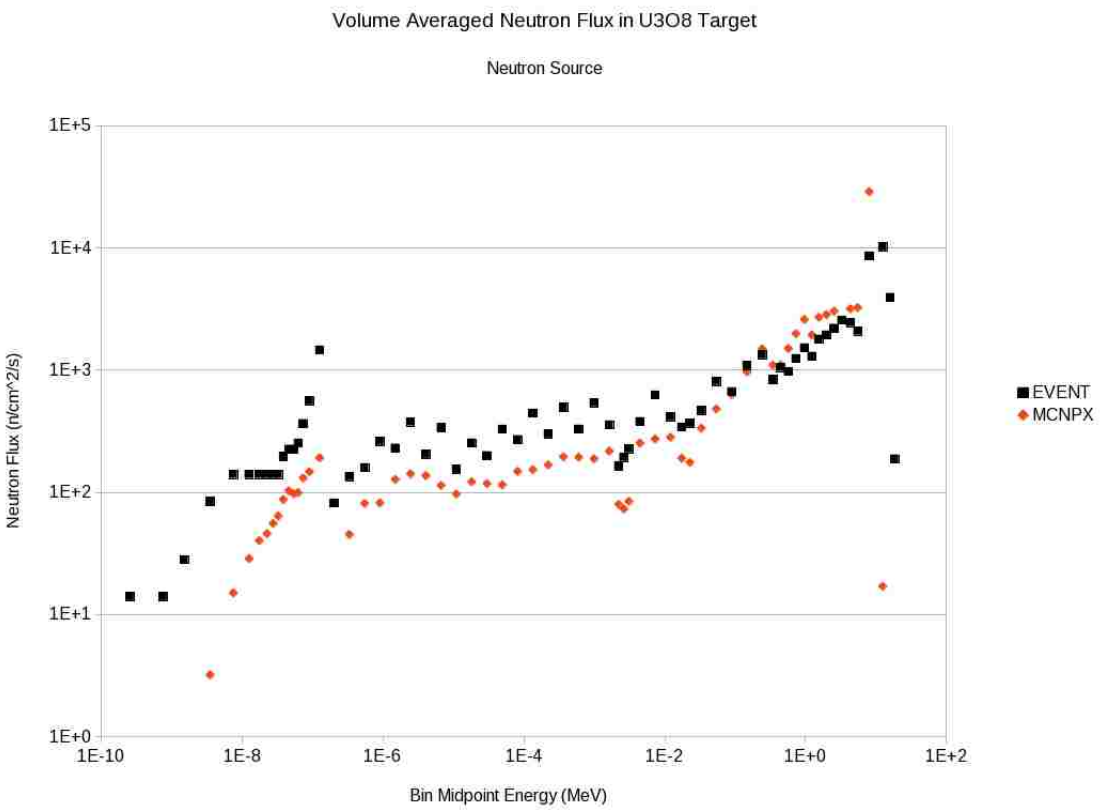

Figure 3.22: Comparison of volume averaged neutron fluxes in the U_3O_8 target due to neutron only source.

MCNPX predicting lower fluxes at low energies but crossing over at about 500 keV and predicting higher fluxes from that point. These discrepancies could be due to the energy of fission neutrons, which will appear in the MeV range then lose their energy as they scatter. Small differences in the representation of this physics could account for the observed discrepancies. It should be noted, though, that notable features are consistent: dips in the flux near 3 and 30 keV, thermal Maxwellian-like peak at low energy and Watt fission-like spectrum peak at high energy. In fact, these features are consistent for both the neutron only source and dual source problems. Although the transport of neutrons seems to diverge slightly between the two codes,

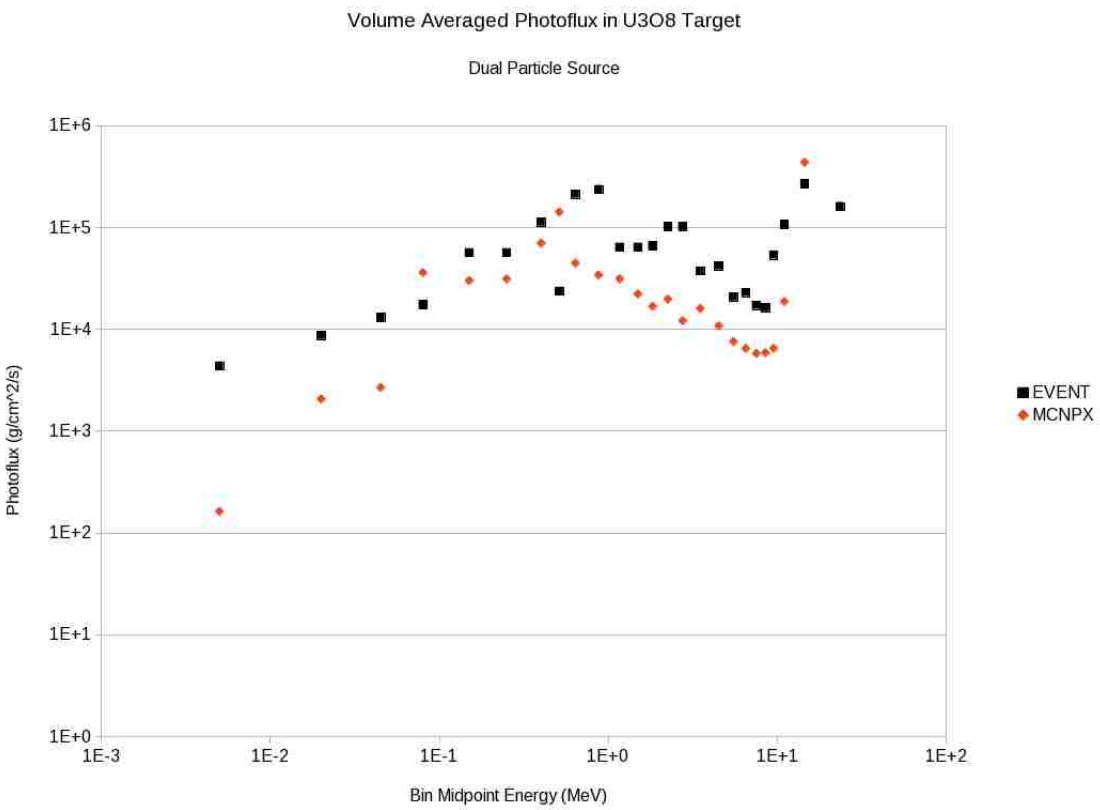

Figure 3.23: Comparison of volume averaged photofluxes in the U_3O_8 target due to dual particle source.

the transport of photons seems to be more similar. This can be observed in Figures 3.23 and 3.24. For the dual particle problem, the trends observed are fairly consistent, especially considering EVENT is using a 12 group energy structure. The modeling of the slowing down through the cargo appears to be similar as their shapes are well correlated. The high energy peak is observed, as well as the increase in the flux around 500 keV. Unlike the neutron fluxes, though, one model is consistently predicting a higher flux throughout the entire spectrum. EVENT tends to predict a higher photoflux when the trends in the data indicate a dip. Again, this is most likely attributed to the data that is supplied to the codes. MCNPX has a much more

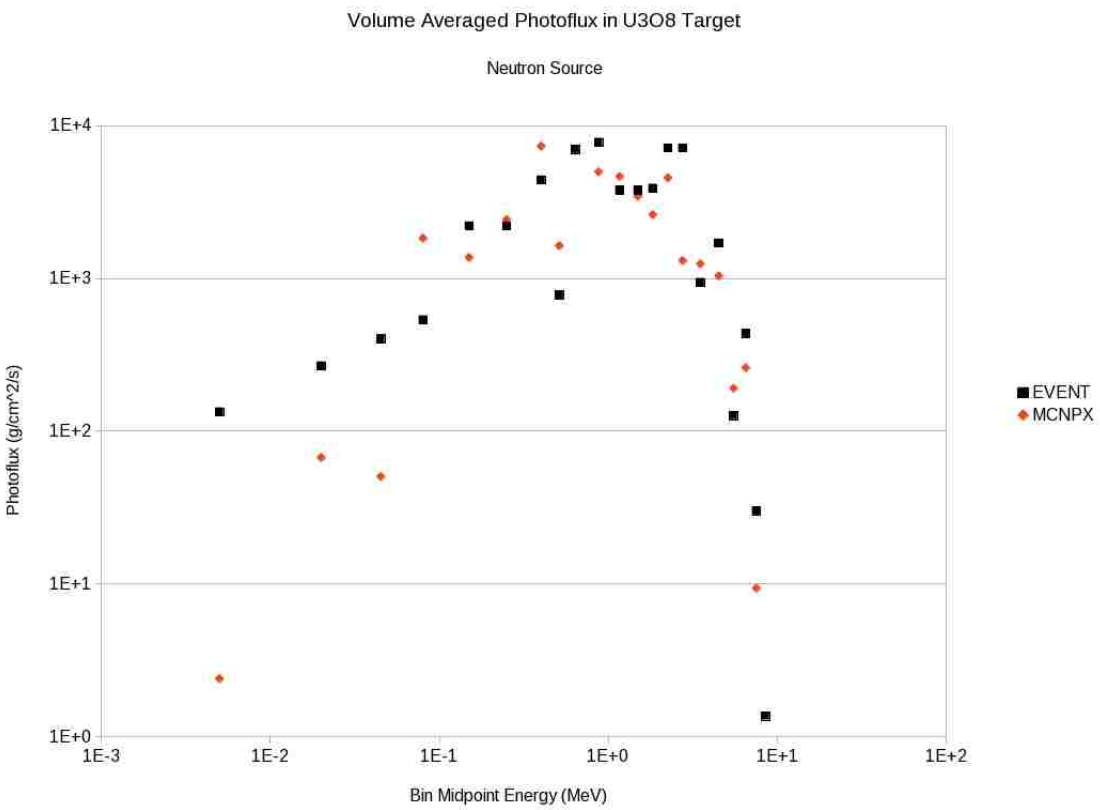

Figure 3.24: Comparison of volume averaged photofluxes in the U_3O_8 target due to neutron only source.

complete representation of the physics with its larger library for this data. Many of the reactions at higher energy in the photon cross sections are not captured, or not captured well, in the MATXS data that is used in EVENT. Therefore, lacking these interactions, especially absorption reactions, can lead to the increase in the prediction of the flux in the target. They simply will not be removed at the same rate in each code. Another possible reason for the higher number of photons in the dual particle source case is the production rate of photons through fission and other neutron induced processes. This could also account for a higher number of photons in the final solution.

This final thought can be seen especially well in the photoflux plot for the neutron only source case, Figure 3.24. This plot shows photons that are solely created in neutron induced reactions, (n, γ), (n, f), etc. Therefore, if the same data was held in both codes, these plots would extremely similar. However, since EVENT shows a generally higher photoflux over all energies, it is safe to assume that the number of photons produced in the EVENT libraries is higher than those in MCNPX. Additionally, if there are fewer removal cross sections, as mentioned, this increase is carried through the calculation. Both of these then can compound into the observed photoflux differences.

Overall, Figures 3.21 through 3.24 show an agreement between the codes on the overall flux profiles, no matter the incident particles.

Although a qualitative comparison is easy, a quantitative measure is more rigorous. The quantitative comparison yields a maximum relative error in the overall flux distribution. For the dual particle case, the neutron and photon fluxes have maximum relative errors of 33 and 29 percent, respectively. The discrepancies are similar for the neutron only case, where the neutron and photon fluxes have a maximum relative error of 37 and 15 percent, respectively. The driver of the higher discrepancies in the neutron fluxes is the discrepancies at very low and very high energy. These differences are less in the photon flux cases as the overall trends are very similar with little to no divergence at the ends of the energy spectrum.

Discrepancies at this level are to be expected, even of 37 percent. This is due to the fact that two codes are using highly different methods, assumptions and data. The trends of each flux spectra are overall fairly consistent, which is promising. Differences in the results could be caused by many factors, as previously mentioned. The first is the inherent physics assumptions in the deterministic transport code. The multigroup approximation is made in energy, which could cause some of the minute details in cross sections and interactions. Additionally, the finite element approximation in space can miss some of the details in spatial heterogeneities. Also, the

isotropic source translation and use can easily cause a slight mismatch in the final resulting flux, due to the scattering of the particles. Finally, the differences in the data supplied to each code could account for many of the discrepancies observed as well. With all these in mind, however, the deterministic method still has its advantages.

The advantages of the deterministic method come mainly in the computation time and effort for the calculation. To get the average flux, it took EVENT 350 times less computational time than with MCNPX. To get within 37 percent in such a small fraction of the time shows the true power of deterministic methods. In fact, the deterministic code could be bolstered with a larger number of energy groups, a finer finite element discretization, and/or a finer angular approximation (all not necessary for this investigation) to bring the results closer if that was needed.

With these flux distributions from each code for the two different cases, CINDER is now ready to be run. As previously noted, the material is "burned" for 30 seconds, followed by 6 seconds of decay time, followed by 1 second more of decay. At that point, the delayed photon spectra is captured for use with the transport codes.

Four different gamma spectra results were found and are displayed in Figure 3.25. As is expected from the flux results, where EVENT generally predicted a higher flux, its delayed gamma spectra are higher. The shapes match extremely well though, as is also expected. The flux is essentially a multiplier on the delayed spectra, so a higher input flux generally will result in a higher spectra. Either way, in the detectable region (>3 MeV), there are plenty of gammas being created.

It is also useful at this point to see what the spectra would look like without irradiation. This will give an idea of how effective the active interrogation can be. The signal that is produced in the activation of the material must overcome this background signal, otherwise no flags may be thrown in the interrogation. Figure 3.26 gives the photon spectra when the material is just decaying – as when using passive methods to interrogate cargo.

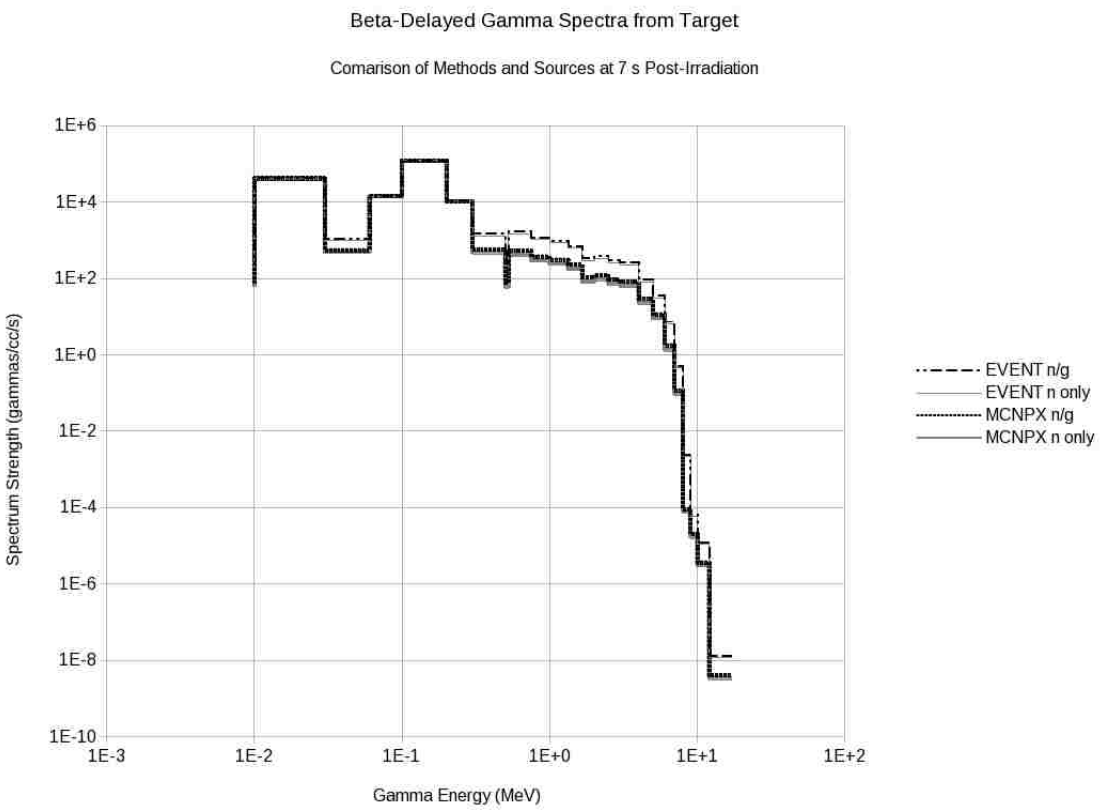

Figure 3.25: Comparison of delayed gamma spectra at 7 seconds post-irradiation calculated by CINDER2008 due to neutron only or dual neutron/photon sources as transported by MCNPX and EVENT. The spectra is as emitted from the U_3O_8 target volume.

As can be seen in the figure, little to no photons are being released in the 3-6 MeV range, the range that is being monitored after irradiation. This shows that neutron and/or photon irradiation holds promise for detection.

Now that the photon spectra have been determined, it can be re-transported out of the cargo and to the detecting surface. By doing this, it shows the potential amount of measurable radiation coming from the interrogation. This source was modeled in both MCNPX and EVENT to track the outgoing current along the detection face. This result can then be compared and contrasted with the experimental result, as-

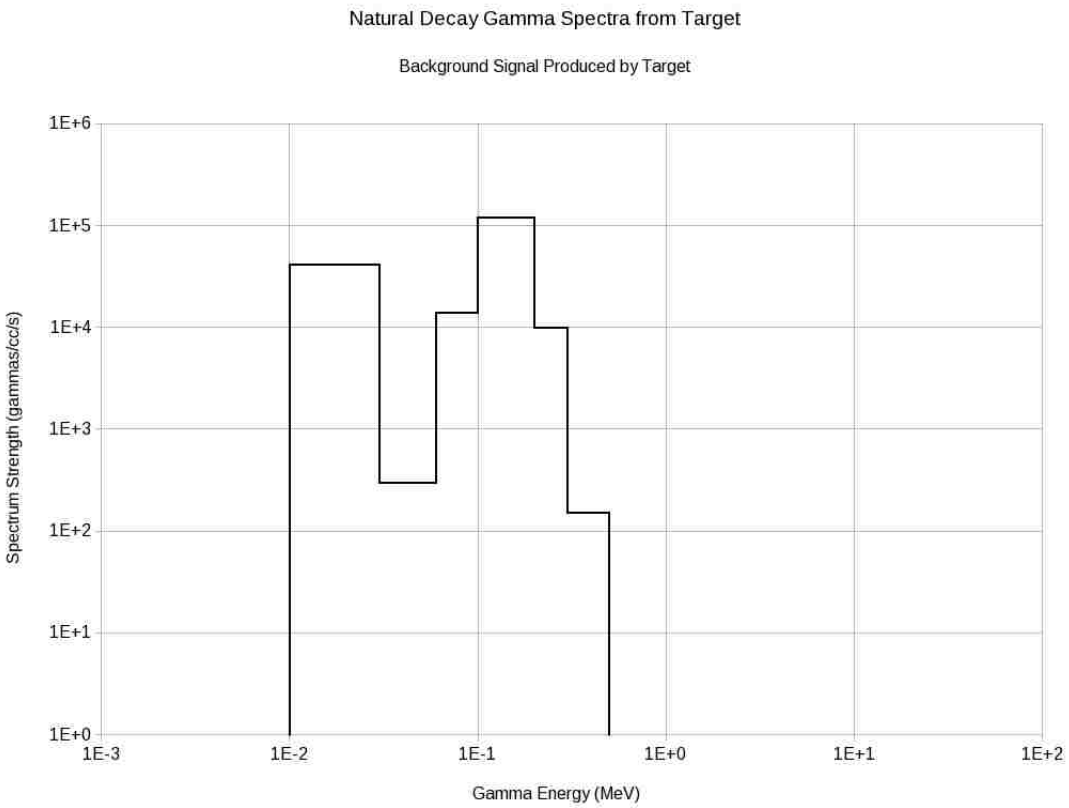

Figure 3.26: Delayed gamma signal produced by the natural decay of uranium in the U_3O_8 target as a constant background signal.

suming a certain detector efficiency.

The experimental results for this value, as presented by Slaughter [84], are not explicitly given. However, they can be extracted from a graph. The value as extracted through this method, at the 6 second post-irradiation mark, is approximately 60 photons per second (approximately 40 photons per second after a background correction). As this data was determined from a graphical representation, it should be assumed to have a high uncertainty, approximately 20%. So long as the calculated values are of the correct order of magnitude, they are assumed to match well. This is especially true due to the assumption of the detector efficiency.

The following table, Table 3.13, gives a summary of the results from these calculations. This table assumes a 30% detector efficiency for both the MCNPX and EVENT models. This means that the current across the detector face of the cargo was multiplied by $^{3}/_{10}{}^{ths}$ to give an approximate detection rate.

The results in Table 3.13 are the ultimate outcome and measure of the active interrogation. These numbers represent the total signal that is observed by the detector. In comparison to the experimental results, the neutron only cases for both MCNPX and EVENT are comparable, off by 8.7 and 135 percent, respectively. Considering the uncertainty experimental result and detector efficiency, matching to about a factor of two is promising, even with all the approximations made with the EVENT model. Note also that the EVENT model is 2D, so there is no leakage through the top and bottom of the cargo. These values for the neutron only case are of the correct order and are therefore taken as a correct representation of the system.

Table 3.13: Detected photons as calculated by EVENT and MCNPX at 7 seconds post-irradiation. Assumes 30% detector efficiency for all photons. Experiment measured approximately 40 photons per second.

(in photons per second)	MCNPX	EVENT
Neutron only case	43.47	94.02
Dual source case	54.55	108.41

Just as important as the comparison to the experimental results is the comparison of the single and dual particle beams. This comparison shows how effective the photon beam was in causing further fission, leading to more detectable signal. For the MCNPX and EVENT models, the addition of the photon beam led to a 20.31 and 15.29 percent increase in the detectable signal, respectively. This is a measurable difference, especially considering the much lower cross sections for the photonuclear reactions.

This increase in the total detectable radiation in the 3-6 MeV range shows that the dual particle beam can make a difference, especially when the cargo material is highly neutron scattering. Hence, a dual particle active interrogation scheme has a great

advantage over a single particle beam.

It is worthwhile to note also the computational times for each set of problems. These are given in Table 3.14[3]. Note that this is the total computational time for the problem run in TINDER, which includes the initial transport, the CINDER calculation, and the final transport model. As can be seen, the EVENT models were by far much less computationally expensive than the MCNPX models. A savings on these problems of approximately 7 hours is huge considering this is simply a scoping problem. Dozens of these could be run with different target and cargo materials, making the expensive MCNPX runs add up quickly. As the final results are comparable to both the experiment and rigorous MCNPX runs, the calculations with EVENT are the best suited for this model.

Table 3.14: Computer time required for full TINDER demonstration calculation.

(in seconds)	MCNPX	EVENT
Neutron only case	17901.9	76.13
Dual source case	18174.6	68.22

3.2.3 Sensitivity Analysis on CINDER2008

A byproduct of the research listed in Section 3.2.2 is the need to have a handle on the sensitivity of the transmutation calculation to the input flux. As the Monte Carlo calculations are expensive, it would be best to be able to run deterministic transport codes to find the volume averaged flux. From the results of the demonstration problem, it appears as if the output spectra from CINDER are not highly sensitive to the input flux. This assertion is to be qualified.

In order to perform the sensitivity analysis, a proper method is needed to vary the input flux, run the CINDER calculation, and track the final results. The DAKOTA

[3]As calculated on the same machine running Fedora 13 Linux, 8GB of memory, and 4 dual core processors.

code from Sandia National Laboratories [87] is well suited for this type of problem. Although designed for massively parallel computations and hundreds of varied inputs used to perform an uncertainty quantification, it is still more than capable of handling a relatively simple sensitivity analysis study. Effectively, Dakota is a wrapper around a "black-box" program. It will send the program a randomized input parameter and will read back response functions that measure the effect of that randomization. Based on the input and response, the sensitivity of the calculation can be determined.

The demonstration problem was chosen as the standard model for the sensitivity analysis to keep in line with the discussion previously. Additionally, as the investigation is into CINDER's sensitivity to the flux inputs, there is no need to run the transport calculation each time. A standard neutron and photon flux is all that is necessary, as it can be subsequently perturbed for the study. Therefore, the MCNPX dual beam model from the previous section was used as the standard. A perturbation is then imposed on that flux.

Now, a fluctuation must be introduced on the flux for each iteration. For this study, a 10 percent maximum individual bin perturbation was used. Therefore, the iteration is assigned a random multiplicative value between -10 and 10 percent. Each bin was then perturbed by a random amount in the range of 0 to that multiplicative value (an introduction of random noise with a maximum value). This led to a perturbed flux distribution which was then used in CINDER. Five hundred iterations were performed to properly characterize the sensitivity. Figure 3.27 gives a graphical example of how this perturbation allocation works.

Not only does a method have to be defined for the inputs, but some sort of metric must be devised to measure its ultimate effect on the output. Since the output in question is the delayed photon spectra at 6 to 7 seconds post-irradiation, the metric is built around that vector. As it is not a scalar quantity, the metric is the L2 norm of the relative error between spectra bin values (unperturbed/standard to perturbed

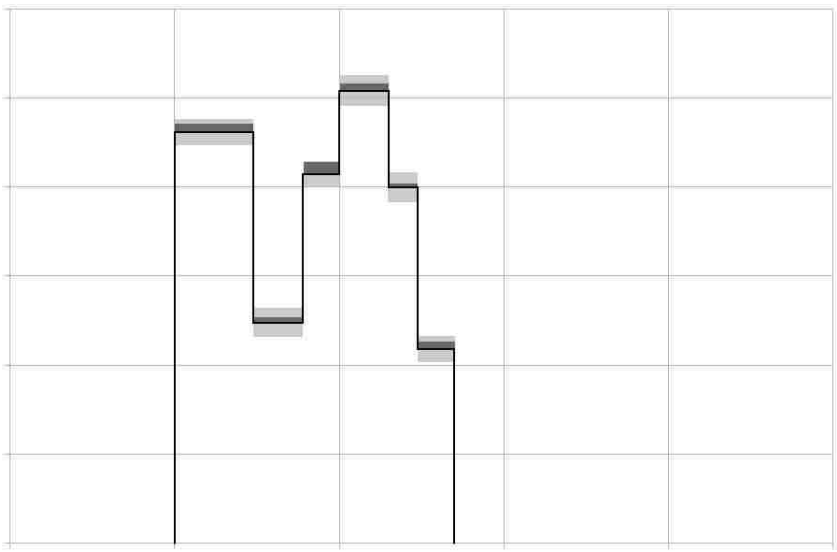

Figure 3.27: Example of how the perturbation is allocated for each group. The light grey region about the black multigroup flux denotes the range that the flux can be perturbed (in one selected direction only). The dark grey denotes the selected value within that range for that bin.

result). This relative error gives a vector of differences, which can then be manipulated. For the L2 norm, these values combined in a root mean square fashion, as the error metric was done in the previous section. This gives a single value measuring the distance from the true delayed spectrum value. An additional norm is also given, the L-infinity norm, which gives the maximum difference of a single value over the whole spectrum.

With the input and outputs defined, the Dakota sensitivity analysis was performed. Three separate cases were run: perturb only the neutron flux, perturb only the photoflux and perturb the neutron and photon fluxes independently but simultaneously. These three cases therefore will show the effect of noise or uncertainty in the fluxes on the final product, individually and combined.

These results are shown in Figures 3.28 through 3.31.

Quite a bit of information can be deduced from these results. To do so, it is necessary

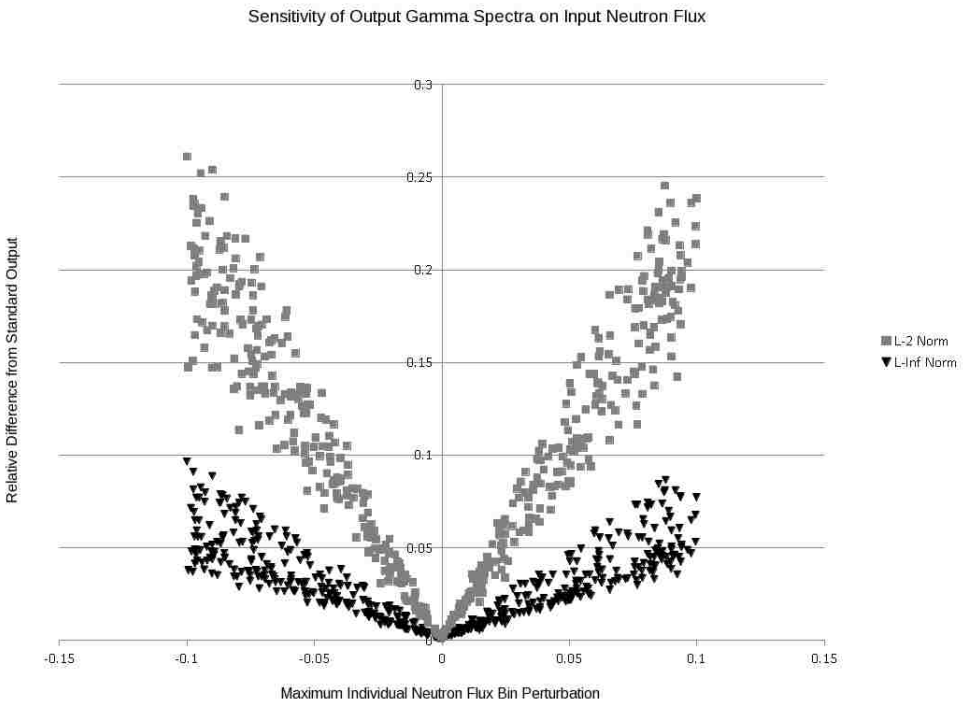

Figure 3.28: Distribution of the error (as measured by norms) due to a random perturbation of the input neutron flux in CINDER2008.

to discuss each plot individually. It should be noted that although a continuum might be anticipated to a norm of zero, due to the numerical precision in CINDER2008 and the probability of getting 25 random zero perturbations, this continuum is not observed with the 500 iterations performed.

Figure 3.28 shows the response of the output beta delayed gamma spectra on the perturbations of the neutron flux. First, the banded nature of the plot is due to the fact that a range was available at each level in terms of the amount of perturbation allowed. If only the maximum was applied to each bin, a single linear response would be observed because that would simply be a multiplier on the entire flux. The grey squares on the plot denote the overall effect of the perturbations. These are based on the L2 norm. The black triangles give the maximum individual response, the L-∞

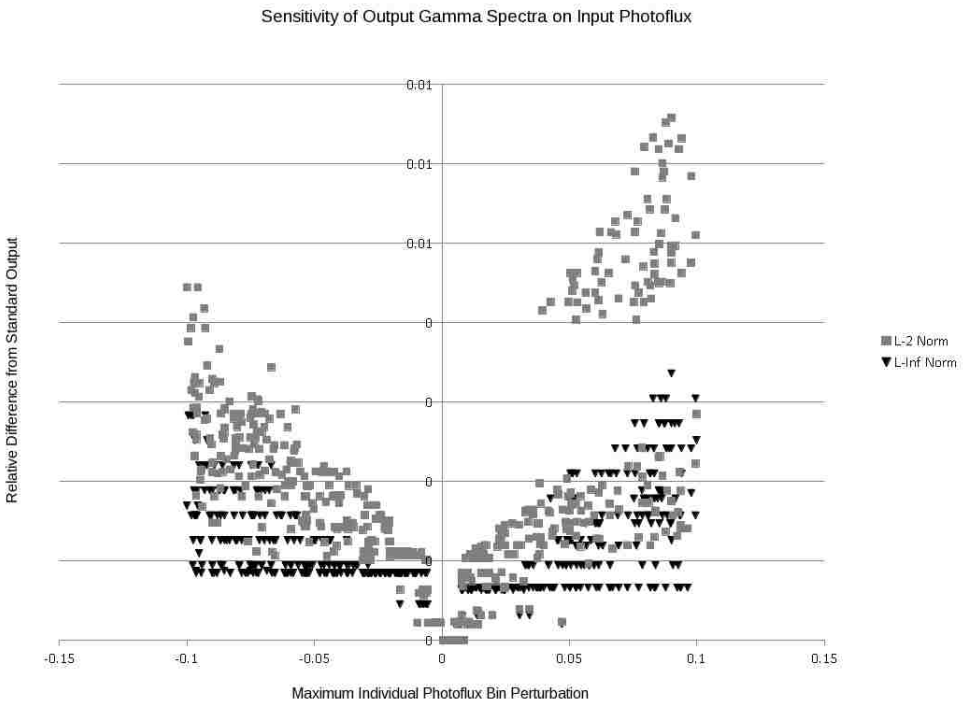

Figure 3.29: Distribution of the error (as measured by norms) due to a random perturbation of the input photoflux in CINDER2008.

norm. The plot shows that the individual effect, on average, is linear and approximately a 5% offset per 10% input perturbation. This is true in both the positive and negative directions.

Overall, the effect of a perturbed neutron flux on the total spectra are approximately 20% per 10% perturbation. Therefore a the uncertainty can be doubled on the whole through the calculation if it is input incorrectly. On the other hand, individual points only take approximately half the uncertainty that was input. Although not dramatically sensitive, the output gamma spectra are sensitive to the neutron flux that is input for this case.

Moving onto the photoflux sensitivity, Figure 3.29 shows the same results but this time for a perturbed photoflux, while holding the neutron flux at the constant level.

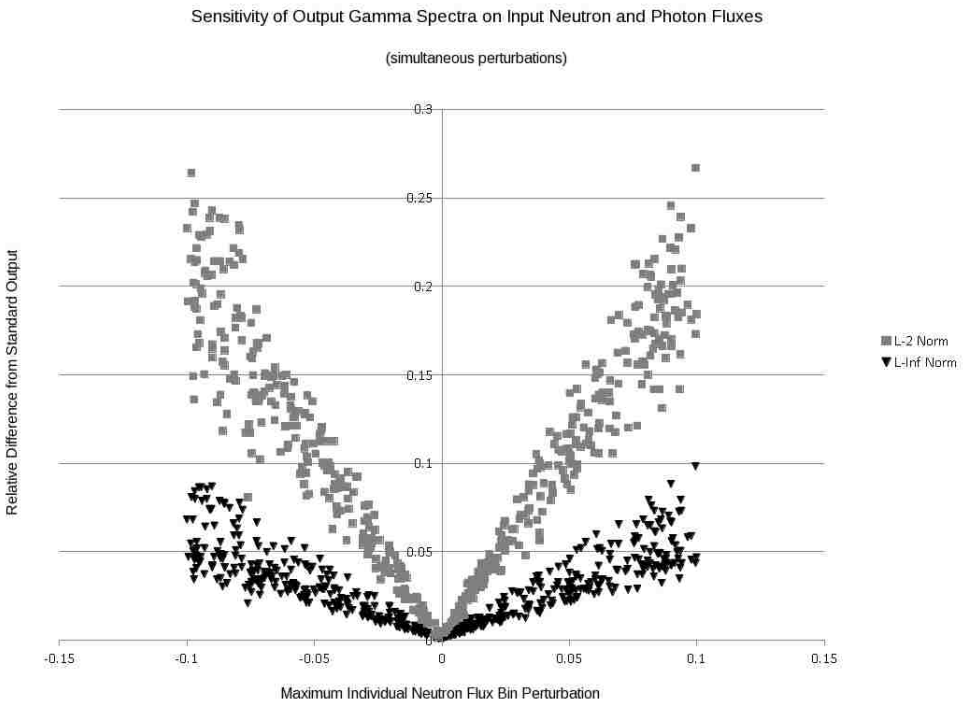

Figure 3.30: Distribution of the error (as measured by norms) due to independent random perturbations of the input neutron and photon flux in CINDER2008, plotted versus the maximum perturbation of the neutron flux.

The limits were kept the same but a much lower effect is observed. Only approximately a 1% change in the total spectra output is observed with a 10% noise on the photoflux. For individual values it is even lower at about 0.4%. As that is an extremely small effect on the output, this problem is insensitive to the photoflux.

This does bring the need for some discussion, however. First, the main reason of the ineffectiveness of noise on the outcome are the very low photonuclear reaction rate. The cross sections for photonuclear reactions are much much lower than those of neutron induced reactions. Therefore, if the neutron and photon flux are approximately on the same order, the photoflux will have very little effect on the overall behavior of the system (although they still contribute measurably to the active interrogation systematics). This low level effect is especially noticeable in the disjointed nature

Figure 3.31: Distribution of the error (as measured by norms) due to independent random perturbations of the input neutron and photon flux in CINDER2008, plotted versus the maximum perturbation of the photoflux.

of the plot in the positive region. Due to the precision of the numbers input into the calculation, low noise has little or no effect on the actual reactions rates. Once the precision level is reached (as with the positive region with higher perturbation levels), the true continuum of values is observed. This is an issue that begins with how CINDER reads data into memory, and its byproduct is a non-physical result.

The next case is shown in Figures 3.30 and 3.31. For this model, both the neutron and photon fluxes were perturbed independently, with the same two responses being measured. As shown with the individual cases, the response based on the perturbations of the neutron flux is dominant. Similar levels of response are observed as well, approximately 18% and 5% for the total and individual measures, respectively. The same trend is observed as above, while when looking at the response based on

the photon flux fluctuations shows effectively no trend. The response of the system to any perturbations in the photoflux are effectively uncorrelated due to the fact that the neutron induced reactions dominate. Therefore, in the dual particle regime, where perturbations in the neutron and photon fluxes can both be present, it will only be the neutron perturbations that affect the output. Again, the sensitivity is not enormous, but there is a definite response.

Effectively, this sensitivity study shows that for the problem at hand, dual particle active interrogation, the main signal will come from the neutron induced reactions. Therefore, knowing it well is the most important step. For every 10% that the signal differs in all energy bins, a response of around 20% in the total output can be observed. The problem is therefore sensitive to the flux input. However, it is insensitive to the photoflux input, as only a 1% response is observed.

As shown in the demonstration in the previous section, even a large difference in the flux and spectra, the detectable amount of photons are still reasonable. This is especially true when knowing the effect of geometric and physics assumptions associated with those results.

3.2.4 Summary of Code Demonstration

To demonstrate the use of the TINDER code system, a sample problem involving active interrogation of nuclear materials was modeled. This model was based off an experiment performed at Lawrence Livermore National Laboratory which involved neutron interrogation of mock cargo systems. A U_3O_8 target was placed in an array of plywood to simulate a hydrogenous cargo. This is typical of most plastics, furniture, and liquids that are shipped.

In this type of system, the neutrons have a difficult time reaching the target due to scattering off the low-Z material. Therefore, the particles could be highly scattered and shielded versus a higher-Z material (e.g. steel or other heavier materials). To

boost the output, adding a photon source can aid in the fissions occurring, therefore increasing the signal. Photons transport well through light materials (not well through high-Z materials unlike neutrons) and therefore would reach the target better in this situation.

To model this dual particle system, including the decay of the fission products from both neutron- and photon-induced fission, TINDER has been assembled to couple the unique dual particle advances in the CINDER transmutation code with transport methods, namely MCNPX and EVENT. MCNPX is taken as the gold standard Monte Carlo code for the high energy particle modeling and EVENT is taken as a representative deterministic method. Each has their specific purpose: MCNPX can give highly detail results using few physics simplifications but the calculations are expensive, and EVENT can give the general results extremely fast but simplifications are required.

To begin the demonstration, the assumptions and model details were presented. Next, the two transport methods were compared to see the differences in the modeling of the irradiation portion. Once these differences were quantified, the differences in the results from CINDER and the retransport of those delayed gammas could take place.

There were notable differences in the calculated fluxes for the irradiation step. Although general trends were consistent, absolute values were slightly different between codes, especially at high and low neutron energies. Overall, the neutron flux spectra were up to 37% between the two codes, mainly due to the mentioned discrepancies. The photoflux results were closer, a maximum difference of 29% between the two results was observed. This is due to the lack of large discrepancies in the data–there were just general trends for EVENT to be higher in these calculations.

These differences are attributed to several factors. First, the physics simplifications that are done in the even-parity deterministic method are bound to cause slight errors as not everything can be captured. This includes the slowing down of neutrons and

photons, which although general trends were captured, they were not the same as the Monte Carlo results. Additionally the nuclear data can play a big role in these results as well. There are fewer removal cross sections represented in the MATXS data for EVENT than in the ACE data for MCNPX, therefore causing higher photofluxes. Other differences could lie in the spatial discretization of the deterministic method as well as angular representation. Overall, though, the simulation results are in agreement.

After that comparison, the transmutation calculation took place. Each transport code's results caused slight differences in the output beta-delayed gamma spectra, but again, trends were all matched. The signal is dominated by the low energy natural decay of the uranium, but in the high energy, fission product decay range, the trends were well matched between all methods. As expected, the introduction of a second beam causes the output signal to increase, especially in the region of interest. This increase is generally caused by the introduction of photofission into the system, even though it is of a low reaction rate compared to others.

Those spectra was then modeled to be retransported out of the system at the time step of 6 to 7 seconds post-irradiation. This was captured in the experiment and allows for the initial background signals to die off. What is left is the signal that should be captured to see if there is special nuclear material in the cargo. This is then modeled again in MCNPX and EVENT to see the response on a face where detectors would be located. These values, along with an assumed detector efficiency, can then be compared to the measured value.

For EVENT, the results are slightly high in terms of the detection rate of photons. This can be attributed to several factors. One could be the assumed detector efficiency, which was 30%. Another could be the fact that the whole calculation showed a trend on the high side for photofluxes, which could be causing the detection rate to also be high. Finally, and perhaps most importantly, the model is based on a 2D (infinite in the vertical direction) representation of the experiment. Therefore, any

leakage that would be seen through the top and bottom of the cargo is not taken into account. This could easily cause the signal to be much higher than what was experimentally measured. Whatever the cause, the dual particle system caused an increase of 15% in the simulation output signal – a good reason to use this method in a real world situation.

For MCNPX, the results match extremely well. Only a few percent error was observed between the MCNPX model and the experimental results, even while assuming a 30% detector efficiency. Additionally, a slightly larger increase in the signal was seen when switching to a dual particle beam, increasing the detected rate by 20.31%. This is a huge increase and the models confirm the worth of this method.

In the end, both methods show promise for this type of modeling. TINDER performed well for this system, keeping human interaction to a minimum and allowing for these calculations to be run in just over a minute using the deterministic transport method. If higher precision is required, MCNPX can be used, but the effort takes nearly 7 hours to process. Either method is suggested depending on the activity at hand. If a simple scoping exercise is needed to provide results quickly, EVENT should be used. For a large calculation where precision is desired over computational time, MCNPX is the better option.

Chapter 4

Conclusions and Further Work

Recently, a need for dual neutral particle transmutation modeling capabilities has arisen. As there has been no previous need for anything more than neutron induced transmutation modeling, a method was needed to fill this need. Additionally, for these programs to fully function, they need the volume averaged scalar flux to be calculated using a dual particle transport code. Therefore, not only is there a need for a dual particle transmutation capability, but it would be best to at the same time couple this directly to a transport code. That was the goal of this research.

The ground work has been laid for this research, beginning with the background and history of existing transmutation methods, photonuclear reactions, and coupled transmutation/transport modeling. From this review, it was found that there is currently no tool that has the capability of modeling the activation and depletion due to photons, let alone photons and neutrons simultaneously. Additionally, there are very limited instances of coupling transport methods to burnup calculations, with the even parity method yet to be used. By doing that coupling with the even parity transport and dual particle transmutation codes, a truly unique tool has been created in the form of the driver code TINDER. Not only has it been coupled to this unique transport method, though, it has been coupled also to a gold standard

in high energy Monte Carlo transport methods, MCNPX. This enables TINDER to calculate not only quick scoping models with EVENT and CINDER, but also high fidelity models with MCNPX and CINDER.

This has not come without some road blocks along the way. First, the data for photonuclear reactions is limited. Evaluated cross section data does exist, in limited quantities, and can easily be formatted into a CINDER library for absorption induced transmutation reactions. Fission product yield data for photofission does not exist in an evaluated form, however. Therefore, a choice had to be made between using unevaluated data sets strewn through journals over the last 50 years or using translated neutron yield data.

It turns out that translating the product yield data from one incident particle to another has been considered before in research, showing that alpha particle induced fission and neutron induced fission have product yields that only differ above 25 MeV, when secondary reactions come into play. Through this translation in energy and mass, a full library could be created for the CINDER code from Los Alamos National Laboratory to handle both neutrons and photons simultaneously (along with some code modifications). This library and method was thoroughly validated and verified versus experimental data, showing that the translation was correct and matched existing, unevaluated data.

Once a dual particle transmutation code had been created, CINDER2008, it then had to be coupled to a transport code to keep human hands off the calculation as much as possible. This also allows for many iterations to take place between the codes for burn-up or similar modeling. The TINDER driver code was created to do just this. It couples a transport code (through a user created wrapper) to CINDER, while keeping track of input files and fluxes, material inventories, and delayed gamma spectra at each step of the calculation.

To verify and demonstrate TINDER, a model was developed that could be compared to real world calculations. As the driver of this research was dual particle active in-

terrogation of cargo, this was the sample problem chosen. No experiments exist for dual particle sources, so using an incident neutron only case along with the validation that had been done of the dual particle portion of CINDER, modeling was able to move forward by verifying single particle source results. After that verification had taken place, a dual incident particle model was created and proved to be fruitful. This regime was able to produce over 15% more photons in the output signal versus the neutron only case.

Not only was a demonstration done in terms of a sample problem, but it was shown that a sensitivity analysis on CINDER was a good idea. Due to the inconsistencies that will always be present between transport codes in calculating the fluxes, CINDER was tested to see how sensitive it would be to perturbations in the flux. In the active interrogation sample problem, the output beta delayed gamma signal was sensitive to variations in the neutron flux, in fact a 10% overall noise in the data could produce a 20% different output spectra. On the other hand, it was extremely insensitive to the photoflux, producing only a 5% difference in the output due to a 10% noise. This sensitivity analysis shows that to properly characterize the problem, the neutron flux for active interrogation is the most important parameter. Through the demonstration problem, though, the flux differences and their effect were shown to not effect the results to the point of non-physicality.

Overall, this research has yielded several unique capabilities. First, the dual particle transmutation code, including the physics translation and validation, is a modeling capability not yet seen. Also, to date there has been no even parity transport method coupled to transmutation. TINDER has accomplished this coupling with no human interaction once started. Additionally, TINDER has brought the first instance of a dual particle coupled transmutation/transport method and has been demonstrated on active interrogation systems. Finally, a sensitivity analysis has been performed on the input to CINDER in terms of the neutron and photon fluxes.

All of this research has come together to fulfill the goal set out at the start – a dual

particle transmutation code coupled to dual particle transport for both scoping and high fidelity modeling.

Although this research has addressed the questions at hand, there is further work that can be done to extend it. One large improvement can be done in the way of fission product yield data. An evaluation of the existing photofission product yields could be performed to possibly improve this data, or at least allow for the use of non-translated data. This would take a large effort and knowledge of how fission product yield evaluations have been performed. A supplement to the current library would be a useful addition.

Additional work could be done in the way of cross section data. Although there is existing data in the library, information is given for about half the nuclides that are given in neutron data. This would require experimental work to fill in the data gaps, but would greatly enhance the results in CINDER2008 by covering more physics. Similar to the fission product yield data, an evaluation would be necessary before this data is used in the code. This was evident in the current research with the ^{238}Np validation case, where a fission product yield set was populated from the translation, but there was no evaluated cross section data.

Another item that would be useful for future efforts is the inclusion of other particles, for example protons, alpha particles, etc., in the transmutation calculation. This would allow for a greater understanding of the large contributors to the transmutation of the media. A difficulty in this would be properly defining the fluxes for these particles as their transport is more difficult to model than neutral particles like neutrons and photons. Additional difficulty would come in the population of the cross section and fission product yield libraries.

A further extension of this work would be the extension of TINDER to other applications, like reactor burn-up. Transport scripts have been written for this purpose but have not been included in this work as it was not the thrust of the effort. Their

comparison to other methods could be done to allow reactor calculations to be performed with EVENT/CINDER in little computational time.

Finally, it would be useful to focus on improvements to the transport side of the code suite. By using deterministic adjoint calculations to improve the biasing of the Monte Carlo calculation, the final calculation could combine the speed of deterministic transport with the fidelity of Monte Carlo methods. This could happen external to the TINDER code, then be brought in once the method is stable. This speed-up is just one method that could be used to improve the transport calculation. Any number of these improvements could be performed to enhance the overall method.

Appendices

Appendix A

Tabulated Photofission Validation Results

The tables in the following sections give the tabular data for the photofisison yield validation presented in Sections 3.1.3 through 3.1.6.

A.1 ^{235}U Photofission Validation Tabulated Results

Table A.1: Photofission yield results for ^{235}U, experiment[1] versus CINDER (6 MeV), 9.7 MeV excitation

Atomic Mass Number	CINDER Yield Fraction	Experimental Yield Fraction	Exerpimental Uncertainty
64	1.77678E-09	-	-
65	1.37242E-10	-	-
66	3.93154E-06	-	-
67	9.34297E-06	-	-
68	2.68236E-05	-	-
69	6.20254E-05	-	-
70	2.06301E-04	-	-
71	5.15715E-04	-	-
72	6.34572E-04	-	-
73	1.07589E-03	-	-
74	4.16541E-03	-	-
75	1.17473E-02	-	-
76	2.60977E-02	-	-
77	5.67596E-02	-	-
78	8.87878E-02	9.50000E-02	4.70000E-02
79	1.44586E-01	-	-
80	2.16871E-01	-	-
81	3.61386E-01	-	-
82	6.53772E-01	-	-
83	1.20761E+00	-	-
84	1.97357E+00	1.18000E+00	1.30000E-01
85	2.16983E+00	1.74000E+00	1.20000E-01
86	3.48165E+00	-	-
87	2.99717E+00	2.94000E+00	2.50000E-01
88	3.96142E+00	3.88000E+00	2.10000E-01
89	5.39372E+00	4.55000E+00	2.40000E-01
90	6.03856E+00	-	-
91	6.42321E+00	5.91000E+00	2.50000E-01
92	6.11191E+00	6.02000E+00	3.70000E-01
93	6.15287E+00	6.17000E+00	5.00000E-01
94	6.42119E+00	6.73000E+00	4.80000E-01
95	6.33396E+00	6.41000E+00	3.60000E-01
96	6.22559E+00	-	-
97	6.07224E+00	6.02000E+00	3.10000E-01
98	5.73079E+00	-	-

Table A.2: Photofission yield results for ^{235}U, experiment[1] versus CINDER (6 MeV), 9.7 MeV excitation, continued

Atomic Mass Number	CINDER Yield Fraction	Experimental Yield Fraction	Exerpimental Uncertainty
99	5.07674E+00	5.58000E+00	2.60000E-01
100	4.13729E+00	-	-
101	3.39360E+00	4.10000E+00	2.50000E-01
102	2.66947E+00	-	-
103	2.41715E+00	2.74000E+00	2.30000E-01
104	1.32089E+00	1.66000E+00	1.30000E-01
105	1.23805E+00	1.03000E+00	7.00000E-02
106	4.28870E-01	-	-
107	2.68342E-01	-	-
108	1.86006E-01	-	-
109	1.22451E-01	-	-
110	1.03608E-01	-	-
111	5.81439E-02	-	-
112	7.22373E-02	2.10000E-01	4.30000E-02
113	5.97338E-02	-	-
114	5.88602E-02	-	-
115	6.85241E-02	1.80000E-01	2.40000E-02
116	5.67781E-02	-	-
117	5.47708E-02	-	-
118	5.47881E-02	-	-
119	5.97648E-02	-	-
120	6.46443E-02	-	-
121	6.96114E-02	-	-
122	8.16007E-02	-	-
123	9.94825E-02	2.18000E-01	4.00000E-02
124	1.19469E-01	-	-
125	1.56503E-01	-	-
126	2.59172E-01	-	-
127	3.88869E-01	8.49000E-01	6.30000E-02
128	6.47380E-01	-	-
129	1.61642E+00	-	-
130	2.54068E+00	-	-
131	3.73564E+00	4.02000E+00	3.30000E-01
132	4.36453E+00	4.73000E+00	1.90000E-01
133	6.46505E+00	5.83000E+00	3.00000E-01

Table A.3: Photofission yield results for ^{235}U, experiment[1] versus CINDER (6 MeV), 9.7 MeV excitation, continued

Atomic Mass Number	CINDER Yield Fraction	Experimental Yield Fraction	Exerpimental Uncertainty
134	5.75234E+00	5.96000E+00	2.40000E-01
135	5.57971E+00	6.59000E+00	2.80000E-01
136	6.49079E+00	-	-
137	5.86468E+00	-	-
138	6.58721E+00	-	-
139	6.00297E+00	-	-
140	5.78625E+00	5.90000E+00	2.00000E-01
141	6.50719E+00	5.73000E+00	3.20000E-01
142	5.98960E+00	5.03000E+00	3.70000E-01
143	6.14341E+00	4.72000E+00	3.80000E-01
144	5.44415E+00	-	-
145	3.98901E+00	-	-
146	3.07189E+00	2.20000E+00	1.60000E-01
147	2.01785E+00	1.86000E+00	1.30000E-01
148	1.43412E+00	-	-
149	1.03579E+00	8.60000E-01	8.00000E-02
150	6.37116E-01	-	-
151	3.18077E-01	4.85000E-01	5.00000E-02
152	2.48648E-01	-	-
153	1.48757E-01	-	-
154	8.05581E-02	-	-
155	5.07201E-02	-	-
156	2.08842E-02	-	-
157	1.09373E-02	-	-
158	6.36522E-03	-	-
159	2.08902E-03	-	-
160	1.09548E-03	-	-
161	4.38053E-04	-	-
162	1.59075E-04	-	-
163	4.97655E-05	-	-
164	2.88882E-05	-	-
165	9.45626E-06	-	-
166	2.48979E-06	-	-
167	5.96633E-07	-	-
168	2.68123E-07	-	-

Table A.4: Photofission yield results for ^{235}U, experiment[1] versus CINDER (6 MeV), 9.7 MeV excitation, continued

Atomic Mass Number	CINDER Yield Fraction	Experimental Yield Fraction	Exerpimental Uncertainty
169	9.44820E-08	-	-
170	2.48358E-08	-	-
171	7.95911E-09	-	-
172	1.19210E-09	-	-

Table A.5: Photofission yield results for ^{235}U, experiment[1] versus CINDER (6 MeV), 11.6 MeV excitation

Atomic Mass Number	CINDER Yield Fraction	Experimental Yield Fraction	Exerpimental Uncertainty
64	1.77678E-09	-	-
65	1.37242E-10	-	-
66	3.93154E-06	-	-
67	9.34297E-06	-	-
68	2.68236E-05	-	-
69	6.20254E-05	-	-
70	2.06301E-04	-	-
71	5.15715E-04	-	-
72	6.34572E-04	-	-
73	1.07589E-03	-	-
74	4.16541E-03	-	-
75	1.17473E-02	-	-
76	2.60977E-02	-	-
77	5.67596E-02	-	-
78	8.87878E-02	9.60000E-02	3.30000E-02
79	1.44586E-01	-	-
80	2.16871E-01	-	-
81	3.61386E-01	-	-
82	6.53772E-01	-	-
83	1.20761E+00	-	-
84	1.97357E+00	1.44000E+00	1.90000E-01
85	2.16983E+00	1.90000E+00	1.40000E-01
86	3.48165E+00	-	-
87	2.99717E+00	3.21000E+00	2.50000E-01
88	3.96142E+00	3.88000E+00	1.60000E-01
89	5.39372E+00	4.74000E+00	2.50000E-01
90	6.03856E+00	-	-
91	6.42321E+00	5.73000E+00	2.50000E-01
92	6.11191E+00	5.76000E+00	3.00000E-01
93	6.15287E+00	6.14000E+00	5.00000E-01
94	6.42119E+00	6.44000E+00	4.80000E-01
95	6.33396E+00	6.33000E+00	2.80000E-01
96	6.22559E+00	-	-
97	6.07224E+00	5.71000E+00	3.00000E-01
98	5.73079E+00	-	-

Table A.6: Photofission yield results for ^{235}U, experiment[1] versus CINDER (6 MeV), 11.6 MeV excitation, continued

Atomic Mass Number	CINDER Yield Fraction	Experimental Yield Fraction	Exerpimental Uncertainty
99	5.07674E+00	5.29000E+00	2.20000E-01
100	4.13729E+00	-	-
101	3.39360E+00	4.18000E+00	2.40000E-01
102	2.66947E+00	-	-
103	2.41715E+00	2.67000E+00	1.90000E-01
104	1.32089E+00	1.77000E+00	1.50000E-01
105	1.23805E+00	1.24000E+00	7.00000E-02
106	4.28870E-01	-	-
107	2.68342E-01	-	-
108	1.86006E-01	-	-
109	1.22451E-01	-	-
110	1.03608E-01	-	-
111	5.81439E-02	-	-
112	7.22373E-02	3.10000E-01	3.20000E-02
113	5.97338E-02	3.07000E-01	4.90000E-02
114	5.88602E-02	-	-
115	6.85241E-02	2.95000E-01	2.90000E-02
116	5.67781E-02	-	-
117	5.47708E-02	-	-
118	5.47881E-02	-	-
119	5.97648E-02	-	-
120	6.46443E-02	-	-
121	6.96114E-02	-	-
122	8.16007E-02	-	-
123	9.94825E-02	3.08000E-01	7.30000E-02
124	1.19469E-01	-	-
125	1.56503E-01	4.54000E-01	9.10000E-02
126	2.59172E-01	-	-
127	3.88869E-01	9.16000E-01	5.50000E-02
128	6.47380E-01	1.38000E+00	1.30000E-01
129	1.61642E+00	-	-
130	2.54068E+00	-	-
131	3.73564E+00	4.16000E+00	2.50000E-01
132	4.36453E+00	4.79000E+00	1.80000E-01
133	6.46505E+00	5.55000E+00	2.80000E-01

Table A.7: Photofission yield results for ^{235}U, experiment[1] versus CINDER (6 MeV), 11.6 MeV excitation, continued

Atomic Mass Number	CINDER Yield Fraction	Experimental Yield Fraction	Exerpimental Uncertainty
134	5.75234E+00	5.88000E+00	2.00000E-01
135	5.57971E+00	6.19000E+00	2.60000E-01
136	6.49079E+00	-	-
137	5.86468E+00	-	-
138	6.58721E+00	-	-
139	6.00297E+00	-	-
140	5.78625E+00	5.62000E+00	2.10000E-01
141	6.50719E+00	5.45000E+00	3.70000E-01
142	5.98960E+00	5.22000E+00	3.90000E-01
143	6.14341E+00	4.40000E+00	3.10000E-01
144	5.44415E+00	3.50000E+00	5.20000E-01
145	3.98901E+00	-	-
146	3.07189E+00	2.24000E+00	1.40000E-01
147	2.01785E+00	1.64000E+00	1.20000E-01
148	1.43412E+00	-	-
149	1.03579E+00	8.11000E-01	9.90000E-02
150	6.37116E-01	-	-
151	3.18077E-01	4.73000E-01	4.10000E-02
152	2.48648E-01	-	-
153	1.48757E-01	2.07000E-01	2.80000E-02
154	8.05581E-02	-	-
155	5.07201E-02	-	-
156	2.08842E-02	-	-
157	1.09373E-02	-	-
158	6.36522E-03	-	-
159	2.08902E-03	-	-
160	1.09548E-03	-	-
161	4.38053E-04	-	-
162	1.59075E-04	-	-
163	4.97655E-05	-	-
164	2.88882E-05	-	-
165	9.45626E-06	-	-
166	2.48979E-06	-	-
167	5.96633E-07	-	-
168	2.68123E-07	-	-

Table A.8: Photofission yield results for ^{235}U, experiment[1] versus CINDER (6 MeV), 11.6 MeV excitation, continued

Atomic Mass Number	CINDER Yield Fraction	Experimental Yield Fraction	Exerpimental Uncertainty
169	9.44820E-08	-	-
170	2.48358E-08	-	-
171	7.95911E-09	-	-
172	1.19210E-09	-	-

Table A.9: Photofission yield results for ^{235}U, experiment[1] versus CINDER(20 MeV), 14.1 MeV excitation

Atomic Mass Number	CINDER Yield Fraction	Experimental Yield Fraction	Exerpimental Uncertainty
64	5.95601E-07	-	-
65	1.33857E-08	-	-
66	4.47395E-04	-	-
67	1.05648E-03	-	-
68	1.47032E-03	-	-
69	2.06106E-03	-	-
70	3.43327E-03	-	-
71	5.29594E-03	-	-
72	1.04271E-02	-	-
73	1.48113E-02	-	-
74	2.26788E-02	-	-
75	3.42713E-02	-	-
76	5.50655E-02	-	-
77	8.38328E-02	-	-
78	1.35466E-01	1.35000E-01	2.70000E-02
79	2.06208E-01	-	-
80	2.60130E-01	-	-
81	4.73007E-01	-	-
82	8.28267E-01	-	-
83	1.17497E+00	-	-
84	1.50725E+00	1.35000E+00	1.90000E-01
85	2.31160E+00	1.95000E+00	1.40000E-01
86	2.25613E+00	-	-
87	3.19226E+00	2.84000E+00	2.10000E-01
88	3.76405E+00	3.63000E+00	1.50000E-01
89	4.30299E+00	4.39000E+00	2.20000E-01
90	4.70745E+00	-	-
91	5.00145E+00	5.64000E+00	2.40000E-01
92	5.18490E+00	5.80000E+00	3.20000E-01
93	5.04070E+00	5.91000E+00	4.40000E-01
94	5.16751E+00	5.98000E+00	4.30000E-01
95	5.03188E+00	6.18000E+00	2.70000E-01
96	5.29306E+00	-	-
97	5.07238E+00	5.55000E+00	2.90000E-01
98	4.82679E+00	-	-

Table A.10: Photofission yield results for ^{235}U, experiment[1] versus CINDER(20 MeV), 14.1 MeV excitation, continued

Atomic Mass Number	CINDER Yield Fraction	Experimental Yield Fraction	Exerpimental Uncertainty
99	4.25552E+00	5.23000E+00	2.40000E-01
100	3.50995E+00	-	-
101	3.16706E+00	3.99000E+00	2.00000E-01
102	2.96973E+00	-	-
103	2.29789E+00	2.73000E+00	2.00000E-01
104	2.08173E+00	1.77000E+00	1.50000E-01
105	2.14024E+00	1.31000E+00	1.10000E-01
106	1.52644E+00	9.53000E-01	1.43000E-01
107	1.23161E+00	-	-
108	1.42043E+00	-	-
109	1.25647E+00	-	-
110	1.42467E+00	-	-
111	1.31787E+00	-	-
112	1.47041E+00	5.68000E-01	4.40000E-02
113	1.30430E+00	5.12000E-01	7.10000E-02
114	1.32484E+00	-	-
115	1.32881E+00	5.22000E-01	4.00000E-02
116	1.17992E+00	-	-
117	1.19230E+00	5.34000E-01	7.10000E-02
118	1.19010E+00	-	-
119	1.17012E+00	-	-
120	1.15048E+00	-	-
121	1.33861E+00	-	-
122	1.22059E+00	-	-
123	1.29961E+00	5.17000E-01	5.10000E-02
124	1.43001E+00	-	-
125	1.61056E+00	7.16000E-01	7.70000E-02
126	2.13486E+00	-	-
127	2.19817E+00	1.17000E+00	6.00000E-02
128	2.50961E+00	1.48000E+00	1.40000E-01
129	3.19224E+00	-	-
130	3.47819E+00	-	-
131	3.70863E+00	4.06000E+00	2.30000E-01
132	5.26158E+00	4.63000E+00	2.10000E-01
133	5.01097E+00	5.46000E+00	2.80000E-01

Table A.11: Photofission yield results for ^{235}U, experiment[1] versus CINDER(20 MeV), 14.1 MeV excitation, continued

Atomic Mass Number	CINDER Yield Fraction	Experimental Yield Fraction	Exerpimental Uncertainty
134	5.54314E+00	5.59000E+00	2.70000E-01
135	5.45936E+00	6.03000E+00	2.50000E-01
136	6.49733E+00	-	-
137	5.03303E+00	6.21000E+00	5.70000E-01
138	5.26202E+00	-	-
139	5.27908E+00	-	-
140	3.93057E+00	5.73000E+00	2.20000E-01
141	3.68137E+00	5.44000E+00	2.90000E-01
142	4.32610E+00	4.78000E+00	3.50000E-01
143	3.28593E+00	4.25000E+00	3.00000E-01
144	2.69541E+00	3.60000E+00	3.00000E-01
145	2.34053E+00	-	-
146	1.91443E+00	2.24000E+00	1.30000E-01
147	1.28241E+00	1.67000E+00	1.10000E-01
148	1.04742E+00	-	-
149	6.22640E-01	8.47000E-01	6.90000E-02
150	4.83258E-01	-	-
151	3.36063E-01	4.08000E-01	3.60000E-02
152	2.37222E-01	-	-
153	1.81964E-01	2.01000E-01	3.40000E-02
154	8.92073E-02	-	-
155	6.42307E-02	-	-
156	4.71195E-02	-	-
157	3.26191E-02	-	-
158	1.97674E-02	-	-
159	1.16376E-02	-	-
160	7.02266E-03	-	-
161	4.55139E-03	-	-
162	2.76810E-03	-	-
163	1.68043E-03	-	-
164	9.89701E-04	-	-
165	5.83335E-04	-	-
166	2.57726E-04	-	-
167	2.07333E-04	-	-
168	1.18622E-04	-	-

Table A.12: Photofission yield results for ^{235}U, experiment[1] versus CINDER(20 MeV), 14.1 MeV excitation, continued

Atomic Mass Number	CINDER Yield Fraction	Experimental Yield Fraction	Exerpimental Uncertainty
169	7.90816E-05	-	-
170	3.89740E-05	-	-
171	2.07542E-05	-	-
172	1.68026E-05	-	-

Table A.13: Photofission yield results for ^{235}U, experiment[1] versus CINDER(20 MeV), 70 MeV endpoint energy

Atomic Mass Number	CINDER Yield Fraction	Experimental Yield Fraction	Exerpimental Uncertainty
64	5.95601E-07	-	-
65	1.33857E-08	-	-
66	4.47395E-04	-	-
67	1.05648E-03	-	-
68	1.47032E-03	-	-
69	2.06106E-03	-	-
70	3.43327E-03	-	-
71	5.29594E-03	-	-
72	1.04271E-02	-	-
73	1.48113E-02	-	-
74	2.26788E-02	-	-
75	3.42713E-02	-	-
76	5.50655E-02	-	-
77	8.38328E-02	-	-
78	1.35466E-01	1.55000E-01	1.90000E-02
79	2.06208E-01	-	-
80	2.60130E-01	-	-
81	4.73007E-01	-	-
82	8.28267E-01	-	-
83	1.17497E+00	-	-
84	1.50725E+00	1.29000E+00	1.40000E-01
85	2.31160E+00	1.81000E+00	1.30000E-01
86	2.25613E+00	-	-
87	3.19226E+00	2.81000E+00	2.10000E-01
88	3.76405E+00	3.55000E+00	1.50000E-01
89	4.30299E+00	4.24000E+00	2.20000E-01
90	4.70745E+00	-	-
91	5.00145E+00	5.36000E+00	2.30000E-01
92	5.18490E+00	5.72000E+00	3.30000E-01
93	5.04070E+00	5.55000E+00	4.00000E-01
94	5.16751E+00	5.95000E+00	4.30000E-01
95	5.03188E+00	6.01000E+00	2.60000E-01
96	5.29306E+00	-	-
97	5.07238E+00	5.27000E+00	2.70000E-01
98	4.82679E+00	-	-

Table A.14: Photofission yield results for ^{235}U, experiment[1] versus CINDER(20 MeV), 70 MeV endpoint energy, continued

Atomic Mass Number	CINDER Yield Fraction	Experimental Yield Fraction	Exerpimental Uncertainty
99	4.25552E+00	5.13000E+00	2.30000E-01
100	3.50995E+00	-	-
101	3.16706E+00	3.98000E+00	2.20000E-01
102	2.96973E+00	-	-
103	2.29789E+00	2.76000E+00	2.00000E-01
104	2.08173E+00	1.84000E+00	1.40000E-01
105	2.14024E+00	1.35000E+00	1.40000E-01
106	1.52644E+00	1.11000E+00	2.40000E-01
107	1.23161E+00	-	-
108	1.42043E+00	-	-
109	1.25647E+00	-	-
110	1.42467E+00	-	-
111	1.31787E+00	-	-
112	1.47041E+00	7.74000E-01	6.00000E-02
113	1.30430E+00	8.08000E-01	8.10000E-02
114	1.32484E+00	-	-
115	1.32881E+00	7.11000E-01	5.10000E-02
116	1.17992E+00	-	-
117	1.19230E+00	7.15000E-01	7.80000E-02
118	1.19010E+00	-	-
119	1.17012E+00	-	-
120	1.15048E+00	-	-
121	1.33861E+00	-	-
122	1.22059E+00	-	-
123	1.29961E+00	-	-
124	1.43001E+00	-	-
125	1.61056E+00	8.47000E-01	7.30000E-02
126	2.13486E+00	-	-
127	2.19817E+00	1.21000E+00	6.00000E-02
128	2.50961E+00	1.48000E+00	1.20000E-01
129	3.19224E+00	-	-
130	3.47819E+00	-	-
131	3.70863E+00	3.93000E+00	2.10000E-01
132	5.26158E+00	4.46000E+00	2.10000E-01
133	5.01097E+00	5.30000E+00	2.80000E-01

Table A.15: Photofission yield results for ^{235}U, experiment[1] versus CINDER(20 MeV), 70 MeV endpoint energy, continued

Atomic Mass Number	CINDER Yield Fraction	Experimental Yield Fraction	Exerpimental Uncertainty
134	5.54314E+00	5.67000E+00	3.70000E-01
135	5.45936E+00	5.80000E+00	2.60000E-01
136	6.49733E+00	-	-
137	5.03303E+00	6.19000E+00	5.30000E-01
138	5.26202E+00	-	-
139	5.27908E+00	-	-
140	3.93057E+00	5.34000E+00	2.30000E-01
141	3.68137E+00	5.18000E+00	3.70000E-01
142	4.32610E+00	4.48000E+00	3.40000E-01
143	3.28593E+00	4.18000E+00	3.00000E-01
144	2.69541E+00	3.62000E+00	2.80000E-01
145	2.34053E+00	-	-
146	1.91443E+00	2.23000E+00	1.30000E-01
147	1.28241E+00	1.60000E+00	9.00000E-02
148	1.04742E+00	-	-
149	6.22640E-01	8.18000E-01	6.00000E-02
150	4.83258E-01	-	-
151	3.36063E-01	4.63000E-01	4.00000E-02
152	2.37222E-01	-	-
153	1.81964E-01	2.15000E-01	3.70000E-02
154	8.92073E-02	-	-
155	6.42307E-02	-	-
156	4.71195E-02	-	-
157	3.26191E-02	-	-
158	1.97674E-02	-	-
159	1.16376E-02	-	-
160	7.02266E-03	-	-
161	4.55139E-03	-	-
162	2.76810E-03	-	-
163	1.68043E-03	-	-
164	9.89701E-04	-	-
165	5.83335E-04	-	-
166	2.57726E-04	-	-
167	2.07333E-04	-	-
168	1.18622E-04	-	-

Table A.16: Photofission yield results for ^{235}U, experiment[1] versus CINDER(20 MeV), 70 MeV endpoint energy, continued

Atomic Mass Number	CINDER Yield Fraction	Experimental Yield Fraction	Exerpimental Uncertainty
169	7.90816E-05	-	-
170	3.89740E-05	-	-
171	2.07542E-05	-	-
172	1.68026E-05	-	-

Table A.17: Photofission yield results for ^{235}U, CINDER(20 MeV), versus ^{234}U(n,f) with 14.8 MeV neutrons [2]

Atomic Mass Number	CINDER Yield Fraction	Experimental Yield Fraction	Exerpimental Uncertainty
64	5.95601E-07	-	-
65	1.33857E-08	-	-
66	4.47395E-04	-	-
67	1.05648E-03	-	-
68	1.47032E-03	-	-
69	2.06106E-03	-	-
70	3.43327E-03	-	-
71	5.29594E-03	-	-
72	1.04271E-02	1.02982E-02	5.82915E-04
73	1.48113E-02	-	-
74	2.26788E-02	-	-
75	3.42713E-02	-	-
76	5.50655E-02	-	-
77	8.38328E-02	-	-
78	1.35466E-01	-	-
79	2.06208E-01	-	-
80	2.60130E-01	-	-
81	4.73007E-01	-	-
82	8.28267E-01	-	-
83	1.17497E+00	-	-
84	1.50725E+00	-	-
85	2.31160E+00	-	-
86	2.25613E+00	-	-
87	3.19226E+00	-	-
88	3.76405E+00	-	-
89	4.30299E+00	-	-
90	4.70745E+00	-	-
91	5.00145E+00	-	-
92	5.18490E+00	-	-
93	5.04070E+00	5.05193E+00	4.85763E-01
94	5.16751E+00	-	-
95	5.03188E+00	5.05193E+00	1.94305E-01
96	5.29306E+00	-	-
97	5.07238E+00	4.91592E+00	2.91458E-01
98	4.82679E+00	-	-

Table A.18: Photofission yield results for ^{235}U, CINDER(20 MeV), versus ^{234}U(n,f) with 14.8 MeV neutrons [2], continued

Atomic Mass Number	CINDER Yield Fraction	Experimental Yield Fraction	Exerpimental Uncertainty
99	4.25552E+00	4.27471E+00	3.88610E-01
100	3.50995E+00	-	-
101	3.16706E+00	-	-
102	2.96973E+00	-	-
103	2.29789E+00	-	-
104	2.08173E+00	-	-
105	2.14024E+00	2.14707E+00	1.74875E-01
106	1.52644E+00	-	-
107	1.23161E+00	-	-
108	1.42043E+00	-	-
109	1.25647E+00	-	-
110	1.42467E+00	-	-
111	1.31787E+00	1.32127E+00	4.85763E-02
112	1.47041E+00	1.47672E+00	9.71525E-02
113	1.30430E+00	-	-
114	1.32484E+00	-	-
115	1.32881E+00	1.30184E+00	1.26298E-01
116	1.17992E+00	-	-
117	1.19230E+00	-	-
118	1.19010E+00	-	-
119	1.17012E+00	-	-
120	1.15048E+00	-	-
121	1.33861E+00	-	-
122	1.22059E+00	-	-
123	1.29961E+00	-	-
124	1.43001E+00	-	-
125	1.61056E+00	-	-
126	2.13486E+00	-	-
127	2.19817E+00	-	-
128	2.50961E+00	-	-
129	3.19224E+00	-	-
130	3.47819E+00	-	-
131	3.70863E+00	-	-
132	5.26158E+00	4.17756E+00	3.88610E-01
133	5.01097E+00	-	-

Table A.19: Photofission yield results for ^{235}U, CINDER(20 MeV), versus ^{234}U(n,f) with 14.8 MeV neutrons [2], continued

Atomic Mass Number	CINDER Yield Fraction	Experimental Yield Fraction	Exerpimental Uncertainty
134	5.54314E+00	-	-
135	5.45936E+00	-	-
136	6.49733E+00	-	-
137	5.03303E+00	4.97421E+00	2.23451E-01
138	5.26202E+00	-	-
139	5.27908E+00	-	-
140	3.93057E+00	3.83753E+00	1.55444E-01
141	3.68137E+00	3.69180E+00	2.91458E-01
142	4.32610E+00	-	-
143	3.28593E+00	3.29347E+00	1.65159E-01
144	2.69541E+00	2.69113E+00	1.94305E-01
145	2.34053E+00	-	-
146	1.91443E+00	-	-
147	1.28241E+00	1.28241E+00	8.74373E-02
148	1.04742E+00	-	-
149	6.22640E-01	-	-
150	4.83258E-01	-	-
151	3.36063E-01	-	-
152	2.37222E-01	-	-
153	1.81964E-01	1.82647E-01	1.45729E-02
154	8.92073E-02	-	-
155	6.42307E-02	-	-
156	4.71195E-02	4.72161E-02	2.13736E-03
157	3.26191E-02	-	-
158	1.97674E-02	-	-
159	1.16376E-02	1.16583E-02	1.16583E-03
160	7.02266E-03	-	-
161	4.55139E-03	4.56617E-03	4.85763E-04
162	2.76810E-03	-	-
163	1.68043E-03	-	-
164	9.89701E-04	-	-
165	5.83335E-04	-	-
166	2.57726E-04	-	-
167	2.07333E-04	-	-
168	1.18622E-04	-	-

Table A.20: Photofission yield results for ^{235}U, CINDER(20 MeV), versus ^{234}U(n,f) with 14.8 MeV neutrons [2], continued

Atomic Mass Number	CINDER Yield Fraction	Experimental Yield Fraction	Exerpimental Uncertainty
169	7.90816E-05	-	-
170	3.89740E-05	-	-
171	2.07542E-05	-	-
172	1.68026E-05	-	-

A.2 ^{238}U Photofission Validation Tabulated Results

Table A.21: Photofission yield results for ^{238}U, experiment[3] versus CINDER (6 MeV), 9.7 MeV excitation

Atomic Mass Number	CINDER Yield Fraction	Experimental Yield Fraction	Exerpimental Uncertainty
64	1.77678E-09	-	-
65	1.37242E-10	-	-
66	3.93154E-06	-	-
67	9.34297E-06	-	-
68	2.68236E-05	-	-
69	6.20254E-05	-	-
70	2.06301E-04	-	-
71	5.15715E-04	-	-
72	6.34572E-04	-	-
73	1.07589E-03	-	-
74	4.16541E-03	-	-
75	1.17473E-02	-	-
76	2.60977E-02	-	-
77	5.67596E-02	-	-
78	8.87878E-02	-	-
79	1.44586E-01	-	-
80	2.16871E-01	-	-
81	3.61386E-01	-	-
82	6.53772E-01	-	-
83	1.20761E+00	-	-
84	1.97357E+00	7.60000E-01	1.40000E-01
85	2.16983E+00	9.30000E-01	6.90000E-02
86	3.48165E+00	-	-
87	2.99717E+00	1.87000E+00	1.40000E-01
88	3.96142E+00	2.27000E+00	1.60000E-01
89	5.39372E+00	3.00000E+00	1.80000E-01
90	6.03856E+00	-	-
91	6.42321E+00	4.41000E+00	1.90000E-01
92	6.11191E+00	4.56000E+00	2.90000E-01
93	6.15287E+00	4.93000E+00	4.30000E-01
94	6.42119E+00	5.52000E+00	4.00000E-01
95	6.33396E+00	5.92000E+00	2.50000E-01
96	6.22559E+00	-	-
97	6.07224E+00	6.03000E+00	3.00000E-01
98	5.73079E+00	-	-

Table A.22: Photofission yield results for ^{238}U, experiment[3] versus CINDER (6 MeV), 9.7 MeV excitation, continued

Atomic Mass Number	CINDER Yield Fraction	Experimental Yield Fraction	Exerpimental Uncertainty
99	5.07674E+00	6.76000E+00	2.80000E-01
100	4.13729E+00	-	-
101	3.39360E+00	5.82000E+00	3.30000E-01
102	2.66947E+00	-	-
103	2.41715E+00	5.61000E+00	4.00000E-01
104	1.32089E+00	3.69000E+00	2.70000E-01
105	1.23805E+00	2.71000E+00	2.80000E-01
106	4.28870E-01	1.74000E+00	1.70000E-01
107	2.68342E-01	-	-
108	1.86006E-01	-	-
109	1.22451E-01	-	-
110	1.03608E-01	-	-
111	5.81439E-02	-	-
112	7.22373E-02	1.15000E-01	2.20000E-02
113	5.97338E-02	-	-
114	5.88602E-02	-	-
115	6.85241E-02	7.50000E-02	7.00000E-03
116	5.67781E-02	-	-
117	5.47708E-02	8.70000E-02	1.10000E-02
118	5.47881E-02	-	-
119	5.97648E-02	-	-
120	6.46443E-02	-	-
121	6.96114E-02	-	-
122	8.16007E-02	-	-
123	9.94825E-02	8.30000E-02	1.50000E-02
124	1.19469E-01	-	-
125	1.56503E-01	-	-
126	2.59172E-01	-	-
127	3.88869E-01	3.07000E-01	1.80000E-02
128	6.47380E-01	-	-
129	1.61642E+00	1.07000E+00	1.30000E-01
130	2.54068E+00	-	-
131	3.73564E+00	3.73000E+00	2.40000E-01
132	4.36453E+00	4.95000E+00	1.60000E-01
133	6.46505E+00	6.80000E+00	3.40000E-01

Table A.23: Photofission yield results for ^{238}U, experiment[3] versus CINDER (6 MeV), 9.7 MeV excitation, continued

Atomic Mass Number	CINDER Yield Fraction	Experimental Yield Fraction	Exerpimental Uncertainty
134	5.75234E+00	6.88000E+00	2.30000E-01
135	5.57971E+00	6.73000E+00	2.80000E-01
136	6.49079E+00	-	-
137	5.86468E+00	6.20000E+00	4.80000E-01
138	6.58721E+00	-	-
139	6.00297E+00	-	-
140	5.78625E+00	6.10000E+00	2.00000E-01
141	6.50719E+00	5.40000E+00	3.80000E-01
142	5.98960E+00	5.07000E+00	4.70000E-01
143	6.14341E+00	4.80000E+00	3.40000E-01
144	5.44415E+00	4.60000E+00	3.20000E-01
145	3.98901E+00	-	-
146	3.07189E+00	3.05000E+00	2.20000E-01
147	2.01785E+00	2.40000E+00	1.70000E-01
148	1.43412E+00	-	-
149	1.03579E+00	1.36000E+00	1.10000E-01
150	6.37116E-01	-	-
151	3.18077E-01	7.92000E-01	6.20000E-02
152	2.48648E-01	-	-
153	1.48757E-01	3.00000E-01	4.70000E-02
154	8.05581E-02	-	-
155	5.07201E-02	-	-
156	2.08842E-02	-	-
157	1.09373E-02	-	-
158	6.36522E-03	-	-
159	2.08902E-03	-	-
160	1.09548E-03	-	-
161	4.38053E-04	-	-
162	1.59075E-04	-	-
163	4.97655E-05	-	-
164	2.88882E-05	-	-
165	9.45626E-06	-	-
166	2.48979E-06	-	-
167	5.96633E-07	-	-
168	2.68123E-07	-	-

Table A.24: Photofission yield results for ^{238}U, experiment[3] versus CINDER (6 MeV), 9.7 MeV excitation, continued

Atomic Mass Number	CINDER Yield Fraction	Experimental Yield Fraction	Exerpimental Uncertainty
169	9.44820E-08	-	-
170	2.48358E-08	-	-
171	7.95911E-09	-	-
172	1.19210E-09	-	-

Table A.25: Photofission yield results for ^{238}U, experiment[3] versus CINDER (6 MeV), 11.6 MeV excitation

Atomic Mass Number	CINDER Yield Fraction	Experimental Yield Fraction	Exerpimental Uncertainty
64	1.77678E-09	-	-
65	1.37242E-10	-	-
66	3.93154E-06	-	-
67	9.34297E-06	-	-
68	2.68236E-05	-	-
69	6.20254E-05	-	-
70	2.06301E-04	-	-
71	5.15715E-04	-	-
72	6.34572E-04	-	-
73	1.07589E-03	-	-
74	4.16541E-03	-	-
75	1.17473E-02	-	-
76	2.60977E-02	-	-
77	5.67596E-02	-	-
78	8.87878E-02	-	-
79	1.44586E-01	-	-
80	2.16871E-01	-	-
81	3.61386E-01	-	-
82	6.53772E-01	-	-
83	1.20761E+00	-	-
84	1.97357E+00	9.00000E-01	9.00000E-02
85	2.16983E+00	1.09000E+00	9.00000E-02
86	3.48165E+00	-	-
87	2.99717E+00	2.12000E+00	1.60000E-01
88	3.96142E+00	2.45000E+00	1.20000E-01
89	5.39372E+00	3.10000E+00	1.70000E-01
90	6.03856E+00	-	-
91	6.42321E+00	4.30000E+00	1.90000E-01
92	6.11191E+00	4.78000E+00	2.50000E-01
93	6.15287E+00	5.15000E+00	3.90000E-01
94	6.42119E+00	5.57000E+00	4.00000E-01
95	6.33396E+00	6.10000E+00	3.40000E-01
96	6.22559E+00	-	-
97	6.07224E+00	5.82000E+00	2.90000E-01
98	5.73079E+00	-	-

Table A.26: Photofission yield results for ^{238}U, experiment[3] versus CINDER (6 MeV), 11.6 MeV excitation, continued

Atomic Mass Number	CINDER Yield Fraction	Experimental Yield Fraction	Exerpimental Uncertainty
99	5.07674E+00	6.13000E+00	2.60000E-01
100	4.13729E+00	-	-
101	3.39360E+00	5.71000E+00	3.10000E-01
102	2.66947E+00	-	-
103	2.41715E+00	5.14000E+00	3.70000E-01
104	1.32089E+00	3.51000E+00	2.60000E-01
105	1.23805E+00	2.67000E+00	1.80000E-01
106	4.28870E-01	1.67000E+00	2.30000E-01
107	2.68342E-01	-	-
108	1.86006E-01	-	-
109	1.22451E-01	-	-
110	1.03608E-01	-	-
111	5.81439E-02	-	-
112	7.22373E-02	1.84000E-01	2.70000E-02
113	5.97338E-02	1.95000E-01	4.00000E-02
114	5.88602E-02	-	-
115	6.85241E-02	1.72000E-01	2.10000E-02
116	5.67781E-02	-	-
117	5.47708E-02	1.71000E-01	2.40000E-02
118	5.47881E-02	-	-
119	5.97648E-02	-	-
120	6.46443E-02	-	-
121	6.96114E-02	-	-
122	8.16007E-02	-	-
123	9.94825E-02	1.76000E-01	2.20000E-02
124	1.19469E-01	-	-
125	1.56503E-01	-	-
126	2.59172E-01	-	-
127	3.88869E-01	5.33000E-01	3.60000E-02
128	6.47380E-01	-	-
129	1.61642E+00	1.38000E+00	1.10000E-01
130	2.54068E+00	-	-
131	3.73564E+00	4.02000E+00	2.60000E-01
132	4.36453E+00	4.68000E+00	3.10000E-01
133	6.46505E+00	6.34000E+00	3.70000E-01

Table A.27: Photofission yield results for ^{238}U, experiment[3] versus CINDER (6 MeV), 11.6 MeV excitation, continued

Atomic Mass Number	CINDER Yield Fraction	Experimental Yield Fraction	Exerpimental Uncertainty
134	5.75234E+00	6.87000E+00	2.50000E-01
135	5.57971E+00	6.58000E+00	2.90000E-01
136	6.49079E+00	-	-
137	5.86468E+00	6.13000E+00	5.50000E-01
138	6.58721E+00	-	-
139	6.00297E+00	-	-
140	5.78625E+00	5.91000E+00	2.00000E-01
141	6.50719E+00	5.38000E+00	2.90000E-01
142	5.98960E+00	5.02000E+00	4.40000E-01
143	6.14341E+00	4.72000E+00	3.40000E-01
144	5.44415E+00	4.24000E+00	4.60000E-01
145	3.98901E+00	-	-
146	3.07189E+00	3.15000E+00	2.10000E-01
147	2.01785E+00	2.22000E+00	1.50000E-01
148	1.43412E+00	-	-
149	1.03579E+00	1.22000E+00	1.50000E-01
150	6.37116E-01	-	-
151	3.18077E-01	7.42000E-01	6.70000E-02
152	2.48648E-01	-	-
153	1.48757E-01	3.24000E-01	5.30000E-02
154	8.05581E-02	-	-
155	5.07201E-02	-	-
156	2.08842E-02	-	-
157	1.09373E-02	-	-
158	6.36522E-03	-	-
159	2.08902E-03	-	-
160	1.09548E-03	-	-
161	4.38053E-04	-	-
162	1.59075E-04	-	-
163	4.97655E-05	-	-
164	2.88882E-05	-	-
165	9.45626E-06	-	-
166	2.48979E-06	-	-
167	5.96633E-07	-	-
168	2.68123E-07	-	-

Table A.28: Photofission yield results for ^{238}U, experiment[3] versus CINDER (6 MeV), 11.6 MeV excitation, continued

Atomic Mass Number	CINDER Yield Fraction	Experimental Yield Fraction	Exerpimental Uncertainty
169	9.44820E-08	-	-
170	2.48358E-08	-	-
171	7.95911E-09	-	-
172	1.19210E-09	-	-

Table A.29: Photofission yield results for ^{238}U, experiment[3] versus CINDER (6 MeV), 13.4 MeV excitation

Atomic Mass Number	CINDER Yield Fraction	Experimental Yield Fraction	Exerpimental Uncertainty
64	1.77678E-09	-	-
65	1.37242E-10	-	-
66	3.93154E-06	-	-
67	9.34297E-06	-	-
68	2.68236E-05	-	-
69	6.20254E-05	-	-
70	2.06301E-04	-	-
71	5.15715E-04	-	-
72	6.34572E-04	-	-
73	1.07589E-03	-	-
74	4.16541E-03	-	-
75	1.17473E-02	-	-
76	2.60977E-02	-	-
77	5.67596E-02	-	-
78	8.87878E-02	-	-
79	1.44586E-01	-	-
80	2.16871E-01	-	-
81	3.61386E-01	-	-
82	6.53772E-01	-	-
83	1.20761E+00	-	-
84	1.97357E+00	8.40000E-01	1.30000E-01
85	2.16983E+00	2.06000E+00	1.50000E-01
86	3.48165E+00	-	-
87	2.99717E+00	2.60000E+00	1.10000E-01
88	3.96142E+00	-	-
89	5.39372E+00	3.01000E+00	1.60000E-01
90	6.03856E+00	-	-
91	6.42321E+00	4.30000E+00	1.90000E-01
92	6.11191E+00	4.80000E+00	2.70000E-01
93	6.15287E+00	5.02000E+00	3.60000E-01
94	6.42119E+00	5.33000E+00	3.80000E-01
95	6.33396E+00	5.70000E+00	2.50000E-01
96	6.22559E+00	-	-
97	6.07224E+00	5.87000E+00	2.90000E-01
98	5.73079E+00	-	-

Table A.30: Photofission yield results for ^{238}U, experiment[3] versus CINDER (6 MeV), 13.4 MeV excitation, continued

Atomic Mass Number	CINDER Yield Fraction	Experimental Yield Fraction	Exerpimental Uncertainty
99	5.07674E+00	6.17000E+00	2.60000E-01
100	4.13729E+00	-	-
101	3.39360E+00	5.59000E+00	3.00000E-01
102	2.66947E+00	-	-
103	2.41715E+00	4.97000E+00	3.70000E-01
104	1.32089E+00	3.56000E+00	2.60000E-01
105	1.23805E+00	2.68000E+00	1.10000E-01
106	4.28870E-01	1.64000E+00	2.40000E-01
107	2.68342E-01	-	-
108	1.86006E-01	-	-
109	1.22451E-01	-	-
110	1.03608E-01	-	-
111	5.81439E-02	-	-
112	7.22373E-02	3.11000E-01	4.80000E-02
113	5.97338E-02	2.90000E-01	3.90000E-02
114	5.88602E-02	-	-
115	6.85241E-02	2.70000E-01	2.50000E-02
116	5.67781E-02	-	-
117	5.47708E-02	2.81000E-01	3.10000E-02
118	5.47881E-02	-	-
119	5.97648E-02	-	-
120	6.46443E-02	-	-
121	6.96114E-02	-	-
122	8.16007E-02	-	-
123	9.94825E-02	2.77000E-01	3.40000E-02
124	1.19469E-01	-	-
125	1.56503E-01	-	-
126	2.59172E-01	-	-
127	3.88869E-01	6.67000E-01	4.20000E-02
128	6.47380E-01	-	-
129	1.61642E+00	1.40300E+00	9.20000E-02
130	2.54068E+00	-	-
131	3.73564E+00	3.90000E+00	2.40000E-01
132	4.36453E+00	4.74000E+00	3.90000E-01
133	6.46505E+00	6.30000E+00	3.50000E-01

Table A.31: Photofission yield results for ^{238}U, experiment[3] versus CINDER (6 MeV), 13.4 MeV excitation, continued

Atomic Mass Number	CINDER Yield Fraction	Experimental Yield Fraction	Exerpimental Uncertainty
134	5.75234E+00	6.84000E+00	2.20000E-01
135	5.57971E+00	6.65000E+00	2.80000E-01
136	6.49079E+00	-	-
137	5.86468E+00	6.11000E+00	5.50000E-01
138	6.58721E+00	-	-
139	6.00297E+00	-	-
140	5.78625E+00	5.59000E+00	2.00000E-01
141	6.50719E+00	5.05000E+00	3.70000E-01
142	5.98960E+00	4.88000E+00	3.70000E-01
143	6.14341E+00	4.53000E+00	3.20000E-01
144	5.44415E+00	3.97000E+00	3.40000E-01
145	3.98901E+00	-	-
146	3.07189E+00	2.90000E+00	1.70000E-01
147	2.01785E+00	2.16000E+00	1.20000E-01
148	1.43412E+00	-	-
149	1.03579E+00	1.38000E+00	1.10000E-01
150	6.37116E-01	-	-
151	3.18077E-01	7.57000E-01	7.00000E-02
152	2.48648E-01	-	-
153	1.48757E-01	3.16000E-01	5.30000E-02
154	8.05581E-02	-	-
155	5.07201E-02	-	-
156	2.08842E-02	-	-
157	1.09373E-02	-	-
158	6.36522E-03	-	-
159	2.08902E-03	-	-
160	1.09548E-03	-	-
161	4.38053E-04	-	-
162	1.59075E-04	-	-
163	4.97655E-05	-	-
164	2.88882E-05	-	-
165	9.45626E-06	-	-
166	2.48979E-06	-	-
167	5.96633E-07	-	-
168	2.68123E-07	-	-

Table A.32: Photofission yield results for ^{238}U, experiment[3] versus CINDER (6 MeV), 13.4 MeV excitation, continued

Atomic Mass Number	CINDER Yield Fraction	Experimental Yield Fraction	Exerpimental Uncertainty
169	9.44820E-08	-	-
170	2.48358E-08	-	-
171	7.95911E-09	-	-
172	1.19210E-09	-	-

Table A.33: Photofission yield results for ^{238}U, experiment[3] versus CINDER (6 MeV), 14.7 MeV excitation

Atomic Mass Number	CINDER Yield Fraction	Experimental Yield Fraction	Exerpimental Uncertainty
64	1.77678E-09	-	-
65	1.37242E-10	-	-
66	3.93154E-06	-	-
67	9.34297E-06	-	-
68	2.68236E-05	-	-
69	6.20254E-05	-	-
70	2.06301E-04	-	-
71	5.15715E-04	-	-
72	6.34572E-04	-	-
73	1.07589E-03	-	-
74	4.16541E-03	-	-
75	1.17473E-02	-	-
76	2.60977E-02	-	-
77	5.67596E-02	-	-
78	8.87878E-02	-	-
79	1.44586E-01	-	-
80	2.16871E-01	-	-
81	3.61386E-01	-	-
82	6.53772E-01	-	-
83	1.20761E+00	-	-
84	1.97357E+00	9.00000E-01	1.00000E-01
85	2.16983E+00	1.20000E+00	9.00000E-02
86	3.48165E+00	-	-
87	2.99717E+00	1.99000E+00	1.40000E-01
88	3.96142E+00	2.62000E+00	1.40000E-01
89	5.39372E+00	3.04000E+00	1.60000E-01
90	6.03856E+00	-	-
91	6.42321E+00	4.20000E+00	1.90000E-01
92	6.11191E+00	4.76000E+00	2.50000E-01
93	6.15287E+00	4.93000E+00	3.50000E-01
94	6.42119E+00	5.32000E+00	3.80000E-01
95	6.33396E+00	5.75000E+00	2.50000E-01
96	6.22559E+00	-	-
97	6.07224E+00	5.69000E+00	2.90000E-01
98	5.73079E+00	-	-

Table A.34: Photofission yield results for ^{238}U, experiment[3] versus CINDER (6 MeV), 14.7 MeV excitation, continued

Atomic Mass Number	CINDER Yield Fraction	Experimental Yield Fraction	Exerpimental Uncertainty
99	5.07674E+00	6.09000E+00	2.50000E-01
100	4.13729E+00	-	-
101	3.39360E+00	5.51000E+00	2.80000E-01
102	2.66947E+00	-	-
103	2.41715E+00	4.82000E+00	3.50000E-01
104	1.32089E+00	3.37000E+00	2.60000E-01
105	1.23805E+00	2.57000E+00	2.40000E-01
106	4.28870E-01	1.75000E+00	1.80000E-01
107	2.68342E-01	-	-
108	1.86006E-01	-	-
109	1.22451E-01	-	-
110	1.03608E-01	-	-
111	5.81439E-02	-	-
112	7.22373E-02	4.91000E-01	4.90000E-02
113	5.97338E-02	4.41000E-01	5.20000E-02
114	5.88602E-02	-	-
115	6.85241E-02	4.44000E-01	3.60000E-02
116	5.67781E-02	-	-
117	5.47708E-02	4.46000E-01	4.50000E-02
118	5.47881E-02	-	-
119	5.97648E-02	-	-
120	6.46443E-02	-	-
121	6.96114E-02	-	-
122	8.16007E-02	-	-
123	9.94825E-02	4.50000E-01	5.90000E-02
124	1.19469E-01	-	-
125	1.56503E-01	5.53000E-01	7.30000E-02
126	2.59172E-01	-	-
127	3.88869E-01	8.94000E-01	5.30000E-02
128	6.47380E-01	-	-
129	1.61642E+00	1.51600E+00	9.50000E-02
130	2.54068E+00	-	-
131	3.73564E+00	3.95000E+00	2.40000E-01
132	4.36453E+00	4.63000E+00	1.50000E-01
133	6.46505E+00	6.10000E+00	3.10000E-01

Table A.35: Photofission yield results for ^{238}U, experiment[3] versus CINDER (6 MeV), 14.7 MeV excitation, continued

Atomic Mass Number	CINDER Yield Fraction	Experimental Yield Fraction	Exerpimental Uncertainty
134	5.75234E+00	6.43000E+00	2.20000E-01
135	5.57971E+00	6.27000E+00	2.60000E-01
136	6.49079E+00	-	-
137	5.86468E+00	5.97000E+00	5.20000E-01
138	6.58721E+00	-	-
139	6.00297E+00	-	-
140	5.78625E+00	5.62000E+00	1.80000E-01
141	6.50719E+00	5.34000E+00	2.90000E-01
142	5.98960E+00	4.60000E+00	3.80000E-01
143	6.14341E+00	4.39000E+00	3.10000E-01
144	5.44415E+00	3.82000E+00	3.20000E-01
145	3.98901E+00	-	-
146	3.07189E+00	2.82000E+00	1.80000E-01
147	2.01785E+00	2.22000E+00	1.30000E-01
148	1.43412E+00	-	-
149	1.03579E+00	1.22200E+00	8.90000E-02
150	6.37116E-01	-	-
151	3.18077E-01	6.94000E-01	6.80000E-02
152	2.48648E-01	-	-
153	1.48757E-01	3.16000E-01	3.80000E-02
154	8.05581E-02	-	-
155	5.07201E-02	-	-
156	2.08842E-02	-	-
157	1.09373E-02	-	-
158	6.36522E-03	-	-
159	2.08902E-03	-	-
160	1.09548E-03	-	-
161	4.38053E-04	-	-
162	1.59075E-04	-	-
163	4.97655E-05	-	-
164	2.88882E-05	-	-
165	9.45626E-06	-	-
166	2.48979E-06	-	-
167	5.96633E-07	-	-
168	2.68123E-07	-	-

Table A.36: Photofission yield results for ^{238}U, experiment[3] versus CINDER (6 MeV), 14.7 MeV excitation, continued

Atomic Mass Number	CINDER Yield Fraction	Experimental Yield Fraction	Exerpimental Uncertainty
169	9.44820E-08	-	-
170	2.48358E-08	-	-
171	7.95911E-09	-	-
172	1.19210E-09	-	-

A.3 ^{239}Pu Photofission Validation Tabulated Results

Table A.37: Photofission yield results for ^{239}Pu, experiment[4] versus CINDER

Atomic Mass Number	CINDER Yield Fraction	Experimental Yield Fraction	Exerpimental Uncertainty
65	7.50635E-10	-	-
66	1.22584E-06	-	-
67	2.03314E-06	-	-
68	6.11606E-06	-	-
69	2.03923E-05	-	-
70	7.13464E-05	-	-
71	1.83420E-04	-	-
72	4.27994E-04	-	-
73	4.61352E-04	-	-
74	1.27162E-03	-	-
75	2.43061E-03	-	-
76	7.86468E-03	-	-
77	2.12828E-02	-	-
78	3.64873E-02	-	-
79	6.73656E-02	-	-
80	1.11574E-01	-	-
81	1.82458E-01	-	-
82	2.75154E-01	-	-
83	3.79096E-01	-	-
84	5.99472E-01	-	-
85	7.23683E-01	8.51000E-01	6.80000E-02
86	1.04064E+00	-	-
87	1.18746E+00	-	-
88	1.60028E+00	1.62000E+00	2.10000E-01
89	2.07679E+00	-	-
90	2.43481E+00	-	-
91	2.94682E+00	2.89000E+00	2.30000E-01
92	3.47785E+00	3.20000E+00	1.60000E-01
93	4.11331E+00	4.02000E+00	2.00000E-01
94	4.74153E+00	-	-
95	4.42442E+00	4.39000E+00	1.30000E-01
96	5.33762E+00	-	-
97	5.69340E+00	4.63000E+00	1.70000E-01
98	5.59012E+00	-	-
99	6.10611E+00	5.76000E+00	2.20000E-01

Table A.38: Photofission yield results for ^{239}Pu, experiment[4] versus CINDER, continued

Atomic Mass Number	CINDER Yield Fraction	Experimental Yield Fraction	Exerpimental Uncertainty
100	6.10998E+00	-	-
101	6.04949E+00	-	-
102	6.13776E+00	-	-
103	5.90050E+00	5.55000E+00	2.80000E-01
104	5.70185E+00	-	-
105	4.76486E+00	3.96000E+00	2.00000E-01
106	4.23817E+00	3.70000E+00	2.60000E-01
107	3.00961E+00	-	-
108	2.14516E+00	-	-
109	1.21290E+00	-	-
110	6.07241E-01	-	-
111	3.06071E-01	1.24200E+00	7.50000E-02
112	1.62843E-01	9.55000E-01	5.70000E-02
113	8.23859E-02	7.10000E-01	6.90000E-02
114	8.16114E-02	-	-
115	8.33658E-02	3.94000E-01	2.70000E-02
116	7.50643E-02	-	-
117	7.50030E-02	3.92000E-01	3.30000E-02
118	7.44174E-02	-	-
119	7.28991E-02	-	-
120	7.48743E-02	-	-
121	7.78659E-02	-	-
122	8.24293E-02	-	-
123	9.27980E-02	-	-
124	1.09903E-01	-	-
125	1.49757E-01	-	-
126	2.30372E-01	-	-
127	3.69309E-01	1.43000E+00	1.50000E-01
128	6.59055E-01	-	-
129	1.11798E+00	-	-
130	2.22807E+00	-	-
131	3.91605E+00	4.67000E+00	1.50000E-01
132	5.30408E+00	4.96000E+00	1.60000E-01
133	5.87451E+00	5.43000E+00	2.10000E-01
134	6.60384E+00	-	-

Table A.39: Photofission yield results for ^{239}Pu, experiment[4] versus CINDER, continued

Atomic Mass Number	CINDER Yield Fraction	Experimental Yield Fraction	Exerpimental Uncertainty
135	6.74514E+00	6.32000E+00	2.60000E-01
136	7.41610E+00	-	-
137	6.51524E+00	-	-
138	6.29692E+00	-	-
139	5.72286E+00	5.18000E+00	2.60000E-01
140	5.61452E+00	4.55000E+00	1.80000E-01
141	4.78549E+00	4.23000E+00	1.40000E-01
142	5.87634E+00	-	-
143	4.53486E+00	3.26000E+00	1.30000E-01
144	3.92533E+00	2.83000E+00	1.10000E-01
145	3.23667E+00	2.33000E+00	1.50000E-01
146	2.76771E+00	-	-
147	2.23685E+00	1.64200E+00	6.40000E-02
148	1.75725E+00	-	-
149	1.59767E+00	-	-
150	9.82320E-01	-	-
151	9.07984E-01	7.45000E-01	7.40000E-02
152	6.78498E-01	-	-
153	4.68989E-01	3.85000E-01	2.70000E-02
154	3.19318E-01	-	-
155	2.39372E-01	1.61000E-01	1.80000E-02
156	1.59656E-01	-	-
157	9.97744E-02	9.80000E-02	1.50000E-02
158	7.97141E-02	-	-
159	3.59214E-02	-	-
160	1.99976E-02	-	-
161	1.02356E-02	-	-
162	3.74426E-03	-	-
163	1.79564E-03	-	-
164	6.97965E-04	-	-
165	2.99283E-04	-	-
166	1.29750E-04	-	-
167	4.49999E-05	-	-
168	6.98389E-06	-	-
169	3.99787E-06	-	-

Table A.40: Photofission yield results for ^{239}Pu, experiment[4] versus CINDER, continued

Atomic Mass Number	CINDER Yield Fraction	Experimental Yield Fraction	Exerpimental Uncertainty
170	1.69791E-06	-	-
171	6.98737E-07	-	-
172	3.79600E-07	-	-

A.4 U-nat Photofission Validation Tabulated Results

Table A.41: Photofission yield results for U-nat, experiment[5] versus CINDER

Atomic Mass Number	CINDER Yield Fraction	Experimental Yield Fraction	Exerpimental Uncertainty
65	1.15258E-08	-	-
66	7.04496E-06	-	-
67	1.68919E-05	-	-
68	2.36467E-05	-	-
69	3.62738E-05	-	-
70	6.24967E-05	-	-
71	1.05613E-04	-	-
72	2.02536E-04	-	-
73	5.13655E-04	-	-
74	1.33051E-03	-	-
75	3.62027E-03	-	-
76	8.05901E-03	-	-
77	1.88395E-02	3.20000E-02	4.00000E-03
78	4.78776E-02	5.90000E-02	2.00000E-03
79	7.70800E-02	-	-
80	1.31108E-01	-	-
81	2.12091E-01	-	-
82	3.15133E-01	-	-
83	4.90291E-01	5.90000E-01	6.00000E-02
84	8.63378E-01	1.03000E+00	1.70000E-01
85	1.05682E+00	-	-
86	1.55402E+00	-	-
87	1.81519E+00	-	-
88	2.75288E+00	-	-
89	3.41669E+00	2.80000E+00	1.00000E-01
90	3.92853E+00	-	-
91	4.37893E+00	3.90000E+00	1.00000E-01
92	4.82874E+00	-	-
93	5.29161E+00	-	-
94	5.46207E+00	-	-
95	5.59957E+00	-	-
96	5.79588E+00	-	-
97	5.92536E+00	5.80000E+00	2.00000E-01
98	5.88561E+00	-	-
99	6.15254E+00	6.60000E+00	-

Table A.42: Photofission yield results for U-nat, experiment[5] versus CINDER, continued.

Atomic Mass Number	CINDER Yield Fraction	Experimental Yield Fraction	Exerpimental Uncertainty
100	5.90492E+00	-	-
101	5.77527E+00	-	-
102	5.63904E+00	-	-
103	4.91664E+00	2.90000E+00	2.00000E-01
104	4.59121E+00	-	-
105	2.69063E+00	2.50000E+00	1.00000E-01
106	2.04681E+00	2.00000E+00	2.00000E-01
107	1.12096E+00	-	-
108	5.12370E-01	-	-
109	1.95090E-01	-	-
110	1.44257E-01	-	-
111	8.83958E-02	7.70000E-01	2.00000E-02
112	7.98277E-02	5.20000E-01	3.00000E-02
113	6.21368E-02	6.00000E-01	3.00000E-02
114	5.58636E-02	-	-
115	6.02471E-02	8.80000E-02	2.20000E-02
116	5.18598E-02	-	-
117	5.15900E-02	5.00000E-01	2.00000E-02
118	5.27585E-02	-	-
119	5.14338E-02	-	-
120	5.11673E-02	-	-
121	5.75532E-02	-	-
122	6.00974E-02	-	-
123	7.47517E-02	-	-
124	9.13389E-02	-	-
125	1.41089E-01	-	-
126	2.06765E-01	-	-
127	2.76802E-01	9.30000E-01	2.00000E-02
128	6.02607E-01	-	-
129	1.04453E+00	-	-
130	2.05023E+00	-	-
131	3.22071E+00	4.30000E+00	1.00000E-01
132	4.76435E+00	4.90000E+00	1.00000E-01
133	5.46436E+00	6.20000E+00	3.00000E-01
134	6.79841E+00	-	-

Table A.43: Photofission yield results for U-nat, experiment[5] versus CINDER, continued.

Atomic Mass Number	CINDER Yield Fraction	Experimental Yield Fraction	Exerpimental Uncertainty
135	6.60395E+00	-	-
136	6.69222E+00	-	-
137	6.47049E+00	4.70000E+00	3.00000E-01
138	6.27650E+00	-	-
139	6.05670E+00	4.60000E+00	1.00000E-01
140	6.61581E+00	5.00000E+00	3.00000E-01
141	5.52866E+00	4.90000E+00	3.00000E-01
142	5.44029E+00	-	-
143	4.79654E+00	3.80000E+00	3.00000E-01
144	4.82314E+00	3.40000E+00	2.00000E-01
145	3.61268E+00	-	-
146	3.10707E+00	-	-
147	2.59569E+00	-	-
148	1.84431E+00	-	-
149	1.43171E+00	-	-
150	1.03476E+00	-	-
151	7.64632E-01	-	-
152	5.20369E-01	-	-
153	3.43871E-01	-	-
154	1.86693E-01	-	-
155	1.17820E-01	-	-
156	5.72038E-02	-	-
157	4.23952E-02	-	-
158	1.49149E-02	-	-
159	6.89985E-03	-	-
160	2.79344E-03	-	-
161	1.09331E-03	-	-
162	3.32442E-04	-	-
163	7.55044E-05	-	-
164	4.18493E-05	-	-
165	1.83628E-05	-	-
166	9.64073E-06	-	-
167	5.38917E-06	-	-
168	2.82103E-06	-	-
169	1.57359E-06	-	-

Table A.44: Photofission yield results for U-nat, experiment[5] versus CINDER, continued.

Atomic Mass Number	CINDER Yield Fraction	Experimental Yield Fraction	Exerpimental Uncertainty
171	3.28252E-07	-	-
172	2.54790E-07	-	-

A.5 ^{238}Np Photofission Validation Comparison Tabulated Results

Table A.45: Photofission yield results for ^{238}Np

Atomic Mass Number	CINDER Yield Fraction	Atomic Mass Number	CINDER Yield Fraction
65	2.42616E-10	100	6.43623E+00
66	1.84857E-07	101	6.12601E+00
67	3.68673E-07	102	5.76821E+00
68	1.87801E-06	103	5.56223E+00
69	6.86196E-08	104	4.12651E+00
70	2.44247E-05	105	3.10737E+00
71	6.19128E-05	106	2.33029E+00
72	1.50497E-04	107	1.71281E+00
73	3.68983E-04	108	1.30535E+00
74	6.67091E-04	109	6.33616E-01
75	1.31879E-03	110	2.96340E-01
76	6.01484E-03	111	9.55255E-02
77	1.04399E-02	112	7.32474E-02
78	2.43615E-02	113	5.15428E-02
79	5.63171E-02	114	5.29653E-02
80	1.11545E-01	115	4.88140E-02
81	2.35704E-01	116	4.78502E-02
82	3.57566E-01	117	4.29612E-02
83	4.83629E-01	118	5.29366E-02
84	7.30778E-01	119	5.32668E-02
85	9.77493E-01	120	5.30229E-02
86	1.30619E+00	121	5.28636E-02
87	1.75145E+00	122	6.04638E-02
88	2.15847E+00	123	7.57198E-02
89	2.54538E+00	124	7.27506E-02
90	3.34114E+00	125	1.31019E-01
91	3.92163E+00	126	1.65212E-01
92	4.38925E+00	127	3.55751E-01
93	5.11532E+00	128	1.49976E+00
94	5.13669E+00	129	1.75844E+00
95	5.66832E+00	130	2.72784E+00
96	5.48742E+00	131	3.60000E+00
97	6.19464E+00	132	4.85378E+00
98	6.06027E+00	133	6.46702E+100
99	6.10888E+00	134	7.07351E+00

Table A.46: Photofission yield results for ^{238}Np, continued

Atomic Mass Number	CINDER Yield Fraction	Atomic Mass Number	CINDER Yield Fraction
135	7.25997E+00	154	1.87276E-01
136	6.70482E+00	155	1.41897E-01
137	6.26179E+00	156	1.00513E-01
138	6.13490E+00	157	3.22163E-02
139	5.63220E+00	158	1.27717E-02
140	5.49556E+00	159	6.49426E-03
141	5.33958E+00	160	2.50882E-03
142	4.79766E+00	161	7.79691E-04
143	4.64979E+00	162	3.02637E-04
144	4.13997E+00	163	1.29642E-04
145	3.45049E+00	164	5.62869E-05
146	2.79973E+00	165	1.92651E-05
147	2.22771E+00	166	1.12573E-05
148	1.71915E+00	167	1.56218E-06
149	1.30298E+00	168	4.03374E-07
150	9.93843E-01	169	1.18961E-07
151	7.27038E-01	170	4.08730E-07
152	4.59944E-01	171	1.19674E-07
153	3.65138E-01	172	4.66060E-07

Appendix B

Sample Input Files

The following are sample input files for the models run in TINDER for Section 3.2.2. The first three files are for EVENT and the second three are for MCNPX.

File: /media/truecrypt1/research/th...nResults/tinder/eventAct/input Page 1 of 1

```
&input
  cinderexec= 'cinder2008g',
  debug=0,
  transexec= 'tinder_event.pl',
  ngrps= 66,
  ggrps= 25,
  burnlibn= "/usr/local/cinder/data/C08lib_fission",
  burnlibg= "/usr/local/cinder/data/C08lib_gamma_v08.2",
  burnlibgl = "/usr/local/cinder/data/cindergl.dat",
  burnlocin="/home/wmartin/cinder/",
  spectraFile="spectra_l"
/

&materials
  u3o8
  u235 2350920 4.92845e-3
  u238 2380920 2.70176e-4
  o16   160080 1.39154e-2

&burnup
calculation="test",
volcc=1.957567e2,
flxmlt=2e8,
flosig=1.000e-21,
signif=1.000e-21,
epsm=0,
epsn=0,
exponmax=0,
kchn=0,
klib=0,
nfe=2,
ltsdnz=-1,
nlintl=0,
nosame=0,
gasopt=1,
run_tab=1,
suffix="",
fine_dg=1000,
coarse_dg=10000,
fine_dn=1000,
coarse_dn=10000,
flxmltg=2e8,
nfeg=2,
description="umix sphere Input Deck for CINDER2008g",
fluxname="tally 14",
gfluxname="tally 24",
ncamp = 2
/
1 13.4168 62.4981
     30.0 's'
2 0.0 0.0
     6.0 's'
     7.0 's'
/
```

File: /media/truecrypt1/research/th...sults/tinder/eventAct/input.x1 Page 1 of 3

```
@@@@@@@@@@@@@@@@@@@@@@@@@@@@@@@@@@@@@@@@@@@@@@@@@@@@@@@@@@@@@@@@@@@
@@@@@@@@@@ gem file  input.x1
@@@@@@@@@@@@@@@@@@@@@@@@@@@@@@@@@@@@@@@@@@@@@@@@@@@@@@@@@@@@@@@@@@@


@@@@@@@@@@@@@@@@@@@@@@@@@@@@@@@@@@@@@@@@@@@@@@@@@@@@@@@@@@@@@@@@@@@
@@@@@@@@@@ problem control parameters
@@@@@@@@@@@@@@@@@@@@@@@@@@@@@@@@@@@@@@@@@@@@@@@@@@@@@@@@@@@@@@@@@@@

title u3o8 puck in a wood box, fixed source problem
problem radiation
case fixed
particle neutron
code event
mode forward
geometry rz
angle 9
groups 42 @30/12 library, MATXS10
scatter 2
upscatter no
fission yes
monitor balance

@@@@@@@@@@@@@@@@@@@@@@@@@@@@@@@@@@@@@@@@@@@@@@@@@@@@@@@@@@@@@@@@@@@
@@@@@@@@@@ geometry definitions/options
@@@@@@@@@@@@@@@@@@@@@@@@@@@@@@@@@@@@@@@@@@@@@@@@@@@@@@@@@@@@@@@@@@@

pnt p1   0.0    -1.685
pnt p2   4.3    -1.685
pnt p3   4.3     1.685
pnt p4   0.0     1.685
pnt p5   0.0   -91.5
pnt p6   4.3   -91.5
pnt p7  97.34  -91.5
pnt p8  97.34   -1.685
pnt p9  97.34    1.685
pnt p10 97.34   91.5
pnt p11  4.3    91.5
pnt p12  0.0    91.5

lin l1  p1  p2
lin l2  p2  p3
lin l3  p3  p4
lin l4  p1  p4
lin l5  p1  p5
lin l6  p5  p6
lin l7  p6  p2
lin l8  p6  p7
lin l9  p7  p8
lin l10 p8  p2
lin l11 p8  p9
lin l12 p9  p3
lin l13 p9  p10
lin l14 p10 p11
lin l15 p11 p3
```

```
lin l16 p11 p12
lin l17 p12 p4

region puck l1  l2  l3  l4
region wd1  l5  l6  l7  l1
region wd2  l7  l8  l9  l10
region wd3  l2  l10 l11 l12
region wd4  l12 l13 l14 l15
region wd5  l3  l15 l16 l17

@@@@@@@@@@@@@@@@@@@@@@@@@@@@@@@@@@@@@@@@@@@@@@@@@@@@@@@@@@@@@@@@@@@@@@@@@@@@@@@
@@@@@@@@@@ meshing options
@@@@@@@@@@@@@@@@@@@@@@@@@@@@@@@@@@@@@@@@@@@@@@@@@@@@@@@@@@@@@@@@@@@@@@@@@@@@@@@

divide 10 l1 l2 l3 l4 l5 l6 l7 l8 l9 l10 l11 l12 l13 l14 l15 l16 l17
default itv 10

@@@@@@@@@@@@@@@@@@@@@@@@@@@@@@@@@@@@@@@@@@@@@@@@@@@@@@@@@@@@@@@@@@@@@@@@@@@@@@@
@@@@@@@@@@ material specifications
@@@@@@@@@@@@@@@@@@@@@@@@@@@@@@@@@@@@@@@@@@@@@@@@@@@@@@@@@@@@@@@@@@@@@@@@@@@@@@@

@ - nuclear data library
library transx matxs10.inp fido

@ - cross section table lengths
xstab 4 5 46

mat u238
mat u235
mat o16
mat cnat
mat h1

mix u3o8
mix u3o8 u235  4.92845e-3
mix u3o8 u238  2.70176e-4
mix u3o8 o16   1.39154e-2
mix wood
mix wood cnat   1.33880e-2
mix wood o16    9.31830e-3
mix wood h1     2.11973e-2

surface t1 0.0000e+00 0.0000e+00 0.0000e+00 0.0000e+00 0.0000e+00 ^
   2.3255e-01 0.0000e+00 0.0000e+00 0.0000e+00 0.0000e+00 ^
   0.0000e+00 0.0000e+00 0.0000e+00 0.0000e+00 0.0000e+00 ^
   0.0000e+00 0.0000e+00 0.0000e+00 0.0000e+00 0.0000e+00 ^
   0.0000e+00 0.0000e+00 0.0000e+00 0.0000e+00 0.0000e+00 ^
   0.0000e+00 0.0000e+00 0.0000e+00 0.0000e+00 0.0000e+00 ^
   2.3255e-01 0.0000e+00 0.0000e+00 0.0000e+00 0.0000e+00 ^
   0.0000e+00 0.0000e+00 0.0000e+00 0.0000e+00 0.0000e+00 ^
   0.0000e+00 0.0000e+00

@@@@@@@@@@@@@@@@@@@@@@@@@@@@@@@@@@@@@@@@@@@@@@@@@@@@@@@@@@@@@@@@@@@@@@@@@@@@@@@
@@@@@@@@@@ define boundary conditions
@@@@@@@@@@@@@@@@@@@@@@@@@@@@@@@@@@@@@@@@@@@@@@@@@@@@@@@@@@@@@@@@@@@@@@@@@@@@@@@
```

File: /media/truecrypt1/research/th...sults/tinder/eventAct/input.x1 Page 3 of 3

```
boundary t1 l6
boundary reflect l17 l4 l5
boundary vacuum l8 l9 l11 l13 l14 l16

@@@@@@@@@@@@@@@@@@@@@@@@@@@@@@@@@@@@@@@@@@@@@@@@@@@@@@@@@@@@@@@@@@@
@@@@@@@@@@ assign properties to regions
@@@@@@@@@@@@@@@@@@@@@@@@@@@@@@@@@@@@@@@@@@@@@@@@@@@@@@@@@@@@@@@@@@@

properties puck u3o8
properties wd1  wood
properties wd2  wood
properties wd3  wood
properties wd4  wood
properties wd5  wood

@@@@@@@@@@@@@@@@@@@@@@@@@@@@@@@@@@@@@@@@@@@@@@@@@@@@@@@@@@@@@@@@@@@
@@@@@@@@@@ define averages
@@@@@@@@@@@@@@@@@@@@@@@@@@@@@@@@@@@@@@@@@@@@@@@@@@@@@@@@@@@@@@@@@@@

average 1 puck
@average 2 wd1 wd2 wd3 wd4 wd5

@@@@@@@@@@@@@@@@@@@@@@@@@@@@@@@@@@@@@@@@@@@@@@@@@@@@@@@@@@@@@@@@@@@
@@@@@@@@@@ mesh the geometry
@@@@@@@@@@@@@@@@@@@@@@@@@@@@@@@@@@@@@@@@@@@@@@@@@@@@@@@@@@@@@@@@@@@

fill

@@@@@@@@@@@@@@@@@@@@@@@@@@@@@@@@@@@@@@@@@@@@@@@@@@@@@@@@@@@@@@@@@@@
@@@@@@@@@@ data
@@@@@@@@@@@@@@@@@@@@@@@@@@@@@@@@@@@@@@@@@@@@@@@@@@@@@@@@@@@@@@@@@@@

data

@@@@@@@@@@@@@@@@@@@@@@@@@@@@@@@@@@@@@@@@@@@@@@@@@@@@@@@@@@@@@@@@@@@
@@@@@@@@@@ stop run
@@@@@@@@@@@@@@@@@@@@@@@@@@@@@@@@@@@@@@@@@@@@@@@@@@@@@@@@@@@@@@@@@@@

stop
```

File: /media/truecrypt1/research/th...sults/tinder/eventAct/input.x2 Page 1 of 3

```
@@@@@@@@@@@@@@@@@@@@@@@@@@@@@@@@@@@@@@@@@@@@@@@@@@@@@@@@@@@@@@@@@@@
@@@@@@@@@@ gem file  input.x2
@@@@@@@@@@@@@@@@@@@@@@@@@@@@@@@@@@@@@@@@@@@@@@@@@@@@@@@@@@@@@@@@@@@


@@@@@@@@@@@@@@@@@@@@@@@@@@@@@@@@@@@@@@@@@@@@@@@@@@@@@@@@@@@@@@@@@@@
@@@@@@@@@@ problem control parameters
@@@@@@@@@@@@@@@@@@@@@@@@@@@@@@@@@@@@@@@@@@@@@@@@@@@@@@@@@@@@@@@@@@@

title u3o8 puck in a wood box, 7/12.2 MeV n/g source
problem radiation
case fixed
particle neutron
code event
mode forward
geometry xy
angle 9
groups 42 @30/12 library, MATXS10
scatter 2
upscatter no
fission yes
monitor balance

@@@@@@@@@@@@@@@@@@@@@@@@@@@@@@@@@@@@@@@@@@@@@@@@@@@@@@@@@@@@@@@@@@@
@@@@@@@@@@ geometry definitions/options
@@@@@@@@@@@@@@@@@@@@@@@@@@@@@@@@@@@@@@@@@@@@@@@@@@@@@@@@@@@@@@@@@@@

pnt p1   0.0    0.0
pnt p2   4.3    0.0
pnt p3   0.0    4.3
pnt p4 122.0    0.0
pnt p5 122.0   61.0
pnt p6   0.0   61.0

line l1 p1 p2
line l2 p2 p3 p1
line l3 p3 p1
line l4 p1 p4
line l5 p4 p5
line l6 p5 p6
line l7 p6 p1

region puck l1 l2 l3
region wd l4 l5 l6 l7

@@@@@@@@@@@@@@@@@@@@@@@@@@@@@@@@@@@@@@@@@@@@@@@@@@@@@@@@@@@@@@@@@@@
@@@@@@@@@@ meshing options
@@@@@@@@@@@@@@@@@@@@@@@@@@@@@@@@@@@@@@@@@@@@@@@@@@@@@@@@@@@@@@@@@@@

default itv 10

@@@@@@@@@@@@@@@@@@@@@@@@@@@@@@@@@@@@@@@@@@@@@@@@@@@@@@@@@@@@@@@@@@@
@@@@@@@@@@ material specifications
@@@@@@@@@@@@@@@@@@@@@@@@@@@@@@@@@@@@@@@@@@@@@@@@@@@@@@@@@@@@@@@@@@@
```

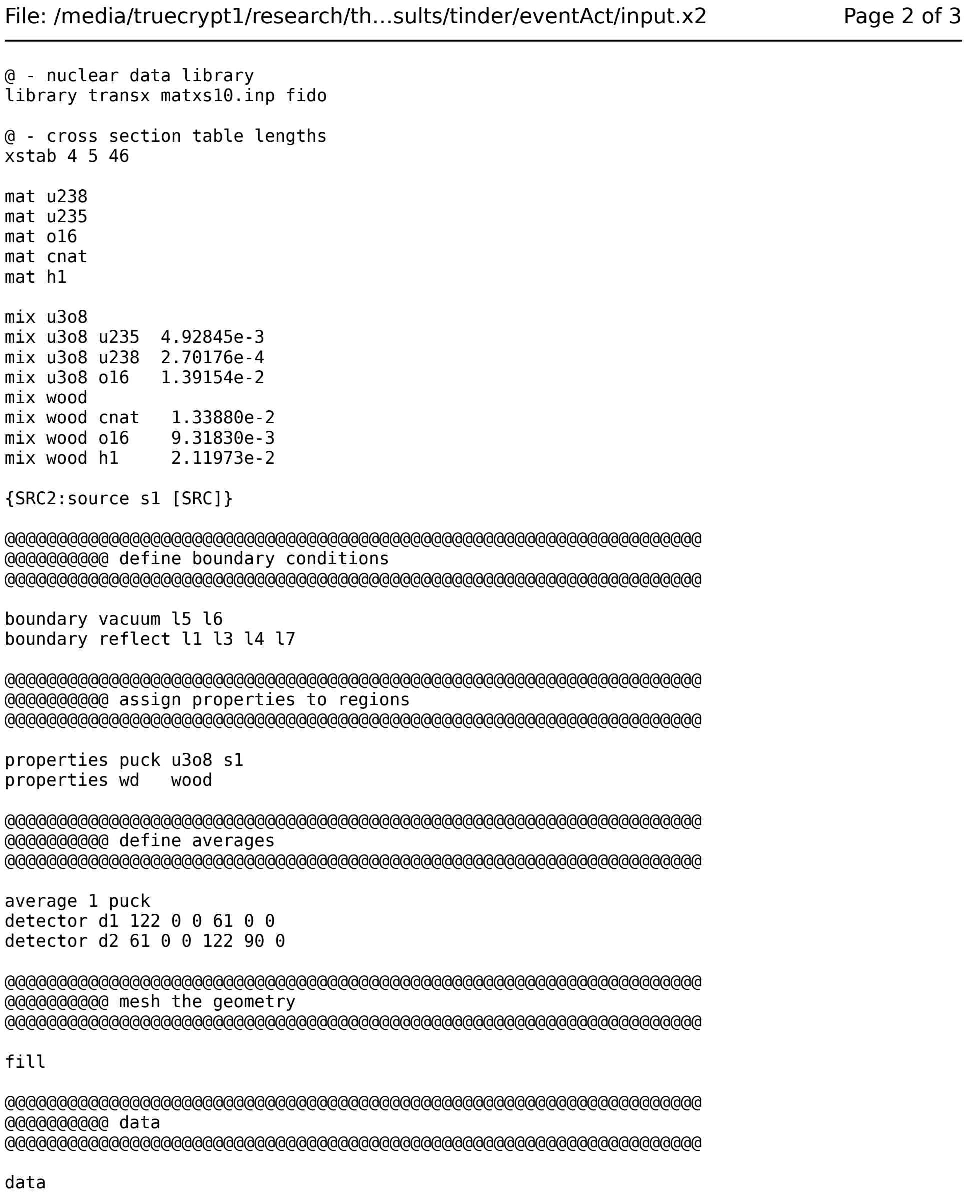

File: /media/truecrypt1/research/th...sults/tinder/eventAct/input.x2 Page 2 of 3

```
@ - nuclear data library
library transx matxs10.inp fido

@ - cross section table lengths
xstab 4 5 46

mat u238
mat u235
mat o16
mat cnat
mat h1

mix u3o8
mix u3o8 u235  4.92845e-3
mix u3o8 u238  2.70176e-4
mix u3o8 o16   1.39154e-2
mix wood
mix wood cnat   1.33880e-2
mix wood o16    9.31830e-3
mix wood h1     2.11973e-2

{SRC2:source s1 [SRC]}

@@@@@@@@@@@@@@@@@@@@@@@@@@@@@@@@@@@@@@@@@@@@@@@@@@@@@@@@@@@@@@@@@@@
@@@@@@@@@@ define boundary conditions
@@@@@@@@@@@@@@@@@@@@@@@@@@@@@@@@@@@@@@@@@@@@@@@@@@@@@@@@@@@@@@@@@@@

boundary vacuum l5 l6
boundary reflect l1 l3 l4 l7

@@@@@@@@@@@@@@@@@@@@@@@@@@@@@@@@@@@@@@@@@@@@@@@@@@@@@@@@@@@@@@@@@@@
@@@@@@@@@@ assign properties to regions
@@@@@@@@@@@@@@@@@@@@@@@@@@@@@@@@@@@@@@@@@@@@@@@@@@@@@@@@@@@@@@@@@@@

properties puck u3o8 s1
properties wd   wood

@@@@@@@@@@@@@@@@@@@@@@@@@@@@@@@@@@@@@@@@@@@@@@@@@@@@@@@@@@@@@@@@@@@
@@@@@@@@@@ define averages
@@@@@@@@@@@@@@@@@@@@@@@@@@@@@@@@@@@@@@@@@@@@@@@@@@@@@@@@@@@@@@@@@@@

average 1 puck
detector d1 122 0 0 61 0 0
detector d2 61 0 0 122 90 0

@@@@@@@@@@@@@@@@@@@@@@@@@@@@@@@@@@@@@@@@@@@@@@@@@@@@@@@@@@@@@@@@@@@
@@@@@@@@@@ mesh the geometry
@@@@@@@@@@@@@@@@@@@@@@@@@@@@@@@@@@@@@@@@@@@@@@@@@@@@@@@@@@@@@@@@@@@

fill

@@@@@@@@@@@@@@@@@@@@@@@@@@@@@@@@@@@@@@@@@@@@@@@@@@@@@@@@@@@@@@@@@@@
@@@@@@@@@@ data
@@@@@@@@@@@@@@@@@@@@@@@@@@@@@@@@@@@@@@@@@@@@@@@@@@@@@@@@@@@@@@@@@@@

data
```

```
@@@@@@@@@@@@@@@@@@@@@@@@@@@@@@@@@@@@@@@@@@@@@@@@@@@@@@@@@@@@@@@@@@@
@@@@@@@@@@ stop run
@@@@@@@@@@@@@@@@@@@@@@@@@@@@@@@@@@@@@@@@@@@@@@@@@@@@@@@@@@@@@@@@@@@

stop
```

File: /media/truecrypt1/research/th...nResults/tinder/mcnpxAct/input Page 1 of 1

```
&input
  cinderexec= 'cinder2008g',
  debug=0,
  transexec= 'tinder_mcnpx_act.pl',
  ngrps= 66,
  ggrps= 25,
  burnlibn= "/media/truecrypt1/cinder/CINDER2008/Data/C08lib_fission",
  burnlibg= "/media/truecrypt1/cinder/CINDER2008/Data/C08lib_gamma_v08.2",
  burnlibgl = "/media/truecrypt1/cinder/CINDER2008/Data/cindergl.dat",
  burnlocin="/media/truecrypt1/cinderrun/",
  spectraFile="spectra_l"
/

&materials
  umix
  u-235 2350920 2.57845134696E-01
  u-238 2380920 1.41349683824E-02
  o-16   160080 7.28019896921E-01


&burnup
calculation="test",
volcc=1.00,
flxmlt=2e8,
flosig=1.000e-15,
signif=1.000e-15,
epsm=0,
epsn=0,
exponmax=0,
kchn=0,
klib=0,
nfe=2,
ltsdnz=-1,
nlintl=0,
nosame=0,
gasopt=1,
run_tab=1,
suffix="",
fine_dg=1000,
coarse_dg=10000,
fine_dn=1000,
coarse_dn=10000,
flxmltg=2e8,
nfeg=2,
description="umix sphere Input Deck for CINDER2008g",
fluxname="tally 14",
gfluxname="tally 24",
ncamp = 2
/
  1 1.0 1.0
    30.0 's'
 2 0.0E+00 0.0
    6.0 's'
    7.0 's'
/
```

File: /media/truecrypt1/research/th...sults/tinder/mcnpxAct/input.x1 Page 1 of 1

```
Bare uranium oxide cylinder surrounded by low-density plywood rcc
C    Cell Cards
1    1  -2.4   -1       imp:n=1 imp:p=1
2    2  -0.55   1  -2   imp:n=1 imp:p=1
3    0          2       imp:n=0 imp:p=0

C    Surface Cards
1    RCC  0 -1.685 0  0 3.37 0  4.3 $ based on 469.7g
2    RPP  -122.0 122.0  -91.5 91.5  -61.0 61.0 $ cm

C    Data Cards
m1    92235 -0.8015 92238 -0.0445 8016 -0.154 $ tweaked per Prussin
m2    6000 -0.4855 8016 -0.45 1001 -0.0645
MODE N P
F14:N 1
c
C   CINDER2008 activation cross sections provided in
C   66 group CINDER2008 fission library neutron energy group structure
E14 1.00000E-11 5.00000E-10 1.00000E-09 2.00000E-09 5.00000E-09 1.00000E-08 &
    1.50000E-08 2.00000E-08 2.50000E-08 3.00000E-08 3.50000E-08 4.20000E-08 &
    5.00000E-08 5.80000E-08 6.70000E-08 8.00000E-08 1.00000E-07 1.52000E-07 &
    2.51000E-07 4.14000E-07 6.83000E-07 1.12500E-06 1.85500E-06 3.05900E-06 &
    5.04300E-06 8.31500E-06 1.37100E-05 2.26000E-05 3.72700E-05 6.14400E-05 &
    1.01300E-04 1.67000E-04 2.75400E-04 4.54000E-04 7.48500E-04 1.23400E-03 &
    2.03500E-03 2.40400E-03 2.84000E-03 3.35500E-03 5.53100E-03 9.11900E-03 &
    1.50300E-02 1.98900E-02 2.55400E-02 4.08700E-02 6.73800E-02 1.11100E-01 &
    1.83200E-01 3.02000E-01 3.88700E-01 4.97900E-01 6.39279E-01 8.20850E-01 &
    1.10803E+00 1.35335E+00 1.73774E+00 2.23130E+00 2.86505E+00 3.67879E+00 &
    4.96585E+00 6.06500E+00 1.00000E+01 1.49182E+01 1.69046E+01 2.00000E+01 &
    2.50000E+01
C
F24:P 1
c
C   25 group CINDER gamma energy group structure
E24 0.000E+00 1.000E-02 3.000E-02 6.000E-02 1.000E-01 2.000E-01 3.000E-01 &
    5.000E-01 5.250E-01 7.500E-01 1.000E+00 1.330E+00 1.660E+00 2.000E+00 &
    2.500E+00 3.000E+00 4.000E+00 5.000E+00 6.000E+00 7.000E+00 8.000E+00 &
    9.000E+00 1.000E+01 1.200E+01 1.700E+01 3.000E+01
C
F11:P 2.1
c
C   3-6 MeV Check
E11 3.0 4.0 5.0 6.0 30.0 $first group will be 0-3
{SRC2:FM11 [SRCTOT]}
c
VOL j 5.45e6 j $ vol of rpp
{SRC1:SDEF SUR=2.4 POS=0 -91.5 0 AXS=0 1 0 RAD=D1 PAR=1 ERG=7.0 VEC=0 1 0 DIR=1
si1 0 6.77
sp1 -21 1}
{SRC2:SDEF CEL=1 PAR=P ERG=d3
si3 [ERG]
sp3 [SRC] }
PHYS:N 25.0 2j -1 j 5
PHYS:P 30.0 2j -1 2j 1
NPS 1e7
PRINT
```

File: /media/truecrypt1/research/th...sults/tinder/mcnpxAct/input.x2 Page 1 of 1

```
Bare uranium oxide cylinder surrounded by low-density plywood rcc
C    Cell Cards
1    1  -2.4   -1       imp:n=1 imp:p=1
2    2  -0.55   1  -2   imp:n=1 imp:p=1
3    0          2       imp:n=0 imp:p=0

C    Surface Cards
1    RCC  0 -1.685 0  0 3.37 0  4.3 $ based on 469.7g
2    RPP  -122.0 122.0  -91.5 91.5  -61.0 61.0 $ cm

C    Data Cards
m1    92235 -0.8015 92238 -0.0445 8016 -0.154 $ tweaked per Prussin
m2    6000 -0.4855 8016 -0.45 1001 -0.0645
MODE N P
F14:N 1
c
C   CINDER2008 activation cross sections provided in
C   66 group CINDER2008 fission library neutron energy group structure
E14 1.00000E-11 5.00000E-10 1.00000E-09 2.00000E-09 5.00000E-09 1.00000E-08 &
    1.50000E-08 2.00000E-08 2.50000E-08 3.00000E-08 3.50000E-08 4.20000E-08 &
    5.00000E-08 5.80000E-08 6.70000E-08 8.00000E-08 1.00000E-07 1.52000E-07 &
    2.51000E-07 4.14000E-07 6.83000E-07 1.12500E-06 1.85500E-06 3.05900E-06 &
    5.04300E-06 8.31500E-06 1.37100E-05 2.26000E-05 3.72700E-05 6.14400E-05 &
    1.01300E-04 1.67000E-04 2.75400E-04 4.54000E-04 7.48500E-04 1.23400E-03 &
    2.03500E-03 2.40400E-03 2.84000E-03 3.35500E-03 5.53100E-03 9.11900E-03 &
    1.50300E-02 1.98900E-02 2.55400E-02 4.08700E-02 6.73800E-02 1.11100E-01 &
    1.83200E-01 3.02000E-01 3.88700E-01 4.97900E-01 6.39279E-01 8.20850E-01 &
    1.10803E+00 1.35335E+00 1.73774E+00 2.23130E+00 2.86505E+00 3.67879E+00 &
    4.96585E+00 6.06500E+00 1.00000E+01 1.49182E+01 1.69046E+01 2.00000E+01 &
    2.50000E+01
C
F24:P 1
c
C   25 group CINDER gamma energy group structure
E24 0.000E+00 1.000E-02 3.000E-02 6.000E-02 1.000E-01 2.000E-01 3.000E-01 &
    5.000E-01 5.250E-01 7.500E-01 1.000E+00 1.330E+00 1.660E+00 2.000E+00 &
    2.500E+00 3.000E+00 4.000E+00 5.000E+00 6.000E+00 7.000E+00 8.000E+00 &
    9.000E+00 1.000E+01 1.200E+01 1.700E+01 3.000E+01
C
F11:P 2.1
c
C   3-6 MeV Check
E11 3.0 4.0 5.0 6.0 30.0 $first group will be 0-3
{SRC2:FM11 [SRCTOT]}
c
VOL j 5.45e6 j $ vol of rpp
{SRC1:SDEF SUR=2.4 POS=0 -91.5 0 AXS=0 1 0 RAD=D1 PAR=2 ERG=12.2 VEC=0 1 0 DIR=1
si1 0 6.77
sp1 -21 1}
{SRC2:SDEF CEL=1 PAR=P ERG=d3
si3 [ERG]
sp3 [SRC] }
PHYS:N 25.0 2j -1 j 5
PHYS:P 30.0 2j -1 2j 1
NPS 5e7
PRINT
```

Appendix C

Sample TINDER Transport Script

The following is an example of the script that can be written to couple a transport code to TINDER. This is the script used for the TINDER/EVENT models run in Section 3.2.2.

File: /media/truecrypt1/research/th...n/tools/tinder/tinder_event.pl Page 1 of 14

```
#!/usr/bin/perl

package tinder_event;

use POSIX;
use strict;
use File::Copy;
use Env '$GEM_DATA','$HOME','$EVENT_OUT';
use Cwd 'abs_path';

#global vars that are problem dependent
our($sname) = "tinder_event.pl";
our($version) = "0.1_Sept_28_2011";
our($low_limit) = 1e-6;            #low limit on %of total material the nuclide must be in
order to be included
our($averageNum) = 1;
our($ntallyName) = "tally  14";
our($ntallyNameOut) = "tally 14";
our($gtallyName) = "tally  24";
our($gtallyNameOut) = "tally 24";
our($Ggrps) = 12;
our($Ngrps) = 30;
our(@energyEg) = (1.000E-01,5.000E-01,1.000E+00,2.000E+00,3.000E+00,4.000E+00,
                  5.000E+00,6.000E+00,7.000E+00,8.000E+00,9.000E+00,2.000E+01);
our(@energyEn) = (1.520E-07,4.140E-07,1.130E-06,3.060E-06,8.320E-06,2.260E-05,
                  6.140E-05,1.670E-04,4.540E-04,1.235E-03,3.350E-03,9.120E-03,
                  2.480E-02,6.760E-02,1.840E-01,3.030E-01,5.000E-01,8.230E-01,
                  1.353E+00,1.738E+00,2.232E+00,2.865E+00,3.680E+00,6.070E+00,
                  7.790E+00,1.000E+01,1.200E+01,1.350E+01,1.500E+01,1.700E+01);
#cinder 25 group energy structure
our(@energyCg) =
(1.000E-02,3.000E-02,6.000E-02,1.000E-01,2.000E-01,3.000E-01,5.000E-01,5.250E-01, #losest
group extent to 0
                7.500E-01,1.000E+00,1.330E+00,1.660E+00,2.000E+00,2.500E+00,3.000E+00,4.000E
+00,5.000E+00,
                6.000E+00,7.000E+00,8.000E+00,9.000E+00,1.000E+01,1.200E+01,1.700E+01,3.000E
+01);
#cinder 66 group energy structure - CINDER2008 standard fission
our(@energyCn) =
(5.00000E-10,1.00000E-09,2.00000E-09,5.00000E-09,1.00000E-08,1.50000E-08,2.00000E-08,
#lowest group extend to 0

2.50000E-08,3.00000E-08,3.50000E-08,4.20000E-08,5.00000E-08,5.80000E-08,6.70000E-08,8.00000E-08,

1.00000E-07,1.52000E-07,2.51000E-07,4.14000E-07,6.83000E-07,1.12500E-06,1.85500E-06,3.05900E-06,

5.04300E-06,8.31500E-06,1.37100E-05,2.26000E-05,3.72700E-05,6.14400E-05,1.01300E-04,1.67000E-04,

2.75400E-04,4.54000E-04,7.48500E-04,1.23400E-03,2.03500E-03,2.40400E-03,2.84000E-03,3.35500E-03,

5.53100E-03,9.11900E-03,1.50300E-02,1.98900E-02,2.55400E-02,4.08700E-02,6.73800E-02,1.11100E-01,

1.83200E-01,3.02000E-01,3.88700E-01,4.97900E-01,6.39279E-01,8.20850E-01,1.10803E
+00,1.35335E+00,
                1.73774E+00,2.23130E+00,2.86505E+00,3.67879E+00,4.96585E+00,6.06500E
+00,1.00000E+01,1.49182E+01,
```

```
                1.69046E+01,2.00000E+01,2.50000E+01);
our($debug) = 0;

#global vars - do not edit
our($grps, @srcErg, @srcVal);     #these should be global since used in multiple
functions, grps is the CINDER spectra structure
our(%mats) = {};
our(%eventMats) = {};
our($cur_dir);

main ();

sub main {
  #definitions
  my($now, $line, @hold, $numden,$fname, $i, $curkey, $atper, $key, $key2);
  my($a2, $b2, $first, $count, $rem, $iter, $nosrc, $srctot);

  #write header line
  $now  = localtime;
  print "tinder_event.pl executed at $now\n";
  print
"------------------------------------------------------------------------------------------------------------
\n";
  print "parsing input ...\n";

  #get the path of this file - delete the script name
  $cur_dir = abs_path($0);
  $cur_dir =~ s/$sname//;
# print $cur_dir."\n";

#----READ MATS FILE---

  #open the materials file if it exists
  if(-e "mats")
  {
    open(MATSIN,"<mats") or die "ERROR: Could not open the mats file"
  }
  else
  {
    die "ERROR: Could not locate the mats file"
  }

  #initialize the total material number density to 0
  $numden = 0.0;

  #read the materials file
  while( $line = <MATSIN> )
  {
    chomp($line);
    @hold = split(/,/,$line);
    @hold[1] = trim(@hold[1]);
    $mats{ @hold[1] } = @hold[2];
    $numden += @hold[2];
    #print "AZID: ".@hold[1]." den: ".$mats{@hold[1]}."\n";
  }
```

```
  #close the file now
  close(MATSIN);

#----READ EVENTDATA FILE---

  #open the eventData file to determine the nuclides present in the event library
  if(-e $cur_dir."eventData"){
    open(eventData,'<'.$cur_dir."eventData") or die "ERROR: Could not open the eventData
file.";
  }
  else{
    die "ERROR: Could not locate the eventData file.";
  }

  #bring in the materials present in the event library
  while( $line = <eventData> )
  {
    chomp($line);
    @hold = split(' ',$line);
    $eventMats{@hold[0]} = @hold[1];
    #print "Name: ".@hold[0]." AZID: ".$eventMats{@hold[0]}."\n";
  }

  #close the file now
  close(eventData);

#----READ SRC FILE---

  #now check to see if there is an src file for the source from CINDER, if not, assume 0
  if(-e "src"){
    open(src,"<src") or die "ERROR: Could not open the src file.";
    #get the first line which is the number of groups, the gamma groups out of CINDER
    $line = <src>;
    chomp($line);
    $grps = $line;

    #now read in the energy edge data
    for($i=0;$i<=$grps;$i++){
      $line = <src>;
      chomp($line);
      @srcErg[$i] = $line;
    }

    #now skip the title line "spectrum"
    $line = <src>;
    #read the actual source spectrum, the first value must be zero for EVENT
    $srctot = 0.0;
    @srcVal[0] = 0.0;
    for($i=1;$i<=$grps;$i++){
      $line = <src>;
      chomp($line);
      @srcVal[$i] = $line;
      $srctot+= @srcVal[$i];
    }
    $nosrc = 0;
    close(src);
```

```
  }
  else{
    $nosrc = 1;
  }

#----COPY EVENT INPUT TEMPLATE FILE---

  #check it the environmental variable is set
  if(length($GEM_DATA) == 0){
    $GEM_DATA = $HOME.'/gem/data/';
  }

  #open the event input file template (the command line argument)
  if($ARGV[1]==1){
    open(template,$ARGV[0]."1") or die "ERROR: Could not open the event template file.\n";
  }
  else{
    open(template,$ARGV[0]."2") or die "ERROR: Could not open the event template file.\n";
  }
  $fname = $GEM_DATA.$ARGV[0];
  if(-e $fname){
    unlink($fname);
  }
  open(input,">$fname") or die "ERROR: could not open the event input file.\n";

  #loop through the template, outputting all the lines to the new event input file
  # until the {MAT}/{MIX}/{SRC: flags are found
  while( $line = <template> ){
    chomp($line);

    #see if material specifier
    if($line =~ m/{MAT}/){
      #loop through the hash determining the output names and write to the input file
      foreach $key (sort {$a<=>$b} keys %mats){
        foreach $key2 (sort {$a2<=>$b2} keys %eventMats){
          $curkey = floor($key/10);
          $rem = $curkey*10-$key;
          if($rem>0){
            #metastable state, adjust appropriately
            $curkey = $curkey+300+100*$rem;
          }
          #print $curkey.' '.$value2."\n";
          if($curkey eq $eventMats{$key2} & $eventMats{$key2} != 0){
            #print $curkey.' '.$eventMats{$key2}."\n";
            $atper = $mats{$key}/$numden;
            if($atper > $low_limit){
              print input "material ".$key2."\n";
            }
          }
        }
      }
      #move on to next line
      next;
    }
    #see if mixture specifier
    if($line =~ m/{MIX:/){
```

```
      #drop the tags
      $line =~ s/{MIX://;
      $line =~ s/}//;

      #first, print the mix instructions line
      print input $line."\n";

      #loop through the hash determining the output names and write to the input file
      foreach $key (sort {$a<=>$b} keys %mats){
        foreach $key2 (sort {$a2<=>$b2} keys %eventMats){
          $curkey = floor($key/10);
          $rem = $curkey*10-$key;
          if($rem>0){
            #metastable state, adjust appropriately
            $curkey = $curkey+300+100*$rem;
          }
          #print $curkey.' '.$value2."\n";
          if($curkey eq $eventMats{$key2} & $eventMats{$key2} != 0){
            #print $curkey.' '.$eventMats{$key2}."\n";
            $atper = $mats{$key}/$numden;
            if($atper > $low_limit){
              print input $line.' '.$key2.' '.$mats{$key}."\n";
            }
          }
        }
      }
      #move on to next line
      next;
    }

    #see if source specifier
    if( $line =~ m/{SRC/ ){
      $iter = $ARGV[1];
      if( $line =~ m/{SRC1:/ ){
        #first source found, only use on iter=1
        $line =~ s/{SRC1://;

        if( $line =~ m/}/ ){
          #single line of source, just take care of it and move on
          $line =~ s/}//;
          if($iter == 1){
            print input $line."\n";
          }
          next;
        }
        else{
          #multiple lines of source, go until the end marker then move on
          if($iter == 1){
            print input $line."\n";
          }

          while( $line = <template> ){
            chomp($line);
            #check for marker, if present, swap, output and move on, otherwise output and
keep going
            if( $line =~ m/}/ ){
```

```
            $line =~ s/}//;
            if($iter == 1){
              print input $line."\n";
            }
            last;
          }
          else{
            if($iter == 1){
              print input $line."\n";
            }
          }
        }
        next;
      }
    }
    elsif( $line =~ m/{SRC2:/ ){
      #second source found, only use on iter=2
      $line =~ s/{SRC2://;

      if( $line =~ m/}/ ){
        #single line of source, just take care of it and move on
        $line =~ s/}//;
        if($iter > 1){
          if($nosrc == 0){
            #there is a source value to search for
            if( $line =~ m/\[SRC\]/ ){ #source spectrum placeholder
              $line =~ s/\[SRC\]// ;
              print input $line."^\n";
              printSRC();
            }
          }
          else{
            #otherwise just print the line
            print input $line."\n";
          }
        }
        next;
      }
      else{
        #multiple lines of source, go until the end marker then move on
        if($iter > 1){
          if($nosrc == 0){
            #there is a source value to search for
            if( $line =~ m/\[SRC\]/ ){ #source spectrum placeholder
              $line =~ s/\[SRC\]// ;
              print input $line."\n";
              printSRC();
            }
          }
          else{
            #otherwise just print the line
            print input $line."\n";
          }
        }

        while( $line = <template> ){
```

```
            chomp($line);
            #check for marker, if present, swap, output and move on, otherwise output and
keep going
            if( $line =~ m/}/ ){
              $line =~ s/}//;
              if($iter > 1){
                if($nosrc == 0){
                  #there is a source value to search for
                  if( $line =~ m/\[SRC\]/ ){ #source spectrum placeholder
                    $line =~ s/\[SRC\]// ;
                    print input $line."\n";
                    printSRC();
                  }
                  else{
                    print input $line."\n";
                  }
                }
                else{
                  #otherwise just print the line
                  print input $line."\n";
                }
              }
              last;
            }
            else{
              if($iter > 1){
                if($nosrc == 0){
                  #there is a source value to search for
                  if( $line =~ m/\[SRC\]/ ){ #source spectrum placeholder
                    $line =~ s/\[SRC\]// ;
                    print input $line."\n";
                    printSRC();
                  }
                  else{
                    print input $line."\n";
                  }
                }
                else{
                  #otherwise just print the line
                  print input $line."\n";
                }
              }
            }
          }
          next;
        }
      }
      else{
        #found some other source, just output it
        print input $line."\n";
      }
    }

    #otherwise
    print input $line."\n";
  }
```

```
  #close the files now
  close(input);
  close(template);

#----RUN EVENT---

  #now run event
  print "running event ...\n";
  system("gem -s $ARGV[0]");
  system("event -dp -wait $ARGV[0] -o $ARGV[0]");

#----WRITE FLUX FILE---

  #now create the flux file
  print "creating transfer files ...\n";
  fluxEVENT();

#---COPY THE INPUT/OUTPUT TO CWD---

  #copy the input file
  my($f1,$f2);
  $f1 = $GEM_DATA.$ARGV[0];
# print $f1."\n";
  mkdir("run".$ARGV[1],0777);
  $f2 = abs_path(getcwd());
  $f2 = $f2."/run".$ARGV[1]."/".$ARGV[0];
# print $f2."\n";
  copy($f1,$f2) or die "WARNING: Could not copy the input file correctly to the current
run folder\n";
  #copy the integral file
  $f1 = $EVENT_OUT."integral/".$ARGV[0];
# print $f1."\n";
  $f2 = abs_path(getcwd());
  $f2 = $f2."/run".$ARGV[1]."/".$ARGV[0].".int";
# print $f2."\n";
  copy($f1,$f2) or die "WARNING: Could not copy the integral file correctly to the current
run folder\n";

  #copy the output file
  $f1 = $EVENT_OUT.$ARGV[0];
# print $f1."\n";
  $f2 = abs_path(getcwd());
  $f2 = $f2."/run".$ARGV[1]."/".$ARGV[0].".out";
# print $f2."\n";
  copy($f1,$f2) or die "WARNING: Could not copy the output file correctly to the current
run folder\n";
}



# Perl trim function to remove whitespace from the start and end of the string
sub trim($)
{
  my $string = shift;
  $string =~ s/^\s+//;
```

```
  $string =~ s/\s+$//;
  return $string;
}
# Left trim function to remove leading whitespace
sub ltrim($)
{
  my $string = shift;
  $string =~ s/^\s+//;
  return $string;
}
# Right trim function to remove trailing whitespace
sub rtrim($)
{
  my $string = shift;
  $string =~ s/\s+$//;
  return $string;
}

sub fmin {
    my($f1, $f2) =@_;
    my ($ff);
    if ($f1 < $f2) {$ff = $f1;}
    else {$ff = $f2;}
    $ff;
}

sub fmax {
    my($f1, $f2) =@_;
    my ($ff);
    if ($f1 < $f2) {$ff = $f2;}
    else {$ff = $f1;}
    $ff;
}

#this sub searches through the output file for the input flux name and outputs that to the
flux file
sub fluxEVENT()
{
  #my($tallyName) = shift;
  my($line, $fname, $count, $i, $j, @Fld, @flux, $n, @nfluxOut,@gfluxOut,$dfde,$ee,
$ee0,@nflux,@gflux);
  my($length,$length0);
  close(output);

  #open the mcnpx output file and pick out the tally14 and tally24 information
  $fname = $EVENT_OUT."integral/".$ARGV[0];
  if(not -e $fname){
    die "ERROR: The EVENT output file was not found.\n";
  }
  open(output,"<$fname") or die "ERROR: Could not open the MCNPX output file for reading.
\n";

  #open the flux file to transfer the tally information, delete it if a copy already exists
  if(-e "flux"){
    unlink("flux");
  }
```

```
  open(flux,">flux") or die "ERROR: Could not open the flux transfer file for writing.\n";
  #skip the header and info line
  $line = <output>; #header
  $line = <output>; #information

  #pick the number of groups from the information line, should equal the total of gamma
and neutron groups
  @Fld = split(' ',$line);
  $n = $Fld[0];

  #make sure things check out before proceeding
  if($n != $Ngrps + $Ggrps){
    die "ERROR: EVENT output groups do not equal those specified in script!";
  }

  #initialize the array in case values are zero and omitted
  for($i=0;$i<$n;$i++){$flux[$i]=0.0;}

  #read through the event integrals file and pick out the flux and group for the given
average set
  while($line = <output>) {
    chomp($line);
    @Fld = split(' ',$line);

    #see if this is an in-between line, if so skip it
    if(scalar @Fld < 7) {next;}

    #get the group's flux
    $flux[$Fld[0]-1] = $Fld[4];
  }
  #close the output file
  close(output);
  #reverse the group orders, EVENT outputs in the standard high to low E grouping, CINDER
needs low to high
  $j=0;
  for($i=$Ngrps-1;$i>=0;$i--){
    #the first portion of the data is neutron
    $nflux[$j] = $flux[$i];
    $j++;
  }
  $j=0;
  for($i=$n-1;$i>=$n-$Ggrps;$i--){
    #the rest is gammas
    $gflux[$j] = $flux[$i];
    $j++;
  }

  #regroup the flux from EVENT to the input structure of CINDER, 66/25 (hardcoded)
  #--neutrons first--

  #initialize the outgoing flux to zero
  for($i=0;$i<66;$i++){$nfluxOut[$i] = 0.0;}
  #loop through the output structure to regroup things
  $length = scalar(@energyEn); #should equal $Ngrps
  $length0 = scalar(@energyCn); #should equal 66 for CINDER2008
```

```
  #loop over outgoing energy structure
  $i = 0; #ctr for input EVENT strcut
  $j = 0; #ctr for output CINDER struct
  $nfluxOut[$j] = 0.0;
  $dfde = $nflux[$i]/$energyEn[$i];
  if($debug>0){
    printf "e0=%10.3e e1=%10.3e flux=%10.3e dfde=%10.3e  \n", 0.0, $energyEn[$i], $nflux
[$i], $dfde;
  }

  $ee0 = 0.0;
  while ($j < $length0 && $i < $length) {
    $ee = fmin($energyCn[$j], $energyEn[$i]);
    if ($ee == $energyCn[$j]) {
      $nfluxOut[$j] += $dfde*($ee-$ee0);
      if($debug>0){
        printf "      flux=%10.3e \n",$nfluxOut[$j];
      }
      $j++;
    }
    else {
      $nfluxOut[$j] += $dfde*($ee-$ee0);
      if($debug>0){
        printf "      flux=%10.3e \n",$nfluxOut[$j];
      }
      $i++;
      $dfde = $nflux[$i]/($energyEn[$i]-$energyEn[$i-1]);
      if($debug>0){
        printf "e0=%10.3e e1=%10.3e flux=%10.3e dfde=%10.3e  \n", $energyEn[$i-1],
$energyEn[$i], $nflux[$i], $dfde;
      }
    }
    if($debug>0){
      printf "ee0=%10.3e  ee=%10.3e  dfde=%10.3e  \n", $ee0, $ee, $dfde;
    }
    $ee0 = $ee;
  }
  #---gammas next---
  #initialize the outgoing flux to zero
  for($i=0;$i<25;$i++){$gfluxOut[$i] = 0.0;}
  #loop through the output structure to regroup things
  $length = scalar(@energyEg); #should equal $Ggrps
  $length0 = scalar(@energyCg); #should equal 25 for CINDER2008

  #loop over outgoing energy structure
  $i = 0; #ctr for input EVENT strcut
  $j = 0; #ctr for output CINDER struct
  $gfluxOut[$j] = 0.0;
  $dfde = $gflux[$i]/$energyEg[$i];
  if($debug>0){
    printf "e0=%10.3e e1=%10.3e flux=%10.3e dfde=%10.3e  \n", 0.0, $energyEg[$i], $gflux
[$i], $dfde;
  }

  $ee0 = 0.0;
  while ($j < $length0 && $i < $length) {
```

```
    $ee = fmin($energyCg[$j], $energyEg[$i]);
    if ($ee == $energyCg[$j]) {
      $gfluxOut[$j] += $dfde*($ee-$ee0);
      if($debug>0){
        printf "     gflux=%10.3e \n",$gfluxOut[$j];
      }
      $j++;
    }
    else {
      $gfluxOut[$j] += $dfde*($ee-$ee0);
      if($debug>0){
        printf "     gflux=%10.3e \n",$gfluxOut[$j];
      }
      $i++;
      $dfde = $gflux[$i]/($energyEg[$i]-$energyEg[$i-1]);
      if($debug>0){
        printf "e0=%10.3e e1=%10.3e flux=%10.3e dfde=%10.3e  \n", $energyEg[$i-1],
$energyEg[$i], $gflux[$i], $dfde;
      }
    }
    if($debug>0){
      printf "ee0=%10.3e  ee=%10.3e dfde=%10.3e  \n", $ee0, $ee, $dfde;
    }
    $ee0 = $ee;
  }

  #now write the fluxes to the flux file, remember they should be in increasing energy
order, so reverse them
  print flux $ntallyNameOut."\n";
  for($i=0;$i<66;$i++){
    #the first portion of the data is neutron
    print flux $nfluxOut[$i]."\n";
  }
  print flux $gtallyNameOut."\n";
  for($i=0;$i<25;$i++){
    #the rest is gammas
    print flux $gfluxOut[$i]."\n";
  }

  #close the open files
  close(flux);

  return;
}


sub printSRC(){
  #this sub prints the energy spectrum for the source specification
  my($l5, $rest, $i,@srcValOut,$grpsTot,@gamSrc,$j,@gamSrcOut);
  my($length,$length0,$dfde,$ee,$ee0);

  #set the total number of groups to the n and g required by EVENT
  $grpsTot = $Ngrps + $Ggrps;
  #regroup the srcVal into padded zeros (neutrons -- no source from CINDER) then the gammas
  #initialize the outgoing source to zero
  for($i=0;$i<$Ggrps;$i++) { $gamSrcOut[$i] = 0.0;}
```

```
  #loop through the output structure to regroup things
  $length = scalar(@energyCg); #should equal 25 for CINDER2008
  $length0 = scalar(@energyEg); #should equal $Ggrps

  #loop over outgoing energy structure
  $i = 0; #ctr for input CINDER strcut
  $j = 0; #ctr for output EVENT struct
  $gamSrcOut[$j] = 0.0;
  $dfde = $srcVal[$i]/$energyCg[$i];
  if($debug>0){
    printf "e0=%10.3e e1=%10.3e flux=%10.3e dfde=%10.3e  \n", 0.0, $energyCg[$i], $srcVal
[$i], $dfde;
  }

  $ee0 = 0.0;
  while ($j < $length0 && $i < $length) {
    $ee = fmin($energyEg[$j], $energyCg[$i]);
    if ($ee == $energyEg[$j]) {
      $gamSrcOut[$j] += $dfde*($ee-$ee0);
      $j++;
    }
    else {
      $gamSrcOut[$j] += $dfde*($ee-$ee0);
      $i++;
      $dfde = $srcVal[$i]/($energyCg[$i]-$energyCg[$i-1]);
      if($debug>0){
        printf "e0=%10.3e e1=%10.3e flux=%10.3e dfde=%10.3e  \n", $energyCg[$i-1],
$energyCg[$i], $srcVal[$i], $dfde;
      }
    }
    if($debug>0){
      printf "ee0=%10.3e  ee=%10.3e dfde=%10.3e  \n", $ee0, $ee, $dfde;
    }
    $ee0 = $ee;
  }
  #reverse the group order to go to decreasing energy (increasing lethargy)
  $j=$Ggrps;
  for($i=0;$i<$Ggrps;$i++){
    $j--;
    $gamSrc[$i] = $gamSrcOut[$j];
  }
  #now take that and translate it into the full EVENT source with n&g in it
  $j=0;
  for($i=0;$i<$grpsTot;$i++) {
    if($i<$Ngrps){
      $srcValOut[$i] = 0.0; #CINDER does not give a neutron source, so set this portion to
zero
    }
    else{
      $srcValOut[$i] = $gamSrc[$j];
      $j++;
    }
  }
  #figure out how many lines of 5 and how many on the extra line
  $l5 = int(($grpsTot+1)/5);
  $rest = ($grpsTot+1) - $l5*5;
```

```
  #loop through the lines of 5,
  for ($i=0;$i<$l5;$i++) {
    if ($i < ($l5-1)) {
      printf input"         %12.5E %12.5E %12.5E %12.5E %12.5E ^\n",
      $srcValOut[$i*5],$srcValOut[$i*5+1],$srcValOut[$i*5+2],
      $srcValOut[$i*5+3],$srcValOut[$i*5+4];
    }
    elsif ($i == ($l5-1) && $rest > 0) {
      printf input"         %12.5E %12.5E %12.5E %12.5E %12.5E ^\n",
      $srcValOut[$i*5],$srcValOut[$i*5+1],$srcValOut[$i*5+2],
      $srcValOut[$i*5+3],$srcValOut[$i*5+4];
    }
    elsif ($i == ($l5-1) && $rest == 0) {
      printf input"         %12.5E %12.5E %12.5E %12.5E %12.5E \n",
      $srcValOut[$i*5],$srcValOut[$i*5+1],$srcValOut[$i*5+2],
      $srcValOut[$i*5+3],$srcValOut[$i*5+4];
    }
  }
  if    ($rest == 4) {
    printf input"         %12.5E %12.5E %12.5E %12.5E\n",
    $srcValOut[$l5*5],$srcValOut[$l5*5+1],$srcValOut[$l5*5+2],
    $srcValOut[$l5*5+3];
  }
  elsif ($rest == 3) {
    printf input"         %12.5E %12.5E %12.5E\n",
    $srcValOut[$l5*5],$srcValOut[$l5*5+1],$srcValOut[$l5*5+2];
  }
  elsif ($rest == 2) {
    printf input"         %12.5E %12.5E\n",
    $srcValOut[$l5*5],$srcValOut[$l5*5+1];
  }
  elsif ($rest == 1) {
    printf input"         %12.5E\n",
    $srcValOut[$l5*5];
  }

  return;
}
```

Bibliography

[1] E. Jacobs, H. Theirens, D. De Frenne, A. De Clercq, P. D'hondt, P. De Gelder, and A. J. Deruytter. Product yields for the photofission of ^{235}U with 12-, 15, 20-, 30-, and 70-MeV bremsstrahlung. *Physical Review C*, 21(1):237–245, 1980.

[2] D. R. Nethaway and B. Mendoza. Fission of ^{234}U and ^{236}U with 14.8 MeV neutrons. *Physical Review C*, 6(5):1821–1826, 1972.

[3] E. Jacobs, H. Theirens, D. De Frenne, A. De Clercq, P. D'hondt, P. De Gelder, and A. J. Deruytter. Product yields for the photofission of ^{238}U with 12-, 15, 20-, 30-, and 70-MeV bremsstrahlung. *Physical Review C*, 19(2):422–432, 1979.

[4] M. Ya. Kondrat'ko, A. V. Mosesov, K. A. Petrzhak, and O. A. Teodorovich. Yields of products of the photofission of ^{239}Pu (translated). *Atomnaya Energiya*, 50(1):33–36, 1981.

[5] R. A. Schmitt and N. Sugarman. Uranium photofission yields. *Physical Review*, 95(5):1260–1267, 1954.

[6] W. L. Myers, C. A. Goulding, C. L. Hollas, and C. E. Moss. Photon and neutron active interrogation of highly enriched uranium. In *International Conference on Nuclear Data for Science and Technology*, Santa Fe, NM, USA, Sept. 26–Oct. 1 2004.

[7] W. R. Martin. Monte carlo depletion. Presentation at CAMS: The Virtual Nuclear Reactor Center Workshop, August 2006.

[8] Z. Xu, J. Rhodes, and K. Smith. Statistical implications in monte carlo depletions. In *PHYSOR 2010: Advances in Reactor Physics to Power the Nuclear Renaissance*, Pittsburgh, PA, USA, May 9–14 2010.

[9] N. Bohr and J. A. Wheeler. The mechanism of nuclear fission. *Physical Review*, 56(5):426–450, 1939.

[10] R. O. Haxby, W. E. Shoupp, W. E. Stephens, and W. H. Wells. Photofission of uranium and thorium. *Physical Review*, 57(1):57–62, 1941.

[11] B. Arakatu, Y. Uemura, M. Sonoda, S. Shimizu, K. Kimura, and K. Muraoka. Photofission of uranium and thorium produced by the γ rays of lithium and fluorine bombarded with high-speed protons. *Proceedings of Physico-Mathematical Society of Japan*, 23:440, 1941.

[12] R. B. Duffield, R. A. Schmitt, and R. A. Sharp. Mass-yield distributions in the photofission of radium and other heavy elements. In *Proceedings of the Second United Nations International Conference on the Peaceful Uses of Atomic Energy*, Geneva, Austria, Sept. 1–13 1958.

[13] B. L. Berman. Atlas of photoneutron cross sections obtained with monoenergetic photons. Technical Report UCRL-78482, Lawrence Livermore Laboratory, Livermore, CA, USA, December 1976.

[14] F. Carrel, M. Agelou, M. Gmar, F. Laine, J. Loridon, J.-L. Ma, C. Passard, and B. Poumarede. New experimental results on the cumulative yields from thermal fission of ^{235}U and ^{239}Pu and from the photofission of ^{235}U and ^{238}U induced by bremsstrahlung. *IEEE Transactions on Nuclear Science*, 58(4):2064–2072, 2011.

[15] D. de Frenne, H. Thierens, B. Proot, E. Jacobs, P. De Gelder, and A. De Clercq. Isotopic distributions and elemental yields for the photofission of ^{235,238}U with 12-30-MeV bremsstrahlung. *Physical Review C*, 29(5):1908–1911, 1984.

[16] E. Jacobs, A. De Clercq, H. Theirens, D. De Frenne, P. D'hondt, P. De Gelder, and A. J. Deruytter. Fragment mass and kinetic energy distributions for the photofission of ^{238}U with 12-, 15, 20-, 30-, and 70-MeV bremsstrahlung. *Physical Review C*, 20(6):2249–2265, 1979.

[17] J. L. Meason and P. K. Kuroda. Photofission of ^{238}u induced by 17.5-MeV monoenergetic gamma rays. *Physical Review C*, 142:691–695, 1966.

[18] H. Theirens, D. De Frenne, E. Jacobs, A. De Clercq, P. D'hondt, and A. J. Deruytter. Product yields for the photofission of ^{235}U and ^{238}U with 25-MeV bremsstrahlung. *Physical Review C*, 14(3):1058–1067, 1976.

[19] H. Theirens, A. De Clercq, E. Jacobs, P. D'hondt, and D. De Frenne. Kinetic energy and fragment mass distributions for the spontaneous and photon-induced fission of ^{244}Pu. *Physical Review C*, 27(3):1117–1125, 1983.

[20] I. N. Vishnevskii, O. I. Davidovskaya, V. A. Zheltonozhskii, and A. N. Savrasov. Investigation of ^{235}U and ^{239}Pu photofission. *Bulletin of the Russian Academy of Sciences: Physics*, 74(4):500–503, 2010.

[21] D. K. Wehe, H. Yang, and M. H. Jones. Observation of ^{238}U photofission products. *IEEE Transactions on Nuclear Science*, 53(3):1430–1434, 2006.

[22] G. C. Baldwin and G. S. Klaiber. Photo-fission in heavy elements. *Physical Review*, 71(1):3–10, 1947.

[23] J. E. Gindler, J. R. Huizenga, and R. A. Schmitt. Photofission and photoneutron emission in thorium and uranium. *Physical Review*, 104(2):425–433, 1956.

[24] D. M. Hiller and D. S. Martin Jr. Radiochemical studies on the photofission of thorium. *Physical Review*, 90(4):581–585, 1953.

[25] J. C. Hogan, A. E. Richardson, J. L. Meason, and H. L. Wright. Photofission of ^{232}Th with 9, 15, and 38 MeV peak bremsstrahlung. *Physical Review C*, 16(6):2296–2305, 1977.

[26] A. De Clercq, E. Jacobs, D. de Frenne, H. Thierens, P. D'hondt, and A. J. Deruytter. Fragment mass and kinetic energy distribution for the photofission of ^{235}U and ^{238}U with 25-MeV end-point bremsstrahlung. *Physical Review C*, 13(4):1536–1543, 1976.

[27] E. Jacobs, A. De Clercq, H. Theirens, D. De Frenne, P. D'hondt, P. De Gelder, and A. J. Deruytter. Fragment mass and kinetic energy distributions for the photofission of ^{235}U with 12-, 15, 20-, 30-, and 70-MeV bremsstrahlung. *Physical Review C*, 24(4):1795–1798, 1981.

[28] M. Verboven, E. Jacobs, M. Piessens, S. Pommé, D. de Frenne, and A. de Clercq. Fragment mass and kinetic energy distributions for the photofission of ^{234}U with 12-, 15, and 20-MeV bremsstrahlung. *Physical Review C*, 42(1):453–456, 1990.

[29] W. Wilke, U. Kneissl, Th. Weber, H. Ströher, L. S. Cardman, P. T. Debevec, D. Hoblit, R. T. Jones, and A. M. Nathan. Photofission of ^{238}U with monochromatic gamma rays in the energy range 11-16MeV. *Physical Review C*, 42(5):2148–2156, 1990.

[30] S. A. Karamian, J. Adam, A. G. Belov, J. J. Carroll, Yu. V. Norseeev, V. I. Stegailov, and P. Chaloun. Light-mass yield and fine structure of mass distributions in ^{232}Th photofission. *Physical Review C*, 62, 2000.

[31] H. Theirens, A. De Clercq, E. Jacobs, D. De Frenne, P. D'hondt, P. De Gelder, and A. J. Deruytter. Kinetic energy and fragment mass distributions for ^{240}Pu(s,f), ^{239}Pu(n$_{th}$,f), and ^{240}Pu(γ,f). *Physical Review C*, 27(3):2104–2113, 1983.

[32] H. Theirens, E. Jacobs, P. D'hondt, A. De Clercq, M. Piessens, and D. De Frenne. Fragment mass and kinetic energy distributions for ^{242}Pu(s,f), ^{241}Pu(n$_{th}$,f), and ^{242}Pu(γ,f). *Physical Review C*, 29(2):498–507, 1984.

[33] A. Alm and L. J. Lindgren. Fission fragment angular distributions and yields of ^{236}U in low-energy photofission. *Nuclear Physics*, A271:1–14, 1976.

[34] H. G. Richter and C. D. Coryell. Low-energy photofission yields of ^{238}U. *Physical Review*, 95(6):1550–1553, 1954.

[35] M. B. Chadwick et al. ENDF/B-VII.0: Next generation evaluated nuclear data library for nuclear science and technology. *Nuclear Data Sheets*, 107:2931–3060, 2006.

[36] E. K. Hyde. *The Nuclear Properties of the Heavy Elements*. Prentice-Hall, Inc., Englewood Cliffs, NJ, USA, 1964.

[37] G. P. Ford. Fission mass yield dependence on angular momentum. *Physical Review*, 137(4B):B826–B836, 1965.

[38] R. Vandenbosch and J. R. Huizenga. *Nuclear Fission*. Academic Press, New York, NY, USA, 1973.

[39] C. Wagemans. *The Nuclear Fission Process*. CRC Press, Boca Raton, FL, USA, 1991.

[40] R. W. Mills. UKFY4.1: A set of prototype fission product yield library for neutron, proton, deuteron, alpha particle, photon and spontaneous fission, developed from UKFY4.0. Technical Report JEF/DOC-1232, UKNSF(2008)P227, Nexia Solutions, Mar 2007.

[41] A. C. Wahl. Systematics of fission-product yields. Report LA-13928, Los Alamos National Laboratory, may 2002.

[42] J. L. Jones, W. Y. Yoon, Y. D. Harker, J. M. Hoggan, K. J. Haskell, and L. A. VanAusdeln. Proof-of-concept assessment of a photofission-based interrogation system for the detection of shielded nuclear material. Technical Report INEEL/EXT-2000-01523, Idaho National Engineering and Environmental Laboratory, Idaho Falls, ID, USA, November 2000.

[43] P. Obložinský. Compilation and evaluation of photonuclear data for applications. Summary Report of the 2nd Research Coordination Meeting INDC(NDS)-384, International Atomic Energy Agency, Vienna, Austria, September 1998.

[44] J. M. Verbeke, C. Hagmann, and D. Wright. Simulation of neutron and gamma ray emission from fission and photofission. Report UCRL-AR-228518, Lawrence Livermore National Laboratory, Livermore, CA, USA, May 2010.

[45] S. M. Bowman and L. C. Leal. ORIGEN-ARP: automatic rapid process for spent fuel depletion, decay, and source term analysis. NUREG NUREG-CR-0200, Oak Ridge National Laboratory, Oak Ridge, TN, USA, May 2000.

[46] A. G. Croff. ORIGEN2 – a revised and updated version of the oak ridge isotope generation and depletion code. report ORNL-5621, Oak Ridge National Laboratory, Oak Ridge, TN, USA, July 1980.

[47] I. C. Gauld, O. W. Hermann, and R. M. Westfall. ORIGEN-S: SCALE system module to calculate fuel depletion, actinide transmutation, fission product buildup and deca, and associated radiation source terms. Manual ORNL/TM-2005/39, Oak Ridge National Laboratory, Oak Ridge, TN, USA, January 2009.

[48] S. T. Holloway, W. B. Wilson, IV C. T. Kelsey, H. Little, and V. Mozin. A manual for CINDER2008 codes and data. Manual LA-UR 11-00006, Los Alamos National Laboratory, Los Alamos, NM, USA, March 2011.

[49] W. B. Wilson, T. R. England, R. J. LaBauve, M. E. Battat, D. E. Wessol, and R. T. Perry. Status of CINDER and ENDF/B-V based libraries for transmutation calculations. report LA-UR-80-2107, Los Alamos Scientific Laboratory, Los Alamos, NM, USA, July 1980.

[50] D. Brown. Translating post-fission β-delayed γ data for ^{239}Pu into ENDF. Technical Report UCRL-TR-223148, Lawrence Livermore National Laboratory, Livermore, CA, USA, July 2006.

[51] M.-L. Giacri, A. Vanalauwe, J.-C. David, D. Dorè, D. Ridikas, I. Raskinyte, E. Dupont, and V. Macary. Photonuclear activation file (PAF) status and perspectives. Prague, Czech Republic, October 2007. Workshop on Activation Data - EAF2007.

[52] M.-L. Giacri-Mauborgne, D. Ridikas, M. B. Chadwick, P. G. Young, and W. B. Wilson. Photonuclear physics in radiation transport–III: Actinide cross-sections and spectra. *Nuclear Science and Engineering*, 153:33–40, 2006.

[53] M.-L. Giacri-Mauborgne, D. Ridikas, J.-C. David, M. B. Chadwick, and W. B. Wilson. Development of the photonuclear activation data library for CINDER'90. In *Proceedings of the International Workshop on Nuclear Data for the Transmutation of Nuclear Waste*, GSI-Darmstadt, Germany, Sept. 1–5 2003.

[54] D. Ridikas, M.-L. Giacri, M. B. Chadwick, J.-C. David, D. Dorè, X. Ledoux, A. Van Lauwe, and W. B. Wilson. Status of the photonuclear activation file: reaction cross-sections, fission fragments and delayed neutrons. *Nuclear Instruments and Methods in Physics Research A*, 562:710–713, 2006.

[55] J. Spanier and E. M. Gelbard. *Monte Carlo Principles and Neutron Transport*. Addison-Wesley Educational Publishers, 1969.

[56] M. D. DeHart and L. M. Petrie. Integrated KENO V.a monte carlo transport for multidimensional depletion within SCALE. *Transactions of the American Nuclear Society*, 91:667–669, 2004.

[57] J. Leppänen and M. Pusa. Burnup calculation capability in the PSG2 / Serpent monte carlo reactor physics code. In *International Conference on Advances in Mathematics, Computational Methods, and Reactor Physics*, Saratoga Springs, NY, USA, May. 3–9 2009.

[58] D. I. Postin and H. R. Trellue. User's manual, version 2.0 for Monteburns, version 5b. Manual LA-UR 99-4999, Los Alamos National Laboratory, Los Alamos, NM, USA, September 1999.

[59] J. J. Duderstadt and W. R. Martin. *Transport Theory*. John Wiley and Sons Inc., 1979.

[60] E. E. Lewis and W. F. Miller. *Computational Methods in Neutron Transport*. American Nuclear Society, Inc., 1993.

[61] B. G. Carlson. Solution of the transport equation by S_{N} approximations. report LA-1599, Los Alamos Scientific Laboratory, Los Alamos, NM, USA, October 1953.

[62] W. B. Wilson, S. T. Cowell, T. R. England, A. C. Hayes, and P. Moller. A manual for CINDER'90 version 07.4 codes and data. Manual LA-UR 07-8412, Los Alamos National Laboratory, Los Alamos, NM, USA, December 2007.

[63] C. R. E. de Oliveira. Finite element techniques for multigroup neutron transport calculations with anisotropic scattering. Ph.D. Thesis, Queen Mary College, London, England, 1987.

[64] D. B. Pelowitz. MCNPX user's manual. Manual LA-CP-07-1473, Los Alamos National Laboratory, Los Alamos, NM, USA, April 2008.

[65] D. B. Pelowitz, J. W. Durkee, J. S. Elson, M. L. Fensin, J. S. Hendricks, M. R. James, R. C. Johns, G. W. McKinney, S. G. Mashnik, J. M. Verbeke, L. S. Waters, and T. A. Wilcox. MCNPX 2.7.e extensions. Manual LA-UR-11-01502, Los Alamos National Laboratory, Los Alamos, NM, USA, March 2011.

[66] H. Bateman. Solution of a system of differential equations occuring in the theory of radioactive transformations. In *Proceedings of the Cambridge Philosophical Society*, 1910.

[67] T. R. England. CINDER - a one-point depletion and fission product program. Manual WAPD-TM-334 (REV), Bettis Atomic Power Laboratory, Pittsburgh, PA, USA, August 1964.

[68] R. E. MacFarlane and D. W. Muir. The NJOY nuclear data processing system. Manual LA-12740-M, Los Alamos National Laboratory, Los Alamos, NM, USA, October 1994.

[69] C. D. Bowman, I. G. Schroder, and C. E. Dick. Very low energy photofission of ^{238}U. *Physical Review C*, 12(3):863–870, 1975.

[70] U. Brosa, S. Grossmann, and Andreas Muller. Nuclear scission. *Physics Reports*, 197(4):167–262, 1990.

[71] P. Talou, T. Kawano, O. Bouland, J. E. Lynn, P. Moller, and M. B. Chadwick. Recent advances in nuclear fission theory: pre- and post-scission physics. report LA-UR-10-03259, Los Alamos National Laboratory, Los Alamos, NM, USA, 2010.

[72] J. J. Duderstadt and L. J. Hamilton. *Nuclear Reactor Analysis*. John Wiley and Sons Inc., 1976.

[73] J. K. Tuli. *Nuclear Wallet Cards*. Brookhaven National Laboratory, Upton, NJ, USA, 2005.

[74] S. Boucher, P. Frigola, M. Ruelas, I. Jovanovic, J. B. Rosenzweig, and G. Travish. Inverse compton scattering gamma ray source. *Nuclear Instruments and Methods in Physics Research A*, 2009.

[75] J. A. Church, D. R. Slaughter, S. Asztalos, P. Biltoft, M.-A. Descalle, J. Hall, D. Manatt, J. Mauger, E. B. Norman, D. Petersen, and S. Prussin. Nuclear car

wash sensitivity in varying thicknesses of wood and steel cargo. report UCRL-TC-225709, Lawrence Livermore National Laboratory, Livermore, CA, USA, October 2006.

[76] J. A. Church, D. R. Slaughter, E. B. Norman, S. Asztalos, P. Biltoft, M.-A. Descalle, J. Hall, T. Luu, D. R. Manatt, G. J. Mauger, D. Petersen, and S. Prussin. Experimental study of variations in background radiation and the effect on nuclear car wash sensitivity. report UCRL-TR-229157, Lawrence Livermore National Laboratory, Livermore, CA, USA, 2007.

[77] J. A. Church, D. R. Slaughter, S. Asztalos, P. Biltoft, M.-A. Descalle, J. Hall, T. Luu, D. Manatt, J. Mauger, E. B. Norman, D. Petersen, and S. Prussin. Signals and interferences in the nuclear car wash. *Nuclear Instruments and Methods in Physics Research B*, B261:351–355, 2007.

[78] J. M. Hall, S. Asztalos, P. Biltoft, J. Church, M.-A. Decalle, T. Luu, D. Manatt, G. Mauger, E. Norman, J. Pruet, S. Prussin, and D. Slaughter. The nuclear car was: neutron interrogation of cargo containers to detect hidden SNM. *Nuclear Instruments and Methods in Physics Research B*, B261:337–340, 2007.

[79] P. Kerr, M. Rowland, D. Dietrich, W. Stoeffl, B. Wheeler, L. Nakae, D. Howard, C. Hagmann, J. Newby, and R. Porter. Active detection of small quantities of shielded highly-enriched uranium using low-dose 60-keV neutron interrogation. *Nuclear Instruments and Methods in Physics Research B*, B261:347–350, 2007.

[80] Y. Liu, B. D. Sowerby, and J. R. Tickner. Comparison of neutron and high-energy x-ray dual-beam radiography for air cargo inspection. *Applied Radiation and Isotopes*, 66:463–473, 2008.

[81] J. Pruet, J. Hall, M.-A. Descalle, and S. Prussin. Monte carlo models for the production of β-delayed gamma-rays following fission of special nuclear materials. *Nuclear Instruments and Methods in Physics Research B*, B222:403–410, 2004.

[82] S. Prussin, D. R. Slaughter, J. Pruet, M.-A. Descalle, A. Bernstein, J. Hall, M. Accatino, O. Alford, S. Asztalos, J. Church, A. Loshak, N. Madden, D. Manatt, T. Moore, E. Norman, and D. Petersen. Nuclear car wash status report, august 2005. report UCRL-TC-214636, Lawrence Livermore National Laboratory, Livermore, CA, USA, August 2005.

[83] S. G. Prussin, M.-A. Descalle, J. M. Hall, J. A. Pruet, D. R. Slaughter, M. R. Accatino, O. J. Alford, S. J. Asztalos, A. Bernstein, J. A. Church, T. Gosnell, A. Loshak, N. W. Madden, D. R. Manatt, G. J. Mauger, A. W. Meyer, T. L.

Moore, E. B. Norman, B. A. Pohl, D. C. Petersen, B. Rusnak, T. B. Sundsmo, W. K. Tenbrook, and R. S. Walling. Comparison of tests with 14-MeV neutrons to a monte carlo model for interrogation of thick cargos for clandestine fissionable materials. *Nuclear Instruments and Methods in Physics Research A*, A569:853–862, 2006.

[84] D. R. Slaughter, M. R. Accatino, A. Bernstein, P. Biltoft, J. A. Church, M. A. Descalle, J. M. Hall, D. R. Manatt, G. J. Mauger, T. L. Moore, E. B. Norman, D. C. Petersen, J. A. Pruet, and S. G. Prussin. The nuclear car wash: a system to detect nuclear weapons in commercial cargo shipments. *Nuclear Instruments and Methods in Physics Research A*, A579:349–352, 2007.

[85] C. E. Moss, C. L. Hollas, G. W. McKinney, and W. L. Myers. Comparison of active interrogation techniques. *IEEE Transactions on Nuclear Science*, 53(4):2242, 2006.

[86] R. E. MacFarlane. TRANSX2: a code for interfacing MATXS cross-section libraries to nuclear transport codes. Manual LA-12312-MS, Los Alamos National Laboratory, Los Alamos, NM, USA, July 1992.

[87] B. M. Adams, K. R. Dalbey, M. S. Eldred, D. M. Gay, L. P. Swiler, W. J. Bohnhoff, J. P. Eddy, and K. Haskell. Dakota, a multilevel parallel object-oriented framework for design optimization, parameter estimation, uncertainty quantification and sensitivity analysis. User's Manual SAND2010-2183, Sandia National Laboratories, Albuquerque, NM, USA, January 2011.